UCLA
UCLA Electronic Theses and Dissertations

Title

The paraspeckle protein Pspc1 promotes adipogenesis through differentiation-dependent nuclear export of adipogenic RNAs

Permalink

https://escholarship.org/uc/item/52p3n3tq

Author

Wang, Jiexin

Publication Date

2016

Peer reviewed|Thesis/dissertation

eScholarship.org Powered by the California Digital Library
University of California

UNIVERSITY OF CALIFORNIA

Los Angeles

The paraspeckle protein Pspc1 promotes adipogenesis through differentiation-dependent nuclear export of adipogenic RNAs

A dissertation submitted in partial satisfaction of the

requirements for the degree Doctor of Philosophy

in Cellular and Molecular Pathology

by

Jiexin Wang

2016

© Copyright by

Jiexin Wang

2016

ABSTRACT OF THE DISSERTATION

The paraspeckle protein Pspc1 promotes adipogenesis through differentiation-dependent nuclear export of adipogenic RNAs

by

Jiexin Wang

Doctor of Philosophy in Cellular and Molecular Pathology

University of California, Los Angeles, 2016

Professor Peter John Tontonoz, Chair

Adipocyte differentiation is accompanied by a robust program of cell-type specific gene expression. Although transcriptional regulators of this process are well defined, the contribution of posttranscriptional factors to the establishment of the adipocyte phenotype is poorly understood. This thesis presents the RNA-binding protein paraspeckle protein 1 (Pspc1), a component of the paraspeckle complex, that promotes adipogenesis *in vitro* and is important for mature adipocyte function *in vivo*. Cross-linking and immunoprecipitation followed by RNA sequencing revealed that Pspc1 binds to intronic and 3′ untranslated regions of a battery of adipocyte RNAs, including that encoding the transcriptional regulator Ebf1. Purification of the paraspeckle complex from adipocytes further showed that Pspc1 associates with the RNA export factor Ddx3x in a differentiation-dependent manner. Remarkably, Pspc1 relocates from the

nucleus to the cytoplasm during differentiation, coinciding with enhanced export of adipogenic RNAs. Mice lacking Pspc1 in fat show reduced lipid storage and adipose tissue mass and are resistant to diet-induced obesity and insulin resistance due to a compensatory increase in energy expenditure. These findings highlight a role for Pspc1-dependent RNA maturation in the posttranscriptional control of adipose development and function.

The dissertation of Jiexin Wang is approved.

Karen Reue

Steven J. Bensinger

Thomas A Drake

Dinesh Subba Rao

Peter John Tontonoz, Committee Chair

University of California, Los Angeles

2016

TABLE OF CONTENTS

Abstract of the Dissertation ii

List of Figures vi

Acknowledgements viii

Vita x

Chapter 1: Introduction

Introduction 1

References 21

Chapter 2: Pspc1 promotes adipogenesis by enhancing nuclear export of adipogenic RNAs

Results 35

Figure Legends 49

Figures and Tables 60

Materials and Methods 79

References 87

Chapter 3: Discussion

Discussion 91

References 98

Appendix: Adipose subtype-selective recruitment of TLE3 or Prdm16 by PPAR gamma specifies lipid storage versus thermogenic gene programs 102

LIST OF FIGURES AND TABLES

Figure 1.1 60

Pscp1 expression is differentiation-dependent and promotes adipogenesis in vitro.

Figure 1.2 61

Tissue distribution of Pspc1 expression.

Figure 1.3 62

Effects of Pspc1 on adipocyte differentiation.

Figure 2.1 63

iCLIP-seq identifies Pspc1 binding sites in adipogenic transcripts.

Figures 2.2 and 2.3 64

UCSC genome browser tracks of Pspc1 binding sites on target mRNAs.

Figure 2.4 66

Pspc1 iCLIP-seq analysis.

Figure 3 67

Pspc1 influences the expression of iCLIP-identified target RNAs.

Figure 4 68

Pspc1 interacts with Ddx3x and translocates from nucleus to cytoplasm during differentiation.

Figure 5.1 69

Pspc1 facilitates nucleocytoplasmic export of target mRNAs.

Figure 5.2 70

Knockdown of Ddx3x does not affect Pspc1 target mRNA levels.

Figure 6.1 71

Pspc1 is important for adipocyte differentiation and maintenance *in vivo.*

Figure 6.2 72

Function of Pspc1 in adipose tissue *in vivo.*

Figure 7.1 73

Adipose-specific Pspc1-deficient mice are resistant to diet-induced obesity.

Figure 7.2 74

Adipose-specific Pspc1-deficient mice exhibit increased energy expenditure and glucose tolerance.

Figure 7.3 75

Energy expenditure of adipose-specific *Pspc1* KO mice.

Table 1 76

Candidate Pspc1-interacting Proteins from IP-mass spec.

Table 2 77

qPCR primers used.

ACKNOWLEDGEMENTS

First, I would like to express my most sincere gratitude to my faculty advisor Dr. Peter Tontonoz for the continuous support of my Ph.D. study and related research, for his patience, motivation, and immense knowledge. His guidance helped me through my research and the writing of this thesis. I could not imagine having a better advisor and mentor.

I would like to extend my appreciation to the rest of my committee members Dr. Karen Reue, Dr. Steven Bensinger, Dr. Thomas Drake, and Dr. Dinesh Rao for their insightful comments and encouragement. Their questions improved my critical thinking and broadened my research perspectives.

I thank my fellow labmates Prashant Rajbhandari, Claudio Villanueva, Xin Rong, Cynthia Hong, Li Zhang, Jie Gao, Ayaka Ito, Stephen Lee, Jon Salazar, and Xiaohui Wu in the Tontonoz lab for the days we were working together, for the stimulating discussions, and for all the fun we have had in the past years. I would also like to thank my collaborators Andrey Damianov and Areum Han in Dr. Douglas Black's lab, who have given tremendous help and advice to my research.

I am also so incredibly thankful for my parents and family members for their supportive words, actions and love during my years of study. Also I must thank my close friends that I have known for years for keeping my spirits high and giving me help when necessary.

Finally, I am extremely grateful to my husband Xinzhe Lin for supporting me spiritually and encouraging me continuously throughout the process of my study and research. This accomplishment would not have been possible without you. Thank you!

Chapter 2 and 3 are a version of the manuscript “Wang J, Rajbhandari P, Damianov A, Han A, Waki H, Villanueva CJ, Nielsen R, Mandrup S, Reue K, Young SG, Whitelegge J, Saez E, Black DL, and Tontonoz P. The paraspeckle protein Pspc1 promotes the differentiation-dependent nuclear export of adipogenic RNAs.” (submitted)

Appendix contains a reprint of the publication “Villanueva CJ, Vergnes L, Wang J, Drew BG, Hong C, Tu Y, Hu Y, Peng X, Feng X, Saez E, Wroblewski K, Hevener AL, Reue K, Fong LG, Young SG, and Tontonoz P. Adipose Subtype-Selective Recruitment of TLE3 or Prdm16 by PPAR gamma Specifies Lipid Storage versus Thermogenic Gene Programs. *Cell metabolism.* 2013, 17(3):423-35.”

VITA

2004－2010 School of Medicine, Zhejiang University, Hangzhou, China

Bachelor's Degree of Medicine

PUBLICATIONS AND PRESENTATIONS

Villanueva CJ, Vergnes L, **Wang J**, Drew BG, Hong C, Tu Y, Hu Y, Peng X, Feng X, Saez E, Wroblewski K, Hevener AL, Reue K, Fong LG, Young SG, and Tontonoz P. Adipose Subtype-Selective Recruitment of TLE3 or Prdm16 by PPAR gamma Specifies Lipid Storage versus Thermogenic Gene Programs. *Cell metabolism.* 2013, 17(3):423-35.

Wang J, Rajbhandari P, Damianov A, Han A, Waki H, Villanueva CJ, Nielsen R, Mandrup S, Reue K, Young SG, Whitelegge J, Saez E, Black DL, and Tontonoz P. The paraspeckle protein Pspc1 promotes the differentiation-dependent nuclear export of adipogenic RNAs. *(submitted)*

Abstract: "Adipose subtype-selective recruitment of TLE3 or Prdm16 by PPARγ specifies lipid-storage versus thermogenic gene expression" **Wang J** and Tontonoz P. (2013) Deuel Conference on Lipids (American Society for Biochemistry and Molecular Biology), Napa Valley, California.

Chapter 1

Introduction

I. Adipose tissue and adipocyte

Adipose tissue is the major organ in human body responsible for maintaining energy and metabolic homeostasis. As the main reservoir for lipid molecules, it was originally thought to function only as the site for energy storage. The majority of lipid in the body is stored in the form of triglyceride within adipose tissue. In times of energy shortage, triglyceride is hydrolyzed through enzyme digestion by hormone sensitive lipase into free fatty acids, in a process known as lipolysis. Free fatty acids are then released into circulation to supply energy to peripheral tissues. Conversely, in time of energy abundance, excessive fat in the blood stream is uptaken by adipose tissue with the help of lipoprotein lipase, and then utilized to synthesize triglyceride in a process known as lipogenesis.

In addition to its role as the energy reservoir, adipose tissue is now recognized as an endocrine organ that plays a vital role in a variety of metabolic processes, including satiety and insulin sensitivity. Malfunction of the adipose compartment is central to the pathophysiology of metabolic disorders such as obesity and type 2 diabetes. Mature adipocytes are able to secrete a number of hormones that are collectively known as adipokines, in particular leptin and adiponectin. Leptin, the product of *lep* gene, possesses profound effects on regulating satiety. Leptin binds its receptor in the hypothalamus to control feeding behavior and energy expenditure according to the fed versus starved state. Leptin secretion is positively associated with degree of adiposity. Severe insulin resistance is the well-known characteristic of mice lacking leptin (*ob/ob*) or its receptor (*db/db*). Leptin replacement in *ob/ob* mice and leptin treatment in normal rodents have both demonstrated the dramatic insulin-sensitizing action of leptin [1]. Adiponectin is another important hormone secreted by mature adipocytes. It normally functions to inhibit hepatic gluconeogenesis and enhance glucose uptake by skeletal muscle. The circulating level of

adiponectin is abnormally reduced in obesity and type 2 diabetes [2]. In murine models of altered insulin sensitivity, decreased expression of adiponectin also correlates with insulin resistance. Adiponectin improves insulin sensitivity by decreasing triglyceride content in muscle and liver in obese mice, through induction of genes involved in fatty-acid combustion or energy dissipation. Moreover, insulin resistance in lipoatrophic mice was completely reversed by the combinatorial treatment of adiponectin and leptin [3]. More recently, the Spiegelman group identified a new secretory factor, Meteorin-like (Metrnl), that is induced and released by white adipose tissue upon cold challenge and by skeletal muscle upon exercise. Increased circulating Metrnl stimulates browning by inducing eosinophil-dependent IL4/IL13 cytokines and M2 macrophage activation to promote energy expenditure and improved glucose tolerance [4].

There are two main types of adipose tissue in the body, white adipose (WAT) and brown adipose (BAT). WAT is composed of white adipocytes that are characterized by large unilocular lipid droplets where neutral lipid is stored. WAT is the primary type of adipose tissue found in adult humans and is distributed throughout the body in subcutaneous regions and surrounding visceral organs. On the other hand, BAT is primarily located discretely in subscapular, paravertebral, supraclavicular and periadrenal regions. Whereas WAT is mainly responsible for energy storage, BAT is the major organ for non-shivering thermogenesis which is the adaptive process to produce heat upon cold exposure. The primary constituents of BAT are brown adipocytes which are morphologically distinct from white adipocytes, containing multilocular lipid droplets and are rich in mitochondria which explains the brown coloring of BAT. Mitochondrial from BAT express a unique transmembrane protein, uncoupling protein 1 (UCP1), that plays a predominant role in heat generation through uncoupling the respiratory chain. UCP1 increases the permeability of the inner mitochondrial membrane thereby decreasing the proton

gradient established by oxidative phosphorylation from ATP production. This allows for energy to be dissipated in the form of heat. It was once thought that BAT is only present in neonatal stage to maintain body temperature upon birth or in adults only after prolonged exposure to cold environment. However, recent studies have proved the presence and importance of functional BAT in adult humans [5-7].

Recently, a third class of adipocytes has emerged from within certain white adipose depots, named ‘beige’ or ‘brite’ adipocytes. These are inducible brown adipocyte-like cells located in white adipose tissue that are formed in response to specific stimuli including cold exposure or beta-adrenergic agonists. The formation of these cells is called ‘browning’ or ‘beiging’. It involves not only the morphologic transformation to form multilocular lipid droplets, but also upregulation of a panel of thermogenic proteins including UCP1. Like white adipocytes, beige cells have extremely low basal expression of UCP1; however, they respond to hypothermia with high UCP1 expression and a robust energy expenditure program like brown adipocytes [8]. The formation of beige adipocytes is now considered a major contributor to the thermogenic capacity of animals in response to cold temperature.

A significant portion of adipose tissue is made up of lipid-storing cells named adipocytes. Mature adipocytes are surrounded by fibroblasts, fibroblast-like preadipocytes, immune cells, and endothelial cells. A current research focus is the crosstalk between adipocytes and local immune cells in the niche, and how this affects the maturation and functionality of adipocytes. Resident immune cells constitute the second largest cellular component in adipose tissue and therefore play an important role in the maintenance of adipose homeostasis. One of the most important hallmarks of obese adipose tissue is inflammation. Obesity-induced changes in the number and activity of immune cells can result in the activation of local and later systemic

inflammatory responses, which contribute to the pathogenesis of metabolic syndrome. One of the earliest examples is the observation that administration of the chief proinflammatory cytokine tumor necrosis factor α (TNFα) led to increased serum glucose level. Subsequently, studies found that TNFα concentration is elevated in obese animals and TNFα neutralizing antibody was able to significantly improve insulin sensitivity [9]. Increased adiposity is also correlated with induction of IL-6, another proinflammatory factor, which is associated with the development of diabetes [10]. Adipose tissue macrophages represent the largest subpopulation of adipose resident immune cells. In humans, they account for about 4% of all cells in lean visceral fat but increase to 12% under an obese state [11]. Obesity not only alters the total number of adipose macrophages, but also induces the switch between the two types of macrophages. In lean individuals alternatively activated (M2) macrophages are the predominant type. Anti-inflammatory cytokines such as IL-4 from eosinophils and IL-13 from T cells regulate M2-polarization. Obesity can decrease these cytokines while increasing the expression of proinflammatory factors such as CD11b, DC11c, TNFα and IL-6, ultimately leading to a phenotypic shift from anti-inflammatory M2 to proinflammatory M1 macrophages [12].

II. Adipogenesis

All adipocytes are derived from mesenchymal stem cells (MSCs), which are the descendants of the mesodermal germ layer during embryonic state. MSCs also give rise to myoblasts, osteocytes, and chondrocytes, in response to appropriate developmental stimuli. The formation of mature functional adipocytes occurs in a process called adipogenesis. Adipogenesis can be further divided into two phases: an early commitment step and a terminal differentiation step. Commitment is the conversion of mesenchymal stem cells to committed preadipocytes.

Preadipocytes are defined as cells that lost their pluripotency and are committed to the adipocyte lineage, with the capacity to become mature adipocytes exclusively. Terminal differentiation is the process where spindle-like preadipocytes differentiate into round mature lipid-laden adipocytes. Preadipocytes feature a growth-arrested state. They do not undergo terminal differentiation spontaneously in the absence of adipogenic signals. Only under certain environmental or nutritional stimuli, the complex adipogenic program within preadipocytes is turned on, driving the terminal differentiation process to form functional mature adipocytes. In this second stage, growth-arrested preadipocytes go through at least one round of mitotic division, termed 'clonal expansion', before they gain the typical characteristics of mature adipocytes.

Developmentally, individual fat depots are formed at distinctive stages. WAT compartment begins to develop in late gestational stage with substantial expansion postnatally in response to the surge in nutritional supply. More specifically, subcutaneous adipose develops prenatally whereas visceral (gonadal) adipose is mainly formed postnatally [13]. By contrast, most BAT primarily develops and expands embryonically, possibly due to the need to maintain body temperature after birth [14]. Whether adipogenesis occurs in adult humans remains controversial. However, adipose tissue undergoes active remodeling throughout adulthood and it has been estimated that approximately 10% white adipocytes in human adults undergo turnover each year [15]. It is also known that the number of white adipocytes remains constant throughout a person's lifetime. These studies suggest that adipogenesis does take place in adult WAT to maintain the balance between adipocyte death and formation of mature functional adipocytes. Moreover, adipogenesis in adulthood might also participate in the pathogenesis of metabolic diseases. Studies have shown that rodents fed with a high-fat diet initially present with enlarged adipocyte size, followed by an increase in adipocyte number as a result of adipogenesis [16, 17].

The past few decades has seen an increased interest and effort to identify the embryological origins of different types of adipocytes. We now know that adipocyte precursor cells reside in the stromal vascular fraction (SVF) of adipose tissue. The SVF fraction is a mixture of cells obtained after enzymatic digestion and centrifugation separation to dissociate mature adipocytes from other cell types in the fat pad. This mixture of cells contains MSCs, endothelial cells, immune cells, fibroblasts and preadipocytes. There is sufficient evidence to support that adipocyte precursors originate from pericytes localized in the microvasculature. The lineage tracing study by Tang et al. based on the master regulator of adipogenesis, PPARγ, traced the source of adipocyte progenitors to the vascular mural compartment [18]. When transplanted back into wild-type mice, these PPARγ^{+} cell precursors are able to differentiate into functional adipocytes. Further studies using flow cytometry have identified a set of markers (Lin^{-}, CD29^{+}, CD34^{+}, Sca-1^{+}, CD24^{+}, PDGFRβ^{+}) that is unique to precursors of the white adipocyte lineage [19].

Historically, it was thought that WAT and BAT adipocytes are derived from the same adipogenic progenitor cell. However, it has been now fully established that brown adipocytes, instead of sharing a common precursor with white adipocytes, developmentally originate from a common precursor cell with skeletal muscle cells. Timmons et al. discovered that the transcriptional profiling features between brown adipocytes and skeletal muscle cells are more similar than when BAT and WAT are compared [20]. Later on, lineage tracing studies in mice further demonstrated the common precursor of BAT and skeletal muscle cells that express the early muscle marker myogenic factor 5 (Myf5) and paired-box 7 (Pax7). It was found that the Myf5^{+} Pax7^{+} precursor cell is driven to differentiate into brown adipocytes by the actions of

many transcription factors including bone morphogenetic protein 7 (BMP7), PPARγ, C/EBPs, and PR domain-containing 16 (PRDM16) [21, 22].

Though beige adipocytes arise with in white adipose depots and their function resembles that of BAT, they neither share the common progenitor as white adipocytes, nor do they originate from the BAT progenitor cells. In fact, beige adipocytes exhibit a unique gene expression profile, compare to WAT and BAT [8]. Recently, Long et al. utilized UCP1-TRAP (translating ribosome affinity purification) mice to identify striking similarities and surprising differences between beige cells and BAT. They concluded that beige adipocytes have a smooth muscle-like origin [23]. Moreover, a lineage tracing study demonstrated that beige adipocytes arise from a population of stellate-like cells that express PDGFRα, Sca-1, and CD34 [24]. Another important question that has attracted a great deal of interest is to what extent beige adipocytes are derived from trans-differentiation of existing white adipocytes versus from de novo differentiation. Though remaining to be controversial, the current view is that in the inguinal WAT β-adrenergic stimulation predominantly triggers de novo differentiation of beige precursor cells to form mature beige adipocytes, whereas in the epididymal WAT bipotential precursor cells differentiate into white adipocytes with calorie excess and differentiate into beige adipocytes with β-adrenergic stimulation [25]. In favor of trans-differentiation, studies found that during cold exposure there is no overall increase in the total number of adipocytes within the fat depot, supporting the idea that existing white adipocytes are directly transformed into beige adipocytes [26]. Furthermore, cold-induced beige cells are found to undergo ‘whitening’ when exposed to warm temperature, suggesting a bi-directional conversion between mature white adipocytes and beige adipocytes in response to environmental stimuli [27]. Therefore, the thermogenic profile of beige adipocytes is reversible.

III. Adipose tissue and metabolic health

A sedentary lifestyle and increased calorie intake lead to a rapidly increasing rate of metabolic syndrome, a cluster of metabolic risk factors that predispose to high likelihood for future cardiovascular disease, type 2 diabetes, and cerebrovascular accidents. These risk factors tend to occur together more often than presenting alone. A joint statement from the World Health Organization, the American Heart Association, and the International Diabetes Federation set the criteria for metabolic syndrome as three or more of the following measurements: central obesity (Waist circumference of 40 inches or above in men, and 35 inches or above in women); triglyceride level of 150 milligrams per deciliter of blood (mg/dL) or greater; HDL cholesterol of less than 40 mg/dL in men or less than 50 mg/dL in women; systolic blood pressure of 130 millimeters of mercury (mm Hg) or greater, or diastolic blood pressure of 85 mm Hg or greater; fasting glucose of 100 mg/dL or greater[28]. As of the year 2004, metabolic syndrome is affecting as many as 47 million Americans and the prevalence is still increasing[29]. Among all the risk factors above, obesity and insulin resistance are considered to be central to the pathogenesis of metabolic syndrome.

Insulin resistance in white adipose tissue has been implicated to play a critical role in the development of metabolic disorders. It is also the fundamental cause of type 2 diabetes. Insulin resistance is defined as the state in which peripheral tissues including adipose, skeletal muscle, and liver exhibit decreased sensitivity to the hormone insulin. As a result, insulin can neither facilitate glucose uptake, metabolism, and storage by peripheral tissues nor can it inhibit hepatic glucose production and output. Typical clinical presentation of insulin resistance consists of compromised ability to tolerate glucose intake in a glucose challenge test. In response to the

impaired sensitivity to insulin, pancreatic β cells compensate by producing more insulin to meet the demand. However, such compensation ultimately fails to produce sufficient insulin and results in clinically evident hyperglycemia and type 2 diabetes.

Central obesity is seen in many insulin resistant individuals. This is largely due to the impaired insulin signaling pathway in insulin target tissues of obese humans, including functional defects in insulin binding to its receptor, receptor phosphorylation, tyrosine kinase activity, and phosphorylation of IRSs [1]. Recent GWAS studies have also identified a strong link between obesity and insulin resistance. SNPs within or near master regulator genes in adipose tissue such as PPARγ and KLF14 have been demonstrated to associate with insulin resistance and type 2 diabetes in humans [30-32]. Moreover, it is known that when on high-fat diet mature adipocytes undergo hypertrophy and that the size of enlarged human adipocytes is inversely correlated with normal adipose function and insulin sensitivity [33]. These insulin resistant hypertrophic adipocytes have lost the ability to regulate lipolysis, leading to increased release of free fatty acids (FFAs). High circulating FFAs further leads to increased gluconeogenesis in the liver as well as impaired glucose uptaking ability for skeletal muscle. In addition, insulin resistant adipocytes by secreting excessive proinflammatory cytokines further exacerbate the metabolic deficits in a systemic manner. For example, TNFα secretion is increased in obesity and can act as a feedback loop to inhibit lipogenesis and increase lipolysis in adipocytes, contributing to insulin resistance [34].

Lipodystrophy and obesity represent two extremes of the adiposity spectrum. On the other end of the spectrum, lipodystrophy, a complete lack of body fat, also predisposes to metabolic dysfunction. WAT is required to maintain the overall metabolic homeostasis by functioning as the major site for fatty acid deposition. For instance, mice that were genetically

modified to possess no WAT were highly insulin resistant with elevated serum levels of glucose, free fatty acids, triglycerides, and insulin [35, 36]. Further study found that surgical implantation of fat cells back into these congenital lipoatrophic mice could restore their normal metabolic homeostasis [37]. Another classical example is the fatty liver dystrophy (*fld*) mutant mice, which had an 80% reduction in both white and brown fat pads. These mice were glucose intolerant, insulin resistant, and prone to atherosclerosis [38].

Interestingly, studies have found that it is not the absolute amount of adipose tissue that determines metabolic health. It is the excess of abdominal or visceral adiposity as measured by waist-to-hip ratio rather than BMI that is now considered the strongest indicator for increased risk of metabolic syndrome [39]. Despite the histological similarities between subcutaneous WAT and visceral WAT, they possess distinct metabolic functions and therefore confer different metabolic risks. Indeed, expansion of visceral fat depots during the development of obesity is closely related to insulin resistance and other metabolic disorders, whereas subcutaneous adipose was proved to be metabolically protective [40]. This is attributable to the higher lipolytic activity and poorer adipogenic capacity of the visceral compartment [41]. Adipokine profiles also vary between different adipose depots: visceral fat secretes lower levels of adiponectin and higher amounts of pro-inflammatory cytokines than subcutaneous WAT [42].

BAT is an organ with a high energy expenditure rate mediated by its thermogenic activity. Because of this, BAT is considered to play a positive role in regulating metabolic health. It is inversely correlated with overall adiposity and type 2 diabetes in humans [5]. Ablation or dysfunction of BAT in rodents causes reduced whole-body energy expenditure and an obese phenotype. *Ucp1* deficient mice exhibited a 50% increase in its fat mass compared with wildtype control mice [43]. Due to its high energy demands, BAT is highly capable of clearing both

glucose and lipids from circulation, protecting against hyperglycemia and hyperlipidemia [44, 45]. BAT is more efficient at glucose disposal than many muscle groups per milligram of tissue [1]. Even though BAT is a small organ, it is an important contributor to the maintenance of metabolic homoeostasis and has become an attractive anti-obesity target. Beige adipocytes with their BAT-like functions have as well been demonstrated with protective effects on metabolic health. Adipocyte-specific *Prdm16* deficient mice displayed markedly deteriorated beige cell function following cold exposure or β3-adrenergic stimulation, while showing minimal effects on classical BAT. These animals developed obesity, insulin resistance, and hepatic steatosis when fed with a high-fat diet [46]. Although rodent data is convincing, the implications of beige adipocyte function in human metabolic health remains to be explored.

IV. Transcriptional regulation of adipogenesis

The process of adipogenesis not only involves marked morphological changes, but also relies on a complex and highly orchestrated gene expression program. Chronological expression of adipose specific genes is achieved by sequentially activation of a network of regulatory factors. To date, numerous factors have been identified to participate in positive or negative control of adipogenesis, among which the most established ones are involved in transcriptional regulation [47].

The nuclear receptor, peroxisome proliferator activated receptor γ (PPARγ), is the master transcriptional regulator of adipocyte differentiation and is proven to be absolutely necessary and sufficient for the development of adipocytes[48, 49]. To date, no factor has been found to be able to rescue the adipogenic defects in the absence of PPARγ. It is also the therapeutic target of the antidiabetic drugs, thiazolidinediones (TZDs). There are two protein isoforms of PPARγ due to

alternative promoters, PPARγ1 and PPARγ2. The major difference between these two is the presence of additional thirty amino acids at the N-terminal end of the PPARγ2 protein isoform. Both isoforms are most abundant in adipose tissue, but PPARγ2 is almost exclusively expressed in adipose tissue and plays a specific role in driving adipocyte differentiation.

PPARγ forms heterodimers with retinoid X receptor-α (RXRα) in the nucleus and binds directly on the promoter region of many characteristic genes of mature adipocyte. These genes regulate lipid metabolism (LPL, SCD1), glucose and lipid transport (GLUT4, CD36), lipid droplet formation (perilipin) and secrete factors that function systemically (adiponectin, adipsin) [50-52]. It is well known that the DNA binding domain of PPARγ confers recognition of the specific binding sequences in target gene promoters, known as peroxisome proliferator response elements (PPREs). PPREs contain imperfect direct repeats of a consensus sequence separated by one nucleotide: AGGTCANAGGTCA (DR-1 sequence).

The importance of PPARγ in adipose development in vivo was demonstrated in multiple mouse models. Although PPARγ global knockout mice are embryonically lethal [53], heterozygous PPARγ deficient mice had reduced body weight and fat mass compared to control mice when fed a high-fat diet[54]. Studies also found that mice chimeric for wild type and PPARγ null cells show little or no contribution of null cells to forming adipose tissue [55]. In a different model, mice that are PPARγ2 deficient throughout the body and PPARγ1 deficient in WAT displayed a severe lipodystrophic phenotype and metabolic abnormalities [56]. In addition, two later models of fat-specific PPARγ knockout mice (aP2-Cre) both exhibited reduced WAT and BAT mass, as well as excessive ectopic fat deposition in the liver [57, 58]. Furthermore, humans with dominant-negative mutations of PPARγ also display abnormal body fat distribution and insulin resistance, suggesting an essential role of PPARγ in human adipose development [59].

The CCAAT/enhancer-binding proteins (C/EBPs) are a family of proteins that are fundamentally important for the regulation of adipogenesis. C/EBPδ and β in response to hormonal stimulation are upregulated and activated at early stage of adipogenesis. They further induce the expression of PPARγ and C/EBPα. In the later stage of adipocyte differentiation, PPARγ and C/EBPα work coordinately to drive adipocyte gene expression and terminal differentiation. Genome-wide ChIP analysis has identified a remarkable degree of colocalization of C/EBPα and PPARγ [60]. C/EBPα is most abundant in mature adipocytes and is important in their function. Studies have shown that inducible whole-body deletion of C/EBPα in adult mice led to substantial reduction in their WAT mass [61]. Undoubtedly, C/EBPα is also crucial for adipose development. Global C/EBPα knockout mice were not viable because of liver defects and failure to accumulate lipid in WAT and BAT [62]. They demonstrated a complete lack of adipose tissue in all WAT depots, which was accompanied by notable metabolic abnormalities including dyslipidemia and hepatosteatosis [63].

Wnt signaling has emerged as a very potent inhibitory pathway of adipogenesis. Wnts are a family of secretory proteins that act in an autocrine or paracrine manner on cell surface receptors. It has been reported that Wnt signaling can regulate adipogenesis through both canonical (β-catenin) and non-canonical pathways [64]. Activation of the Wnt pathway in 3T3-L1 preadipocytes prevented adipogenesis in vitro[65]. Reciprocal repression might exist between Wnt signaling and PPARγ or E/CBPα [66], and repression of Wnt must occur prior to the initiation of adipocyte differentiation [67]. The two Wnt proteins that have been most extensively studied for their role in regulating adipogenesis are Wnt10b and Wnt5a, which inhibit differentiation through canonical and non-canonical pathways respectively [68, 69].

Many other adipogenic regulators have been identified that control adipocyte differentiation on the transcriptional level. The Kruppel-like (KLF) family comprises of a large family of zinc-finger transcription factors that act either as activators or repressors of adipogenesis [70-72]. Cell cycle proteins are also involved in the very early phase of adipocyte differentiation, especially during the mitotic clonal expansion upon hormonal induction. Cyclin D3, cyclin-dependent kinases (Cdk4, Cdk6) as well as E2F factors were all shown to influence adipogenesis [73-75]. Early B-cell factor 1 (Ebf1), which has established roles in B-lymphocyte development, was found to promote differentiation by activating PPARγ and C/EBPα transcription [76]. GATA factors (GATA2 and GATA3) have abundant expression in preadipocytes that progressively decrease during adipogenesis. They inhibit terminal differentiation partly through repressing transcriptional activity of PPARγ [77]. More repressors include interferon-regulatory factors (IRF3 and IRF4), forkhead box proteins (FOXO1 and FOXC2) and preadipocyte factor 1 (Pref-1) [78]. Furthermore, several extracellular factors have been implicated to affect adipocyte differentiation, including bone morphogenesis proteins (BMP2 and BMP4 in WAT, BMP7 in BAT), transforming growth factor β (TGFβ), fibroblast growth factors (FGF1, FGF2), insulin, extracellular matrix proteins, etc. [79-83].

In recent years, multiple transcriptional cofactors have been found to interact with key transcription factors in order to fine-tune the adipogenic program and/or specify white *versus* brown adipocyte fate. Some of these are general cofactors that are able to interact with various nuclear receptors, including coactivators (CBP/p300, SRC family) and corepressors (SMRT, NcoR) [84-86]. Others selectively interact with adipogenic transcription factors, mainly PPARγ. The most well studied ones are PPARγ coactivator-1α (Pgc-1α) and PR domain-containing 16 (Prdm16), which are both coactivators of PPARγ. Cold-inducible Pgc-1α coactivates PPARγ to

drive the expression of thermogenic genes [87], whereas Prdm16 functions to promote the development of brown adipocyte from $Myf5^+$ progenitor cells [21]. More recently, transducin-like enhancer of split 3 (TLE3) has emerged as a dual-function protein that coactivates PPARγ while concurrently repressing Wnt signaling [88]. Furthermore, genome-wide analysis has revealed dynamic changes in chromatin structure during adipocyte differentiation [89]. Specific histone acetyltransferases, deacetylases, and methyltransferases have been implicated in the regulation of adipogenesis [90, 91].

V. Posttranscriptional regulation of adipogenesis

Alongside the discovery of an increasing number of transcriptional regulators of adipogenesis, several other mechanisms have also emerged. Alternative splicing is an effective mechanism to spatiotemporally expand the eukaryotic proteome, which contributes to the modulation of cell differentiation, specification and organogenesis [92-94]. Adipogenesis-related alternative splicing events have shown potential influence on adipose tissue development and serve as an important mechanism of posttranscriptional regulation of adipocyte differentiation. Multiple studies identified several adipocyte regulatory genes with alternatively spliced isoforms that exert different or even opposing effects on adipogenesis. One example is the nuclear receptor corepressor NCoR, which is documented to encode various splicing variants that differ in their receptor interaction domains. Inclusion of exon 37b in the mature transcripts give rise to the NCoRω variants that mainly distribute in brain, testes and WAT progenitors, whereas exclusion of exon 37b generates the NCoRδ variant that is predominantly expressed in heart, skeletal muscle, and mature WAT [95]. A ω-to-δ variant switch by alternative splicing has been found during the course of adipocyte differentiation. Increased expression of the δ isoform has

been shown to enhance the development and function of white adipocytes[96]. Another example is Pref-1, which encodes the constitutive full-length isoform Pref-1A that dramatically inhibits adipogenesis. Two other alternative-splicing products, Pref-1C and Pref-1D, have no effect because they do not generate the biologically active large soluble fragment [97]. Insulin receptor (IR) mRNA is also alternatively spliced, producing two isoforms, IR_A, which lacks exon 11, and IR_B, which contains exon 11. IR_A has higher affinity to insulin and exhibits faster internalization rate compared to IR_B [98]. During brown adipocyte differentiation, there is not only an increase in total IR amount but also a shift from the IR_A to IR_B isoform [99].

More recent studies focused on how splicing factors affect adipogenesis by modulating alternative splicing events. Src-associated in mitosis of 68 kDa (Sam68) as a known RNA-binding protein and splicing factor was found to inhibit adipogenesis via controlling the alternative splicing profiles of mTOR [100] and ribosomal S6 kinase (S6K) [101]. *Sam68* whole-body knockout mice exhibited resistance to diet-induced obesity, increased energy consumption and thermogenesis [102]. Another splicing factor, serine/arginine-rich splicing factor 10 (SRSF10), dictates the alternative splicing of Lipin1. SRSF10 binds to exon 8 of Lipin1 pre-mRNA resulting in the exclusion of exon 7, which was required for the early differentiation of preadipocytes. On the other hand, the retention of exon 7 is crucial to lipid accumulation in mature adipocytes [103]. RNA-binding motif protein 4a (RBM4a) is an example of splicing regulation in BAT. RBM4a protein expression is upregulated during brown adipocyte differentiation, which further mediates the splicing profiles of several important adipogenic transcripts including IR, PPARγ, and Pref-1. As a result, RBM4a plays a positive role in driving brown adipose development, which was demonstrated by the reduced interscapular BAT mass in *RBM4a* global knockout mice [104].

A number of microRNAs have been identified to positively or negatively control specific adipogenic gene expression. MiR-143 is one of the most extensively studied microRNAs associated with adipogenesis. It was found to be induced during both human and murine adipocyte differentiation [105, 106]. *In vitro*, ectopic overexpression of miR-143 in 3T3-L1 preadipocytes can accelerate adipogenesis and enhance lipid accumulation [106], whereas inhibition of miR-143 resulted in decreased adipogenic potential in human preadipocytes[105]. However, *in vivo* studies showed discrepancy in the regulated expression of miR-143 in obese animals. While miR-143 was shown to be upregulated in mesenteric adipose tissue of high-fat diet-induced obese mice [107], it was found to be downregulated in epididymal WAT of ob/ob mice [106]. The proposed target of miR-143 is extracellular-signal-regulated kinase 5 (ERK5), which has no known function in adipogenesis [105]. The miR-27 family has been implicated as negative regulators of adipogenesis and are downregulated during differentiation [108]. Both miR-27a and miR-27b can repress adipogenesis *in vitro* by directly targeting PPARγ and decreasing its expression [109, 110]. Additional proadipogenic microRNAs include miR-103, miR-21, and the miR-30 family; more antiadipogenic microRNAs include let-7, miR-130, and miR-488 [111].

Long noncoding RNAs (lncRNAs) are a novel group of players in the regulation of various biological processes. Recent publications have revealed the influence of lncRNAs on adipogenesis. One study profiled the transcriptome of primary white and brown adipocytes, preadipocytes, and cultured adipocytes, from which they identified 175 lncRNAs that are specifically regulated in adipogenesis [112]. Many of them are direct targets of the master regulators of adipogenesis, PPARγ or C/EBPα. To date, several lncRNAs have been investigated and demonstrated a role in regulating either white or brown adipogenesis. The paraspeckle

component *NEAT1* has been shown to potentiate the phosphorylation and activation of splicing factor SRp40, thereby facilitating PPARγ2 expression and promoting differentiation [113]. *Blinc1* was reported to promote brown adipocyte differentiation with both gain-of-function and loss-of-function studies *in vitro*. Mechanistically *Blinc1* forms ribonucleoprotein complex with the transcription factor EBF2, by which it induces the expression of the thermogenic program genes [114].

Overall, adipogenesis or adipose tissue development constitutes a complex morphological and functional conversion that requires tightly regulated control at different levels. However, in contrast with the well-established transcriptional cascade of adipogenesis, regulation of adipogenic gene expression on the post-transcriptional level is still largely unexplored.

VI. Paraspeckle

Paraspeckles are subnuclear bodies located in the interchromatin space. These RNA–protein complexes are composed of the long noncoding RNA nuclear paraspeckle assembly transport 1 (*Neat1*) and three core protein components from the Drosophila behavior/human splicing (DBHS) family: paraspeckle protein 1 (Pspc1), non-POU domain-containing octamer-binding protein (Nono), and splicing factor proline- and glutamine-rich (Sfpq) [115]. Prior to the identification of paraspeckles, Nono and Sfpq as confirmed RNA-binding proteins were implicated in various aspects of RNA production and processing [116-120]. However, comparatively little is known about the cellular functions of Pspc1, although it has been suggested to be important for spermatogenesis [121, 122]. Whether and how Pspc1 may play a role in RNA processing is as well unknown.

In this thesis, we describe Pspc1 as an adipogenic factor, which we identified through a phenotype-based high-throughput cDNA screen [88, 123]. We further show that Pspc1 is a *bona fide* RNA binding-protein that shuttles from the nucleus to the cytoplasm during adipocyte differentiation. Pspc1 directly interacts with adipose-specific RNAs and promotes their export, ultimately leading to increased protein expression. Loss of Pspc1 compromises adipogenesis and adipocyte gene expression both *in vitro* and *in vivo,* and affects the development of diet-induced obesity and insulin resistance. These studies shed light on the importance of Pspc1-dependent RNA maturation in adipogenesis and expand our knowledge of post-transcriptional processes contributing to adipocyte development and adipose function.

References

1. Kahn, B.B. and J.S. Flier, *Obesity and insulin resistance.* J Clin Invest, 2000. **106**(4): p. 473-81.
2. Weyer, C., et al., *Hypoadiponectinemia in obesity and type 2 diabetes: close association with insulin resistance and hyperinsulinemia.* J Clin Endocrinol Metab, 2001. **86**(5): p. 1930-5.
3. Yamauchi, T., et al., *The fat-derived hormone adiponectin reverses insulin resistance associated with both lipoatrophy and obesity.* Nat Med, 2001. **7**(8): p. 941-6.
4. Rao, R.R., et al., *Meteorin-like is a hormone that regulates immune-adipose interactions to increase beige fat thermogenesis.* Cell, 2014. **157**(6): p. 1279-91.
5. Cypess, A.M., et al., *Identification and importance of brown adipose tissue in adult humans.* N Engl J Med, 2009. **360**(15): p. 1509-17.
6. van Marken Lichtenbelt, W.D., et al., *Cold-activated brown adipose tissue in healthy men.* N Engl J Med, 2009. **360**(15): p. 1500-8.
7. Virtanen, K.A., et al., *Functional brown adipose tissue in healthy adults.* N Engl J Med, 2009. **360**(15): p. 1518-25.
8. Wu, J., et al., *Beige adipocytes are a distinct type of thermogenic fat cell in mouse and human.* Cell, 2012. **150**(2): p. 366-76.
9. Mraz, M. and M. Haluzik, *The role of adipose tissue immune cells in obesity and low-grade inflammation.* J Endocrinol, 2014. **222**(3): p. R113-27.
10. Dandona, P., A. Aljada, and A. Bandyopadhyay, *Inflammation: the link between insulin resistance, obesity and diabetes.* Trends Immunol, 2004. **25**(1): p. 4-7.

11. Harman-Boehm, I., et al., *Macrophage infiltration into omental versus subcutaneous fat across different populations: effect of regional adiposity and the comorbidities of obesity.* J Clin Endocrinol Metab, 2007. **92**(6): p. 2240-7.

12. Lumeng, C.N., et al., *Increased inflammatory properties of adipose tissue macrophages recruited during diet-induced obesity.* Diabetes, 2007. **56**(1): p. 16-23.

13. Wang, Q.A., et al., *Tracking adipogenesis during white adipose tissue development, expansion and regeneration.* Nat Med, 2013. **19**(10): p. 1338-44.

14. Frontini, A. and S. Cinti, *Distribution and development of brown adipocytes in the murine and human adipose organ.* Cell Metab, 2010. **11**(4): p. 253-6.

15. Spalding, K.L., et al., *Dynamics of fat cell turnover in humans.* Nature, 2008. **453**(7196): p. 783-7.

16. Lemonnier, D., *Effect of age, sex, and sites on the cellularity of the adipose tissue in mice and rats rendered obese by a high-fat diet.* J Clin Invest, 1972. **51**(11): p. 2907-15.

17. Faust, I.M., et al., *Diet-induced adipocyte number increase in adult rats: a new model of obesity.* Am J Physiol, 1978. **235**(3): p. E279-86.

18. Tang, W., et al., *White fat progenitor cells reside in the adipose vasculature.* Science, 2008. **322**(5901): p. 583-6.

19. Rodeheffer, M.S., K. Birsoy, and J.M. Friedman, *Identification of white adipocyte progenitor cells in vivo.* Cell, 2008. **135**(2): p. 240-9.

20. Timmons, J.A., et al., *Myogenic gene expression signature establishes that brown and white adipocytes originate from distinct cell lineages.* Proc Natl Acad Sci U S A, 2007. **104**(11): p. 4401-6.

21. Seale, P., et al., *PRDM16 controls a brown fat/skeletal muscle switch.* Nature, 2008. **454**(7207): p. 961-7.

22. Tseng, Y.H., et al., *New role of bone morphogenetic protein 7 in brown adipogenesis and energy expenditure.* Nature, 2008. **454**(7207): p. 1000-4.

23. Long, J.Z., et al., *A smooth muscle-like origin for beige adipocytes.* Cell Metab, 2014. **19**(5): p. 810-20.

24. Lee, Y.H., et al., *In vivo identification of bipotential adipocyte progenitors recruited by beta3-adrenoceptor activation and high-fat feeding.* Cell Metab, 2012. **15**(4): p. 480-91.

25. Harms, M. and P. Seale, *Brown and beige fat: development, function and therapeutic potential.* Nat Med, 2013. **19**(10): p. 1252-63.

26. Vitali, A., et al., *The adipose organ of obesity-prone C57BL/6J mice is composed of mixed white and brown adipocytes.* J Lipid Res, 2012. **53**(4): p. 619-29.

27. Rosenwald, M., et al., *Bi-directional interconversion of brite and white adipocytes.* Nat Cell Biol, 2013. **15**(6): p. 659-67.

28. Alberti, K.G., et al., *Harmonizing the metabolic syndrome: a joint interim statement of the International Diabetes Federation Task Force on Epidemiology and Prevention; National Heart, Lung, and Blood Institute; American Heart Association; World Heart Federation; International Atherosclerosis Society; and International Association for the Study of Obesity.* Circulation, 2009. **120**(16): p. 1640-5.

29. Steinbaum, S.R., *The metabolic syndrome: an emerging health epidemic in women.* Prog Cardiovasc Dis, 2004. **46**(4): p. 321-36.

30. Deeb, S.S., et al., *A Pro12Ala substitution in PPARgamma2 associated with decreased receptor activity, lower body mass index and improved insulin sensitivity.* Nat Genet, 1998. **20**(3): p. 284-7.

31. Altshuler, D., et al., *The common PPARgamma Pro12Ala polymorphism is associated with decreased risk of type 2 diabetes.* Nat Genet, 2000. **26**(1): p. 76-80.

32. Voight, B.F., et al., *Twelve type 2 diabetes susceptibility loci identified through large-scale association analysis.* Nat Genet, 2010. **42**(7): p. 579-89.

33. Cornier, M.A., et al., *The metabolic syndrome.* Endocr Rev, 2008. **29**(7): p. 777-822.

34. Peraldi, P. and B. Spiegelman, *TNF-alpha and insulin resistance: summary and future prospects.* Mol Cell Biochem, 1998. **182**(1-2): p. 169-75.

35. Sovik, O., et al., *Studies of insulin resistance in congenital generalized lipodystrophy.* Acta Paediatr Suppl, 1996. **413**: p. 29-37.

36. Moitra, J., et al., *Life without white fat: a transgenic mouse.* Genes Dev, 1998. **12**(20): p. 3168-81.

37. Gavrilova, O., et al., *Surgical implantation of adipose tissue reverses diabetes in lipoatrophic mice.* J Clin Invest, 2000. **105**(3): p. 271-8.

38. Reue, K., et al., *Adipose tissue deficiency, glucose intolerance, and increased atherosclerosis result from mutation in the mouse fatty liver dystrophy (fld) gene.* J Lipid Res, 2000. **41**(7): p. 1067-76.

39. Yusuf, S., et al., *Obesity and the risk of myocardial infarction in 27,000 participants from 52 countries: a case-control study.* Lancet, 2005. **366**(9497): p. 1640-9.

40. Hamdy, O., S. Porramatikul, and E. Al-Ozairi, *Metabolic obesity: the paradox between visceral and subcutaneous fat.* Curr Diabetes Rev, 2006. **2**(4): p. 367-73.

41. Tchkonia, T., et al., *Mechanisms and metabolic implications of regional differences among fat depots.* Cell Metab, 2013. **17**(5): p. 644-56.

42. Hilton, C., F. Karpe, and K.E. Pinnick, *Role of developmental transcription factors in white, brown and beige adipose tissues.* Biochim Biophys Acta, 2015. **1851**(5): p. 686-96.

43. Feldmann, H.M., et al., *UCP1 ablation induces obesity and abolishes diet-induced thermogenesis in mice exempt from thermal stress by living at thermoneutrality.* Cell Metab, 2009. **9**(2): p. 203-9.

44. Bartelt, A., et al., *Brown adipose tissue activity controls triglyceride clearance.* Nat Med, 2011. **17**(2): p. 200-5.

45. Arbeeny, C.M., et al., *Metabolic alterations associated with the antidiabetic effect of beta 3-adrenergic receptor agonists in obese mice.* Am J Physiol, 1995. **268**(4 Pt 1): p. E678-84.

46. Cohen, P., et al., *Ablation of PRDM16 and beige adipose causes metabolic dysfunction and a subcutaneous to visceral fat switch.* Cell, 2014. **156**(1-2): p. 304-16.

47. Rosen, E.D. and O.A. MacDougald, *Adipocyte differentiation from the inside out.* Nat Rev Mol Cell Biol, 2006. **7**(12): p. 885-96.

48. Tontonoz, P., et al., *Mppar-Gamma-2 - Tissue-Specific Regulator of an Adipocyte Enhancer.* Genes & Development, 1994. **8**(10): p. 1224-1234.

49. Tontonoz, P., E.D. Hu, and B.M. Spiegelman, *Stimulation of Adipogenesis in Fibroblasts by Ppar-Gamma-2, a Lipid-Activated Transcription Factor.* Cell, 1994. **79**(7): p. 1147-1156.

50. Tontonoz, P., et al., *PPAR gamma 2 regulates adipose expression of the phosphoenolpyruvate carboxykinase gene.* Mol Cell Biol, 1995. **15**(1): p. 351-7.

51. Schoonjans, K., et al., *PPARalpha and PPARgamma activators direct a distinct tissue-specific transcriptional response via a PPRE in the lipoprotein lipase gene.* EMBO J, 1996. **15**(19): p. 5336-48.

52. Dalen, K.T., et al., *Adipose tissue expression of the lipid droplet-associating proteins S3-12 and perilipin is controlled by peroxisome proliferator-activated receptor-gamma.* Diabetes, 2004. **53**(5): p. 1243-52.

53. Barak, Y., et al., *PPAR gamma is required for placental, cardiac, and adipose tissue development.* Mol Cell, 1999. **4**(4): p. 585-95.

54. Kubota, N., et al., *PPAR gamma mediates high-fat diet-induced adipocyte hypertrophy and insulin resistance.* Mol Cell, 1999. **4**(4): p. 597-609.

55. Rosen, E.D., et al., *PPAR gamma is required for the differentiation of adipose tissue in vivo and in vitro.* Mol Cell, 1999. **4**(4): p. 611-7.

56. Koutnikova, H., et al., *Compensation by the muscle limits the metabolic consequences of lipodystrophy in PPAR gamma hypomorphic mice.* Proc Natl Acad Sci U S A, 2003. **100**(24): p. 14457-62.

57. He, W., et al., *Adipose-specific peroxisome proliferator-activated receptor gamma knockout causes insulin resistance in fat and liver but not in muscle.* Proc Natl Acad Sci U S A, 2003. **100**(26): p. 15712-7.

58. Jones, J.R., et al., *Deletion of PPARgamma in adipose tissues of mice protects against high fat diet-induced obesity and insulin resistance.* Proc Natl Acad Sci U S A, 2005. **102**(17): p. 6207-12.

59. Agostini, M., et al., *Non-DNA binding, dominant-negative, human PPARgamma mutations cause lipodystrophic insulin resistance.* Cell Metab, 2006. **4**(4): p. 303-11.

60. Lefterova, M.I., et al., *PPARgamma and C/EBP factors orchestrate adipocyte biology via adjacent binding on a genome-wide scale.* Genes Dev, 2008. **22**(21): p. 2941-52.

61. Yang, J., et al., *Metabolic response of mice to a postnatal ablation of CCAAT/enhancer-binding protein alpha.* J Biol Chem, 2005. **280**(46): p. 38689-99.

62. Wang, N.D., et al., *Impaired energy homeostasis in C/EBP alpha knockout mice.* Science, 1995. **269**(5227): p. 1108-12.

63. Linhart, H.G., et al., *C/EBPalpha is required for differentiation of white, but not brown, adipose tissue.* Proc Natl Acad Sci U S A, 2001. **98**(22): p. 12532-7.

64. Kennell, J.A. and O.A. MacDougald, *Wnt signaling inhibits adipogenesis through beta-catenin-dependent and -independent mechanisms.* J Biol Chem, 2005. **280**(25): p. 24004-10.

65. Ross, S.E., et al., *Inhibition of adipogenesis by Wnt signaling.* Science, 2000. **289**(5481): p. 950-3.

66. Moldes, M., et al., *Peroxisome-proliferator-activated receptor gamma suppresses Wnt/beta-catenin signalling during adipogenesis.* Biochem J, 2003. **376**(Pt 3): p. 607-13.

67. Prestwich, T.C. and O.A. Macdougald, *Wnt/beta-catenin signaling in adipogenesis and metabolism.* Curr Opin Cell Biol, 2007. **19**(6): p. 612-7.

68. Longo, K.A., et al., *Wnt10b inhibits development of white and brown adipose tissues.* J Biol Chem, 2004. **279**(34): p. 35503-9.

69. Takada, I., et al., *A histone lysine methyltransferase activated by non-canonical Wnt signalling suppresses PPAR-gamma transactivation.* Nat Cell Biol, 2007. **9**(11): p. 1273-85.

70. Birsoy, K., Z. Chen, and J. Friedman, *Transcriptional regulation of adipogenesis by KLF4.* Cell Metab, 2008. **7**(4): p. 339-47.

71. Oishi, Y., et al., *Kruppel-like transcription factor KLF5 is a key regulator of adipocyte differentiation.* Cell Metabolism, 2005. **1**(1): p. 27-39.

72. Sue, N., et al., *Targeted disruption of the basic Kruppel-like factor gene (Klf3) reveals a role in adipogenesis.* Mol Cell Biol, 2008. **28**(12): p. 3967-78.

73. Sarruf, D.A., et al., *Cyclin D3 promotes adipogenesis through activation of peroxisome proliferator-activated receptor gamma.* Mol Cell Biol, 2005. **25**(22): p. 9985-95.

74. Abella, A., et al., *Cdk4 promotes adipogenesis through PPARgamma activation.* Cell Metab, 2005. **2**(4): p. 239-49.

75. Fajas, L., et al., *E2Fs regulate adipocyte differentiation.* Dev Cell, 2002. **3**(1): p. 39-49.

76. Jimenez, M.A., et al., *Critical role for Ebf1 and Ebf2 in the adipogenic transcriptional cascade.* Mol Cell Biol, 2007. **27**(2): p. 743-57.

77. Tong, Q., et al., *Function of GATA transcription factors in preadipocyte-adipocyte transition.* Science, 2000. **290**(5489): p. 134-138.

78. Smas, C.M. and H.S. Sul, *Pref-1, a Protein Containing Egf-Like Repeats, Inhibits Adipocyte Differentiation.* Cell, 1993. **73**(4): p. 725-734.

79. Huang, H., et al., *BMP signaling pathway is required for commitment of C3H10T1/2 pluripotent stem cells to the adipocyte lineage.* Proc Natl Acad Sci U S A, 2009. **106**(31): p. 12670-5.

80. Zamani, N. and C.W. Brown, *Emerging roles for the transforming growth factor-{beta} superfamily in regulating adiposity and energy expenditure.* Endocr Rev, 2011. **32**(3): p. 387-403.

81. Widberg, C.H., et al., *Fibroblast growth factor receptor 1 is a key regulator of early adipogenic events in human preadipocytes.* Am J Physiol Endocrinol Metab, 2009. **296**(1): p. E121-31.

82. Xiao, L., et al., *Disruption of the Fgf2 gene activates the adipogenic and suppresses the osteogenic program in mesenchymal marrow stromal stem cells.* Bone, 2010. **47**(2): p. 360-70.

83. Divoux, A. and K. Clement, *Architecture and the extracellular matrix: the still unappreciated components of the adipose tissue.* Obes Rev, 2011. **12**(5): p. e494-503.

84. Gelman, L., et al., *p300 interacts with the N- and C-terminal part of PPARgamma2 in a ligand-independent and -dependent manner, respectively.* J Biol Chem, 1999. **274**(12): p. 7681-8.

85. Leo, C. and J.D. Chen, *The SRC family of nuclear receptor coactivators.* Gene, 2000. **245**(1): p. 1-11.

86. Yu, C., et al., *The nuclear receptor corepressors NCoR and SMRT decrease peroxisome proliferator-activated receptor gamma transcriptional activity and repress 3T3-L1 adipogenesis.* J Biol Chem, 2005. **280**(14): p. 13600-5.

87. Puigserver, P., et al., *A cold-inducible coactivator of nuclear receptors linked to adaptive thermogenesis.* Cell, 1998. **92**(6): p. 829-39.

88. Villanueva, C.J., et al., *TLE3 is a dual-function transcriptional coregulator of adipogenesis.* Cell Metab, 2011. **13**(4): p. 413-27.

89. Steger, D.J. and M.A. Lazar, *Adipogenic hotspots: where the action is.* EMBO J, 2011. **30**(8): p. 1418-9.

90. Guan, H.P., et al., *Corepressors selectively control the transcriptional activity of PPARgamma in adipocytes.* Genes Dev, 2005. **19**(4): p. 453-61.

91. Cho, Y.W., et al., *Histone methylation regulator PTIP is required for PPARgamma and C/EBPalpha expression and adipogenesis.* Cell Metab, 2009. **10**(1): p. 27-39.

92. Pimentel, H., et al., *A Dynamic Alternative Splicing Program Regulates Gene Expression In A Differentiation Stage-Specific Manner During Terminal Erythropoiesis.* Blood, 2013. **122**(21).

93. Mazin, P., et al., *Widespread splicing changes in human brain development and aging.* Molecular Systems Biology, 2013. **9**.

94. Revil, T., et al., *Alternative splicing is frequent during early embryonic development in mouse.* Bmc Genomics, 2010. **11**.

95. Malartre, M., S. Short, and C. Sharpe, *Alternative splicing generates multiple SMRT transcripts encoding conserved repressor domains linked to variable transcription factor interaction domains.* Nucleic Acids Res, 2004. **32**(15): p. 4676-86.

96. Snyder, C.A., et al., *Regulation of corepressor alternative mRNA splicing by hormonal and metabolic signaling.* Mol Cell Endocrinol, 2015. **413**: p. 228-35.

97. Mei, B., et al., *Only the large soluble form of preadipocyte factor-1 (Pref-1), but not the small soluble and membrane forms, inhibits adipocyte differentiation: role of alternative splicing.* Biochem J, 2002. **364**(Pt 1): p. 137-44.

98. Mosthaf, L., et al., *Functionally distinct insulin receptors generated by tissue-specific alternative splicing.* EMBO J, 1990. **9**(8): p. 2409-13.

99. Entingh, A.J., C.M. Taniguchi, and C.R. Kahn, *Bi-directional regulation of brown fat adipogenesis by the insulin receptor.* J Biol Chem, 2003. **278**(35): p. 33377-83.

100. Huot, M.E., et al., *The Sam68 STAR RNA-binding protein regulates mTOR alternative splicing during adipogenesis.* Mol Cell, 2012. **46**(2): p. 187-99.

101. Song, J. and S. Richard, *Sam68 Regulates S6K1 Alternative Splicing during Adipogenesis.* Mol Cell Biol, 2015. **35**(11): p. 1926-39.

102. Zhou, J., et al., *Inhibition of Sam68 triggers adipose tissue browning.* J Endocrinol, 2015. **225**(3): p. 181-9.

103. Li, H., et al., *SRSF10 regulates alternative splicing and is required for adipocyte differentiation.* Mol Cell Biol, 2014. **34**(12): p. 2198-207.

104. Lin, J.C., W.Y. Tarn, and W.K. Hsieh, *Emerging role for RNA binding motif protein 4 in the development of brown adipocytes.* Biochimica Et Biophysica Acta-Molecular Cell Research, 2014. **1843**(4): p. 769-779.

105. Esau, C., et al., *MicroRNA-143 regulates adipocyte differentiation.* Journal of Biological Chemistry, 2004. **279**(50): p. 52361-52365.

106. Xie, H.M., B. Lim, and H.F. Lodish, *MicroRNAs Induced During Adipogenesis that Accelerate Fat Cell Development Are Downregulated in Obesity.* Diabetes, 2009. **58**(5): p. 1050-1057.

107. Takanabe, R., et al., *Up-regulated expression of microRNA-143 in association with obesity in adipose tissue of mice fed high-fat diet.* Biochemical and Biophysical Research Communications, 2008. **376**(4): p. 728-732.

108. Lin, Q., et al., *A role of miR-27 in the regulation of adipogenesis.* FEBS J, 2009. **276**(8): p. 2348-58.

109. Kim, S.Y., et al., *miR-27a is a negative regulator of adipocyte differentiation via suppressing PPARgamma expression.* Biochem Biophys Res Commun, 2010. **392**(3): p. 323-8.

110. Karbiener, M., et al., *microRNA miR-27b impairs human adipocyte differentiation and targets PPARgamma.* Biochem Biophys Res Commun, 2009. **390**(2): p. 247-51.

111. Peng, Y., et al., *MicroRNAs: emerging roles in adipogenesis and obesity.* Cell Signal, 2014. **26**(9): p. 1888-96.

112. Sun, L., et al., *Long noncoding RNAs regulate adipogenesis.* Proc Natl Acad Sci U S A, 2013. **110**(9): p. 3387-92.

113. Cooper, D.R., et al., *Long Non-Coding RNA NEAT1 Associates with SRp40 to Temporally Regulate PPAR gamma 2 Splicing during Adipogenesis in 3T3-L1 Cells.* Genes, 2014. **5**(4): p. 1050-1063.

114. Zhao, X.Y., et al., *A long noncoding RNA transcriptional regulatory circuit drives thermogenic adipocyte differentiation.* Mol Cell, 2014. **55**(3): p. 372-82.

115. Fox, A.H., et al., *Paraspeckles: A novel nuclear domain.* Current Biology, 2002. **12**(1): p. 13-25.

116. Patton, J.G., et al., *Cloning and characterization of PSF, a novel pre-mRNA splicing factor.* Genes Dev, 1993. **7**(3): p. 393-406.

117. Yang, Y.S., et al., *NonO, a non-POU-domain-containing, octamer-binding protein, is the mammalian homolog of Drosophila nonAdiss.* Mol Cell Biol, 1993. **13**(9): p. 5593-603.

118. Peng, R., et al., *PSF and p54nrb bind a conserved stem in U5 snRNA.* RNA, 2002. **8**(10): p. 1334-47.

119. Kaneko, S., et al., *The multifunctional protein p54nrb/PSF recruits the exonuclease XRN2 to facilitate pre-mRNA 3' processing and transcription termination.* Genes Dev, 2007. **21**(14): p. 1779-89.

120. Kameoka, S., P. Duque, and M.M. Konarska, *p54(nrb) associates with the 5' splice site within large transcription/splicing complexes.* EMBO J, 2004. **23**(8): p. 1782-91.

121. Kuwahara, S., et al., *PSPC1, NONO, and SFPQ are expressed in mouse Sertoli cells and may function as coregulators of androgen receptor-mediated transcription.* Biol Reprod, 2006. **75**(3): p. 352-9.

122. Myojin, R., et al., *Expression and functional significance of mouse paraspeckle protein 1 on spermatogenesis.* Biol Reprod, 2004. **71**(3): p. 926-32.

123. Waki, H., et al., *The small molecule harmine is an antidiabetic cell-type-specific regulator of PPAR gamma expression.* Cell Metabolism, 2007. **5**(5): p. 357-370.

Chapter 2

Pspc1 promotes adipogenesis by enhancing nuclear export of adipogenic RNAs

Results

Pspc1 expression is responsive to PPARγ and is increased during adipogenesis

We previously performed a high-throughput screen for cDNAs affecting adipocyte differentiation [1]. This screen identified TLE3 as a transcriptional modulator of PPARγ and Wnt signaling that selectively promotes white adipogenic gene expression [2, 3]. Another "hit" in this screen was the cDNA encoding the paraspeckle component Pspc1. Pspc1 has not been previously linked with adipogenesis, and the biological function of paraspeckle complex proteins is poorly understood. To begin to address a potential function for Pspc1 in adipocytes, we first examined Pspc1 expression during the time course of differentiation of 10T1/2 and 3T3-L1 preadipocyte cell lines. *Pspc1* mRNA expression rose during differentiation in both cell lines (Figure 1.1A), and Pspc1 protein expression was even more prominently increased (Figure 1.1B).

We next examined whether the *Pspc1* gene was a direct target of the master adipogenic regulator PPARγ. To address whether PPARγ bound directly to the *Pspc1* promoter, we analyzed genome-wide ChIP-sequencing data from 3T3-L1 cells [4]. We identified peaks for PPARγ and its heterodimeric partner RXRα –0.2 kb from the transcription start site in the *Pspc1* promoter (Figure 1.2A), and sequence analysis identified a DR-1 sequence associated with this region (AGGTCAAGGGTTA). Directed ChIP-qPCR assays confirmed that this –0.2-kb region was bound by PPARγ in a differentiation-dependent manner in 3T3-L1 cells (Figure 1.2B). These results indicate that *Pspc1* is a direct target of PPARγ.

Pspc1 has previously been reported to form a complex with other paraspeckle components [5]. We therefore tested whether the expression of other paraspeckle components was altered in a similar fashion as Pspc1 during differentiation. *Sfpq* and *Nono* were modestly

induced during differentiation in at least one cell line, and expression of *Neat1* was markedly increased in both (Figure 1.2C), in agreement with a recent report [6]. We also investigated whether Pspc1 level was altered in murine obesity models. We found that *ob/ob* mice expressed less *Pspc1* mRNA in white adipose tissue (WAT) compared to wild-type controls (Figure 1.1C). We also observed reduced expression of Pspc1 in WAT from mice fed a high-fat diet. Interestingly, the expression pattern of Pspc1 in these models resembles that of PPARγ and adiponectin (Figure 1.1C). Examination of *Pspc1* mRNA tissue distribution revealed prominent expression in metabolically active tissues including WAT, brown adipose tissue (BAT), liver, heart, and kidney (Figure 1.2D).

Pspc1 promotes adipogenesis *in vitro*

To elucidate the role of Pspc1 in adipogenesis, we employed *in vitro* differentiation assays. Chronic overexpression of Pspc1 in 10T1/2 preadipocytes was achieved *via* retroviral transduction [7] (Figure 1.1D). We obtained stable cell lines derived from a large population of individual clones. These stable cell lines were then induced to differentiate for 7–8 days with the DMI + GW cocktail. Retroviral expression of Pspc1 increased the capacity of 10T1/2 cells to differentiate, as judged by oil-red O staining (Figure 1.1E). Real-time PCR analysis at multiple time points during the differentiation time course confirmed a marked increase in expression of adipocyte-selective genes in cells overexpressing Pspc1 (Figure 1.1F and 1.2E). Comparable results were obtained in parallel studies in the 3T3-L1 system (Figures 1.3A and 1.3B).

As a complement to these gain-of-function studies, we investigated the combinatorial effect of Pspc1 and PPARγ expression. We employed the NIH-3T3 fibroblast system that lacks endogenous PPARγ expression and is therefore unable to differentiate into mature adipocytes.

Consistent with earlier work, introduction of PPARγ conferred the ability to differentiate, as shown by the induction of adipocyte-specific genes [7]. Expression of Pspc1 alone had little, if any, effect, whereas co-expression of Pspc1 and PPARγ resulted in a synergistic effect (Figure 1.3C). These data suggest that Pspc1 is able to drive the adipogenic program and acts synergistically with PPARγ.

In order to assess the requirement for endogenous Pspc1 expression during adipocyte differentiation, we generated retroviruses encoding shRNA sequences against *Pspc1*. Knockdown of *Pspc1* expression in 10T1/2 stable cell lines was confirmed by immunoblotting (Figure 1.1G). Morphological differentiation, as assessed by Oil-red O staining, was impaired in cells with reduced Pspc1 expression (Figure 1.1H). Reduced expression of Pspc1 was also associated with reduced expression of adipocyte genes at multiple time points during differentiation (Figure 1.1I). Importantly, two different shRNA sequences targeting Pspc1 were confirmed to impair adipogenesis, and the degree of knockdown correlated with the effect on adipocyte gene expression. In agreement with the gene expression analysis, we observed the same effects in 3T3-L1 preadipocytes engineered to stably express these shRNA sequences (Figures 1.3D and 1.3E).

We also evaluated whether Nono and Sfpq were capable of promoting adipogenesis, because all three paraspeckle proteins have high sequence homology and are known to form heterodimers. While ectopic expression of Pspc1 markedly increased differentiation, expression of either Nono or Sfpq alone did not have any effect (Figure 1.3F). This finding suggests that either the adipogenic activity of Pspc1 is paraspeckle-independent or that only Pspc1 levels are limiting during preadipocyte differentiation *in vitro*.

The adipogenic capacity of Pspc1 depends on RNA binding

Next, we addressed the mechanism of Pspc1 action in adipogenesis. All three DBHS members, Pspc1, Nono, and Sfpq, contain two tandem RNA recognition motifs (RRMs) that exhibit >50% sequence identity [8]. RRMs typically engage in sequence-specific recognition of short RNA motifs [9]. We investigated whether the two RRMs were required for Pspc1 to drive adipogenesis. We generated stable cell lines that expressed Pspc1 deletion mutants of RRM1, RRM2, or both RRMs (Figure 2.1A). Remarkably, while Pspc1 promoted adipocyte differentiation, none of the RRM mutants promoted differentiation (Figure 2.1B). Immunoblotting for PPARγ in these differentiated stable cells further confirmed an almost complete loss of Pspc1 adipogenic function when either RRM was deleted (Figure 2.1C). These data indicate that the two RRMs of Pspc1 are required for its adipogenic capacity.

RRM domains are documented to mediate binding to a multitude of RNA molecules. RRM proteins can bind RNA with sequence-specificity. Structural elements within the RRM as well as flanking domains contribute to this specificity. Interestingly, prior studies have shown that the presence of a second RRM in a protein confers additional affinity and specificity for RNA recognition [9, 10]. We therefore postulated that Pspc1 might drive adipogenesis through interacting with certain mRNA transcripts of differentiation-relevant genes. To test this idea, we employed individual-nucleotide resolution cross-linking and immunoprecipitation (iCLIP) as a genome-wide approach to explore whether Pspc1 binds RNA, and if so which specific species [11, 12]. We utilized 10T1/2 stable cells expressing vector or Flag-tagged Pspc1. Cells before (day 0) and after (day 6) differentiation were subjected to UV cross-linking, lysed, and then protein–RNA complexes were immunoprecipitated with Flag antibody. Purified Pspc1-bound RNAs were enzymatically fragmented and radioactively labeled. When this purified Pspc1–RNA

complex was resolved by SDS-PAGE, we detected a radioactive signal at the exact molecular weight of Flag-Pspc1 with full RNA digestion, and shifted above the size of Flag-Pspc1 as a smear with partial RNA digestion (Figure 2.1D). Radioactive signal was undetectable in the control pull-down samples. These data strongly suggest that Pspc1 binds to RNA directly.

To identify genome-wide RNA targets of Pspc1, we performed high-throughput sequencing on the Pspc1-bound RNA samples recovered from the gel. We obtained 3.6 and 3.0 million nonredundant reads from Pspc1-bound RNA on differentiation day 0 and day 6, respectively (Figure 2.1D). We confirmed the quality of the reads (Figure 2.4A) and analyzed their length distribution (Figure 2.4B). Using the TopHat mapping tool, 1,024,730 (day 0) and 894,301 (day 6) reads were uniquely aligned to the mouse (NCBI37/mm9) genome (Figure 2.1E) [13]. We next utilized the CLIP-seq cluster-finding algorithm CLIPper to identify 25,743 (day 0) and 38,084 (day 6) significant clusters ($P < 0.05$) (Figure 2.1E) [14]. We further analyzed the genomic distribution of Pspc1 binding sites. The majority of the binding sites (97% on day 0 and 93% on day 6) were located within intronic regions, indicating that Pspc1 preferentially interacts with pre-mRNA in the nucleus. A minority of clusters was identified within 3′ UTRs. Interestingly, we observed a 2.5-fold increase in 3′ UTR binding on day 6, suggesting a possible shift in preference or subcellular localization of the Pspc1-RNA interaction upon differentiation (Figure 2.1F). Furthermore, *de novo* motif search with the HOMER algorithm identified AU-rich elements, UAAUU and UAUAU, within Pspc1-bound RNA sequences (Figure 2.4C) [15].

Pspc1 binds and regulates mRNA transcripts of adipocyte-selective genes

Next, we analyzed the target mRNAs of Pspc1 based on the CLIP-defined binding sites. We identified several candidate transcripts with remarkably high read numbers that were

previously known to play important roles in adipogenesis, including Ebf1, PPARγ, Acsl1, and Scd1 (Figures 2.2 and 2.3). Neat1, a known binding partner of Pspc1, was one of the RNAs with the highest read number, confirming the validity of the assay. Scanning through a 15-Mb region flanking Ebf1 on the chromosome revealed very few Pspc1 binding peaks (Figure 2.3A). To provide a global view of Pspc1 target genes, we performed pathway analysis. This analysis revealed that the "insulin signaling" and "PPAR signaling" pathways were highly enriched (Figure 2.4D).

We next addressed whether physical binding of these adipogenic transcripts by Pspc1 had functional consequences. We hypothesized that modulating the amount of Pspc1 in the cell might affect target mRNA or protein expression. To verify whether Pspc1 promotes expression of its binding targets during differentiation, we examined RNA and protein levels of these targets in differentiated 10T1/2 adipocytes on day 7. Stable expression of untagged, N-terminal Flag-tagged (F-Psp) or C-terminal Flag-tagged Pspc1 (Psp-F) all conferred increased levels of target mRNAs and proteins (Figures 3A and 3B). By contrast, two point mutations within the 8-amino acid RNP consensus sequence in each RRM abolished these effects of Pspc1. Although these studies confirmed that Pspc1 had effects on expression of its mRNA targets, they did not discriminate between direct or indirect—or between transcriptional or post-transcriptional—effects. We therefore assessed the effects of Pscp1 in undifferentiated preadipocytes to eliminate secondary effects due to changes in the differentiation state of the cells. Remarkably, while native Pspc1 expression in 10T1/2 preadipocytes did not significantly affect target mRNA levels (Figure 3C), protein levels were nonetheless increased (Figure 3D), suggesting a post-transcriptional mechanism of regulation. This effect was not observed with the RRM mutants. Conversely, loss of endogenous Pspc1 strongly reduced protein levels of Pspc1 targets, with only

minimal or no detectable effect on mRNA expression (Figures 3E and 3F). Since these effects of Pspc1 expression and knockdown were observed in the absence of differentiation, they were likely to be primary effects of Pspc1 modulation rather than secondary effects reflecting changes in overall differentiation.

Pspc1 interacts with Ddx3x in a differentiation- and RNA-dependent manner

RNA-binding proteins tend to form protein complexes that work cooperatively on the target RNA molecule. Paraspeckle complexes have not heretofore been studied in adipocytes, and therefore their composition in this cell type is unknown. It is also unknown whether their composition changes during differentiation. We hypothesized that determining the Pspc1 protein interactome in adipocytes might provide insight into the mechanism by which Pspc1–RNA binding regulates gene expression. We employed co-immunoprecipitation (co-IP) coupled with mass spectrometry to investigate the constituents of Pspc1 complexes in preadipocytes and adipocytes. We analyzed 10T1/2 stable cell lines that expressed Flag-Pspc1 on two differentiation time points (days 0 and 7). Silver staining of the immunoprecipitated proteins revealed a number of bands that seemed to be enriched in the Flag-Pscp1 sample on day 7 of differentiation (Figure 4A arrows). Mass spectrometry analysis of the immunoprecipitated proteins generated a list of proteins that were putative Pspc1 binding partners. To eliminate nonspecific binding, the list of candidates was compared with the sample from cells lacking Flag-Pspc1. Importantly, the two known Pspc1 interaction partners, Nono and Sfpq, had the highest confidence scores, confirming the validity of our approach. Among the other top interaction candidates, the majority were known RNA-binding proteins, reinforcing the idea that

Pspc1 is involved in RNA biology. Notably, the two categories with the highest number of interaction candidates were “RNA transport” and “protein synthesis” (Table 1).

We verified the interaction of several top candidates from our list using co-immunoprecipitation studies (Figure 4B and data not shown). One interacting protein, DEAD-box RNA helicase 3 (Ddx3x), was of particular interest. First, it ranked alongside the known direct interactors, Nono and Sfpq; second, it was associated with Pspc1 in a differentiation-dependent manner in immunoprecipitation studies (Figure 4B). The finding that Pspc1-Ddx3x association was induced by the differentiation program suggested it could have functional relevance to adipogenesis. Since both Pspc1 and Ddx3x are known to be RNA-binding proteins [16], we examined whether their interaction was RNA-dependent. Treatment with RNase prior to immunoprecipitation of Pspc1 from adipocyte lysates abolished the Pspc1-Ddx3x interaction, indicating that it was indeed RNA-dependent (Figure 4C).

Pspc1 translocates from nucleus to cytoplasm upon adipocyte differentiation

Ddx3x is an ATP-dependent RNA helicase that participates in various aspects of mRNA metabolism, including mRNA nuclear export [17-19]. Prior studies have shown that Ddx3x interacts with mRNA ribonucleoprotein complexes in the nucleus and is exported along with the ribonucleoproteins to the cytoplasm [20-22]. We therefore speculated that Pspc1, in a complex with Ddx3x, might be exported out of the nucleus (together with its target mRNA) during adipogenesis. To test this hypothesis, we performed nuclear-cytoplasmic fractionation on undifferentiated and differentiated adipocytes. Before differentiation (day 0), Pspc1 was present solely in the nuclear fraction. Surprisingly, despite previous reports that Pspc1 was a constitutively nuclear protein, we detected a substantial fraction of Pspc1 protein in the

cytoplasmic fraction on day 7 (Figure 4D). This finding suggested that Pspc1 might accompany its target mRNA transcripts from nucleus into the cytoplasm during differentiation.

To provide additional evidence for Pspc1 translocation, we employed confocal immunofluorescence microscopy to visualize Pspc1 localization in preadipocytes and adipocytes. In preadipocytes, Pspc1 expression entirely colocalized with DAPI staining, consistent with nuclear localization. However, in mature adipocytes, there was a remarkable shift of Pspc1 staining into the cytoplasm, consistent with results of our cell fractionation studies. In particular, the lipid-laden cells displayed prominent cytoplasmic Pspc1 localization. Parallel studies were carried out with both epitope-tagged and endogenous Pspc1 protein (Figures 4E and 4F). These data indicate that Pspc1 shuttles from the nucleus to the cytoplasm during adipocyte differentiation.

Pspc1 promotes nuclear export of adipogenic mRNAs

The discovery of Pspc1 translocation to the cytoplasm suggested that Pspc1 might facilitate adipocyte differentiation through mechanism(s) affecting mRNA processing, transport, or stability. We initially tested whether Pspc1 enhanced target mRNA stability in the cytoplasm. We treated differentiated 10T1/2 adipocytes with actinomycin D to inhibit transcription and analyzed target transcript levels at multiple time points. We were unable to detect any alteration in rates of target mRNA degradation in cells with either increased or decreased Pspc1 expression (Figures 5.1A and 5.1B), suggesting that Pspc1 does not stabilize these mRNA transcripts.

We next addressed whether Pspc1 was able to facilitate target mRNA export from the nucleus. We performed nuclear-cytoplasmic fractionation and extracted RNA from each fraction to analyze the transcript levels of Pspc1-interacting RNAs. 10T1/2 adipocytes stably expressing

either native or Flag-tagged Pspc1 exhibited an elevated cytoplasmic-to-nuclear ratio of a number of mRNA transcripts compared to control cells, including *Ebf1*, *Pparγ*, *Acsl1*, *Scd1,* and *Cd36* (Figure 5.1C). Importantly, this finding did not appear to reflect a general effect on all mRNAs, as those not found to interact with Pspc1, such as *LXRβ*, were not different between control and Pspc1-expressing cells. These observations suggest that Pspc1 facilitates adipocyte differentiation by promoting the nuclear export of a subset of mRNAs, resulting in augmented protein expression. In support of this idea, we found that expression of the putative mRNA export factor Ddx3x, which interacts with Pspc1 (Fig. 4), was important for Pspc1 effects on its target proteins. We knocked down Ddx3x expression in undifferentiated preadipocytes expressing retroviral vector alone or Pspc1with siRNA. Even partial loss of Ddx3x protein led to a reduction in protein levels of Ebf1, Scd-1, Ascl1, and PPARγ without affecting levels of their corresponding mRNAs and without affecting protein levels of Pspc1 itself (Figures 5.1D, 5.1E and 5.2). This affect was most evident in cells overexpressing Pspc1 (Figure 5.1E right), consistent with the hypothesis that Ddx3x facilitates the actions of Pspc1.

Pspc1 is required for adipogenesis *in vivo*

Finally, we tested the importance of Pspc1 for adipocyte differentiation and maintenance *in vivo*. To address whether Pspc1 activity contributes to adipocyte development, we assessed the capacity of Pspc1-knockdown preadipocytes to form fat pads when transplanted into immunocompromised mice. We used the 3T3-F442A preadipocyte cell line for these studies, as it efficiently forms fat pads *in vivo* [23]. Four weeks after subcutaneous transplantation, preadipocytes transduced with Pspc1 shRNA gave rise to markedly smaller fat pads. The average fat pad weight in the Pspc1 shRNA group was less than the control group, suggesting that fewer

adipocytes were derived from Pspc1 knockdown preadipocytes compared to controls, despite the same number of cells injected (Figure 6.1A). Histological analysis of the control fat pads revealed primarily mature adipocytes with large unilocular lipid droplets, resembling the normal histological features of white adipose tissue. By contrast, fat pads from the Pspc1-shRNA group contained more stromal fibrous tissue and relatively few mature adipocytes, suggesting that cells with decreased Pspc1 expression had impaired differentiation capacity *in vivo* (Figure 6.1B). Gene expression analysis also revealed lower levels of mature adipocyte mRNAs in the Pspc1-shRNA fat pads (Figure 6.1C). Comparable results were obtained for multiple shRNA constructs in multiple independent experiments (Figure 6.2A).

As a complementary approach to address Pspc1 function *in vivo*, we generated *Pspc1*-floxed mice (*Pspc1*$^{F/F}$) (Figures 6.2B and 6.2C) and used Cre-expressing adenovirus to delete Pspc1 in inguinal adipose tissue (see Experimental Procedures). We injected inguinal fat pads of *Pspc1*$^{F/F}$ mice with Ad-Cre virus on one side and Ad-Gfp control virus on the other. All comparisons were made between the two fat pads within the same animal. The efficacy of adenoviral transduction was confirmed by the markedly diminished Pspc1 protein expression in the Ad-Cre injected fat pads (Figure 6.1D). Pspc1 expression was not altered in the nearby quadriceps muscle or in the liver, suggesting minimal systemic effects from the adenoviral injection (Figure 6.2D). Adipocyte-specific gene expression was lower in Ad-Cre-injected fat pads compared with their Ad-Gfp-injected counterpart, including a number of the CLIP-identified Pspc1 target genes (Figure 6.1E). The results of Figure 6.1 indicate that endogenous Pspc1 is indispensable for adipose tissue development and maintenance *in vivo*.

Resistance to diet-induced obesity in adipose-specific Pspc1-knockout mice

To address the consequence of chronic loss of Pspc1 in mature adipose tissue in a physiological context we generated adipose tissue-specific *Pspc1*-null mice. *Pspc1*-floxed mice were crossed with adiponectin-*Cre* transgenic mice. Subsequent comparisons were made between homozygous *Pspc1*-floxed mice in the presence or absence of the *Cre* transgene. As expected, mice expressing adiponectin-*Cre* showed markedly reduced Pspc1 mRNA expression in whole white and brown adipose tissue (Figure 7.3A). Adipose Pspc1-deficient mice had comparable body weight to floxed controls when maintained on chow diet (Figure 7.1A). However, when the mice were switched to high-fat diet (60% calories from fat), they gained much less weight (Figure 7.1A) and were visibly much leaner (Figure 7.1B). Analysis of tissue weights after 10 weeks on high-fat diet confirmed markedly reduced body fat in adipose Pspc1-deficient mice compared to floxed controls with no change in body lean mass (Figure 7.1C). On visual inspection after laparotomy adipose Pspc1-deficient mice had much less adipose tissue, and the size and weight of isolated inguinal white, epididymal white, and subscapular brown fat pads (iWAT, eWAT, BAT) were correspondingly reduced in adipose Pspc1-deficient mice (Figures 7.1D, 7.1E, and 7.1F). We found that the size of white adipocytes in both the iWAT and eWAT depots was smaller in adipose Pspc1-deficient mice (Figure 7.1G). Both the BAT and liver of adipose Pspc1-deficient mice showed histological evidence of recued lipid accumulation compared to tissues from floxed controls (Figure 7.1G). Spleen and liver size was not different between groups.

As adipose tissue serves as a major organ controlling systemic metabolic and energy homeostasis, we next asked whether adipose-specific *Pspc1* deletion might result in altered systemic energy balance. Surprisingly, metabolic cage analysis revealed a dramatic elevation in

VO_2, VCO_2, and energy expenditure in mice lacking adipose Pspc1 compared to floxed controls mice (Figure 7.2A, 7.2B, 7.2C, and 7.3C). Food intake was not different between genotypes (Figure 7.2D). Activity was slightly increased in adipose Pspc1-deficient mice (Figure 7.3D). We went on to explore whether chronic loss of Pspc1 expression in mature adipose tissue affected systemic glucose metabolism in the setting of a high-fat diet challenge. Mice lacking Pspc1 in adipose tissue fed high-fat diet had improved glucose tolerance compared to controls as determined by IP glucose tolerance test (Figure 7.2E). Furthermore, insulin tolerance tests revealed an improved response to exogenous insulin in Pspc1-deficient mice, consistent with the interpretation that loss of Pspc1 expression in fat ameliorates the development of HFD-induced insulin resistance (Figure 7.2F). We did not detect difference in serum triglyceride or serum cholesterol levels between genotypes (Figure 7.3B).

Finally, consistent with our mechanistic findings showing that Pspc1 expression affects adipose gene expression, we found reduced expression of multiple genes in iWAT from adipose Pspc1-deficient mice (Figure 7.2G). Interestingly, we also observed increased expression of thermogenic genes in BAT in adipose Pspc1-deficient mice compared to their floxed counterparts (Figure 7.2G). Furthermore, despite the fact that Pspc1 deletion was specific for adipose tissue, we also found elevated expression of genes involved in fatty acid utilization, including that encoding acyl-CoA oxidase, in skeletal muscle of adiponectin-Cre+$Pspc1^{Fl/Fl}$ mice (Figure 7.2G). These data suggest that loss of Pspc1 expression in adipose tissue provokes compensatory changes in systemic energy balance that offset the impairment in adipose tissue lipid storage. In addition, Glut4 expression levels were elevated in the skeletal muscle of adipose Pspc1-deficient mice, potentially contributing to their improved glucose tolerance. Collectively,

our results indicate that the ability of Pspc1 to regulate adipocyte mRNA maturation is important for both adipocyte development and the function of mature adipose tissue *in vivo*.

Figure Legends

Figure 1.1 Pscp1 expression is differentiation-dependent and promotes adipogenesis in vitro.

(A) Real-time PCR analysis of Pspc1 mRNA expression during the differentiation of 10T1/2 and 3T3-L1 preadipocytes. Cells were stimulated to differentiate with dexamethasone (1 μM), IBMX (0.5 μM), insulin (5 μg/ml), and GW1929 (20 nM) for 7 days. Unless mentioned otherwise, mRNA expression in this and all subsequent figures were normalized to 36B4 control. Results are representative of three independent experiments. Error bars represent mean ± SD.

(B) Immunoblot analysis of Pspc1 protein expression during differentiation of 10T1/2 and 3T3-L1 preadipocytes. Cells were treated as in (A). (C) Real-time PCR analysis of Pspc1, PPARγ, and adiponectin mRNA expression in epididymal white adipose tissue from control, ob/ob mice and WT C57BL/6 mice fed with high fat diet (HFD) for 12 weeks. n = 8–10 per group. Statistical analysis was performed using student's t-test compared to chow or WT control groups. $*p < 0.05$, $**p < 0.01$.

(D) Immunoblot analysis of Pspc1 protein expression in retrovirally-derived 10T1/2 stable cell lines expressing vector or Pspc1.

(E) Oil-red O staining of 10T1/2 stable cells described in (D). Cells were stimulated to differentiate with DMI + 20 nM GW for 8 days.

(F) Real-time PCR analysis of adipogenic gene expression in 10T1/2 stable cells described in (A) on different days during differentiation. Cells were stimulated to differentiate as in (B).(G) Immunoblot analysis of Pspc1 protein expression in retrovirally-derived 10T1/2 stable cell lines expressing Pspc1 shRNAs (sh#1 and sh#2) or lacZ shRNA control.

(H) Oil-red O staining of the 10T1/2 stable cells described in (E). Cells were stimulated to differentiate with DMI + 20 nM GW for 7 days.

(I) Real-time PCR analysis of adipogenic gene expression in 10T1/2 stable cells described in (E) on different days during differentiation. Cells were stimulated to differentiate as in (F).

Figure 1.2 Tissue distribution of Pspc1 expression.

(A) High-resolution ChIP-seq analysis of PPARγ and RXRα binding sites within the mouse *Pspc1* locus from 3T3-L1 cells on differentiation day 0 and day 6. Red square indicates putative PPARγ/RXRα binding site at -200 bp from *Pspc1* transcription start site. Data are from the deep sequencing study of Nielsen et al. [4].

(B) Real-time PCR validation of PPARγ occupancy in the –200 bp region of *Pspc1* promoter at the indicated time points during differentiation. A region of the β-globin promoter served as a negative control.

(C) mRNA expression of paraspeckle components during adipocyte differentiation. Error bars represent mean ± SD in this and all subsequent figures.

(D) Real-time PCR analysis of the relative tissue distribution of Pspc1 mRNA. Tissues were harvested from 12-week old C57BL/6 mice fasted for 6 h, $n = 3$.

(E) Real-time PCR analysis of adipogenic gene expression in 10T1/2 stable cell lines expressing vector or Pspc1. Cells were stimulated to differentiate with DMI + 20 nM GW.

Figure 1.3 Effects of Pspc1 on adipocyte differentiation.

(A) Immunoblot analysis of Pspc1 protein expression in retrovirally-derived 3T3-L1 stable cell lines expressing vector or Pspc1.

(B) Real-time PCR analysis of adipogenic gene expression in 3T3-L1 stable cells described in (A) on different days during differentiation. Cells were stimulated to differentiate with DMI + 20 nM GW.

(C) Real-time PCR analysis of adipogenic gene expression in NIH-3T3 cells stably expressing Pspc1, PPARγ, or both. Cells were stimulated to differentiate with dexamethasone (2 μM), insulin (5 μg/ml), and GW1929 (20 nM) for 8 days.

(D) Immunoblot analysis of Pspc1 protein expression in retrovirally-derived 3T3-L1 stable cell lines expressing Pspc1 shRNAs (sh#1 and sh#3) or lacZ shRNA control.

(E) Real-time PCR analysis of adipogenic gene expression in 3T3-L1 stable cells described in (C) on different days during differentiation. Cells were stimulated to differentiate with DMI + 20 nM GW.

(F) Real-time PCR analysis of adipogenic gene expression in 10T1/2 stable cell lines expressing vector, Pspc1, Nono, or Sfpq. Cells were stimulated to differentiate with DMI + 20 nM GW.

Figure 2.1 iCLIP-seq identifies Pspc1 binding sites in adipogenic transcripts.

(A) Immunoblot analysis of V5-Pspc1 in retrovirally-derived 10T1/2 stable cell lines expressing WT Pspc1 or RRM deletion mutants.

(B) Real-time PCR analysis of adipogenic gene expression in 10T1/2 stable cells described in (A). Cells were stimulated to differentiate with DMI + 20 nM GW for 6 days.

(C) Immunoblot analysis of PPARγ in retrovirally-derived 10T1/2 stable cell lines expressing WT Pspc1 or RRM deletion mutants.

(D) Autoradiograph of cross-linked Pspc1-RNA complexes using denaturing gel electrophoresis. Pspc1-RNA complexes were immunopurified from 10T1/2 cells expressing vector or Flag-

tagged Pspc1 (Fl-Pspc1) using Flag antibody. RNA was partially or fully digested using different concentrations of MNase. Complexes extending 20–40 kDa upwards from the size of Pspc1 (59 kDa) were excised for further analysis (area indicated in squares).

(E) Summary of total reads, mapped reads (by TopHat), and significant clusters (by CLIPper) from iCLIP-seq assay on control cells (Vect) and Flag-Pspc1 cells (Fl-Pspc1) on differentiation day 0 and day 6.

(F) Genomic distribution of iCLIP-identified Pspc1 binding clusters on differentiation day 0 and day 6, as compared to percentage of nucleotides in the annotated transcriptome.

Figures 2.2 and 2.3 UCSC genome browser tracks of Pspc1 binding sites on target mRNAs. Pspc1 iCLIP-seq clusters mapped to the mouse Ebf1 and Acsl1 gene (UCSC genome browser track). Four tracks in green, blue, yellow, and red represent day 0 vector, day 0 Flag-Pspc1, day 6 vector, and day 6 Flag-Pspc1, respectively. Peaks are piles of 30-nt significant clusters (cross-linking site ± 15 nt). Height of the peaks indicates the number of clusters identified within the region.

Figure 2.4 Pspc1 iCLIP-seq analysis.

(A) Quality scores of total trimmed reads at each nucleotide position, using the FastQC tool from Babraham Bioinformatics. Scores within the green area indicate high quality.

(B) Length distribution of trimmed reads from vector control samples and Flag-Pspc1 samples at two time points.

(C) De novo motif analysis using the Homer's findMotifsGenome program. Pentamers and hexamers with top p-value rankings are displayed.

(D) Pathway analysis on CLIP-identified Pspc1 target genes using the DAVID Bioinformatics Database. Pathways displayed were ranked by *p* values.

Figure 3 Pspc1 influences the expression of iCLIP-identified target RNAs.

(A) Real-time PCR analysis of target gene mRNA expression in differentiated 10T1/2 cells stably expressing vector (Vect), N-terminal Flag-tagged Pspc1 (F-Psp), C-terminal Flag-tagged Pspc1 (Psp-F), untagged Pspc1 (Psp), or Pspc1 RNP mutant (RNP). Cells were stimulated to differentiate with DMI + 20 nM GW for 7 days.

(B) Immunoblot analysis of target gene protein expression in differentiated 10T1/2 stable cell lines described in (A).

(C) Real-time PCR analysis of target gene mRNA expression in undifferentiated 10T1/2 cells expressing vector (Vect), V5-tagged WT Pspc1 (Psp), V5-tagged RRM1 deletion mutant (ΔRRM1), or V5-tagged RRM2 deletion mutant (ΔRRM2).

(D) Immunoblot analysis of target gene protein expression in undifferentiated 10T1/2 cells described in (C).

(E) Real-time PCR analysis of target gene mRNA expression in undifferentiated 10T1/2 cells expressing Pspc1 shRNAs (shPsp#1 and shPsp#3) or lacZ shRNA control (shLacZ).

(F) Immunoblot analysis of target gene protein expression in undifferentiated 10T1/2 cells described in (E).

Figure 4 Pspc1 interacts with Ddx3x and translocates from nucleus to cytoplasm during differentiation.

(A) Silver staining of Flag-Pspc1 co-immunoprecipitated proteins on a gradient Bis-Tris gel. Co-IP with Flag antibody was performed in 10T1/2 cells stably expressing Flag-Pspc1 or vector control. Arrows point to protein bands exclusively present in the Flag-Pspc1 lane.
(B) Immunoblot analysis of proteins co-immunoprecipitated with Flag-Pspc1 in 10T1/2 cells on differentiation day 0 and day 6. Cells were stimulated to differentiate with DMI + 20 nM GW. The known interaction partner Nono served as a positive control.
(C) Immunoblot analysis of Ddx3x co-immunoprecipitated with Flag-Pspc1 in 10T1/2 cells on differentiation day 6 (middle panel). Cell lysates treated with control or RNase prior to immunoprecipitation (right panel).
(D) Immunoblot analysis of Pspc1 and Nono in the nuclear (Nucl) and cytoplasmic (Cyto) fractions of 10T1/2 cells on differentiation day 0 and day 7. Cells were stimulated to differentiate with DMI + 20 nM GW. Hmg1 and αTubulin served as nuclear and cytoplasmic markers, respectively.
(E) Pspc1 subcellular localization visualized by fluorescent confocal microscopy in undifferentiated (Pre) and differentiated (Ad) 10T1/2 adipocytes stably expressing V5-tagged Pspc1. Cells were stimulated to differentiate with DMI + 20 nM GW for 7 days. V5-Pspc1 (red) colocalizes exclusively with DAPI (blue)-stained nuclei in undifferentiated state, whereas in BODIPY (green)-stained mature adipocytes Pspc1 localizes in nucleus as well as cytoplasm.
(F) Pspc1 subcellular localization visualized by fluorescent confocal microscopy in undifferentiated (Pre) and differentiated (Ad) 10T1/2 adipocytes stably expressing untagged Pspc1. Antibody against Pspc1 (red) was used for detecting endogenous Pspc1.

Figure 5.1 Pspc1 facilitates nucleocytoplasmic export of target mRNAs.

(A) Real-time PCR analysis of Pspc1 target transcripts at multiple time points following actinomycin D treatment in differentiated 10T1/2 cells stably expressing vector (Vect), Flag-tagged Pspc1 (Fl-Pspc1), or untagged Pspc1 (Pspc1) were used for this assay.
(B) Real-time PCR analysis of Pspc1 target transcripts at multiple time points following actinomycin D treatment in differentiated 10T1/2 cells stably expressing Pspc1 shRNA (shPspc1) or lacZ shRNA (shLacZ).
(C) Real-time PCR analysis of Pspc1 target transcripts in the nuclear and cytoplasmic fractions of 10T1/2 cells expressing vector (Vect), Flag-tagged Pspc1 (Fl-Pspc1), or untagged Pspc1 (Pspc1). Values represent the cytoplasmic-to-nuclear ratio of each transcript. LXRβ served as a negative control.
(D) Real-time PCR analysis of gene expression in control or Pspc1-transduced 10T1/2 cells transfected with non-targeting siRNA control (siNC) or siRNA directed against Ddx3x (siDdx3x).
(E) Immunoblot analysis of protein extracts from control or Pspc1-transduced 10T1/2 cells transfected with non-targeting siRNA control (siNC) or siRNA directed against Ddx3x (siDdx3x)

Figure 5.2 Knockdown of Ddx3x does not affect Pspc1 target mRNA levels.
Real-time PCR analysis of gene expression in 10T1/2 stable cell lines expressing retroviral vector control, or Pspc1.

Figure 6.1 Pspc1 is important for adipocyte differentiation and maintenance *in vivo.*

(A) Weight of the fat pad formed from subcutaneous transplantation of 3T3-F442A preadipocytes expressing lacZ shRNA or Pspc1 shRNA. Mice were sacrificed 4 weeks post transplantation. 6-week old male NCr nude mice were used, $n = 4$ per group. Statistical analysis was performed using student's *t*-test. $^{**}p < 0.01$.

(B) Histological analysis of the fat pad formed from subcutaneous preadipocytes transplantation described in (A).

(C) Real-time PCR analysis of Pspc1 and adipose-specific genes in the fat pads formed from the subcutaneous preadipocytes transplantations described in (A). $^{*}p < 0.05$, $^{**}p < 0.01$.

(D) Immunoblot analysis of Pspc1 and PPARγ protein expression in the inguinal WAT of each *Pspc1*$^{F/F}$ mice injected with GFP adenovirus in one inguinal fat pad and Cre adenovirus in the contralateral pad. Mice were sacrificed 7 days post adenovirus injection. 8-week old male *Pspc1*$^{F/F}$ mice were used, $n = 5$. Results from 3 representative mice are shown.

(E) Real-time PCR analysis of adipose specific-genes in the inguinal WAT injected with adenovirus as described in (D). $^{*}p < 0.05$, $^{**}p < 0.01$. Results from 3 representative mice are shown.

Figure 6.2 Function of Pspc1 in adipose tissue *in vivo.*

(A) Weight of the fat pad formed from subcutaneous transplantation of 3T3-F442A preadipocytes expressing lacZ shRNA or different Pspc1 shRNA constructs. $n = 4$ per group. $^{**}p < 0.01$.

(B) Strategy for the generation of *Pspc1*-floxed mice. The targeting vector was electroporated into C57BL/6N ES cells to generate the conditional-potential allele. Validated ES cell clones were subjected to *in vitro* Flp recombination followed by blastocyst injection. Resulting chimeric

mice were mated with C57BL/6N mice to generate heterozygous *Pspc1*-floxed mice. forward/reverse, genotyping primer binding sites for detection of the inserted *loxP* site. Homozygous *Pspc1*-floxed mice were used for Adeno-Cre injection or mated with adiponectin-*Cre* mice.

(C) PCR genotyping of *Pspc1*-floxed mice.

(D) Real-time PCR analysis of Pspc1 mRNA expression in liver and quadriceps muscle of $Pspc1^{F/F}$ mice injected with adenovirus. Results from 3 representative mice are shown.

Figure 7.1 Adipose-specific Pspc1-deficient mice are resistant to diet-induced obesity.

(A) Body weight of $Pspc1^{F/F}$ (F/F) and $Pscp1^{F/F}$ *Cre*+ (KO) mice fed chow diet for 10 weeks and then switched to 60% high-fat diet. $n = 8$ per group, female mice.

(B) External appearance of representative F/F and KO mice shown in (A) at 20 weeks of age after 10 weeks on HFD.

(C) Body fat and lean mass in F/F and KO mice at 8 weeks old on chow diet and at 20 weeks old after 10 weeks on HFD determined by Echo MRI. $n = 8$ per group, female mice.

(D) Average weight of individual white and brown adipose fat pads from F/F and KO mice after 10 weeks on HFD. $n = 8$ per group, 20-week old female mice.

(E) Representative F/F and KO mice after 10 weeks on HFD showing grossly reduced adipose tissue content in the absence of Pspc1.

(F) Gross appearance of tissues from F/F and KO mice after 10 weeks on HFD.

(G) Histology of tissues from F/F and KO mice after 10 weeks on HFD.

Figure 7.2 Adipose-specific Pspc1-deficient mice exhibit increased energy expenditure and glucose tolerance.

(A-C) Energy expenditure rate (kCal/hr), VO_2 (ml/kg/hr), and VCO_2 of F/F and KO mice was analyzed by Columbus Oxymax metabolic chambers after 4 weeks on HFD. 12 hr light/dark cycles, 66hr total duration, each light/dark bar represents 12 hr duration. n = 8 per group, female mice.

(D) Daily food intake normalized to body weight. n = 8 per group, female mice.

(E) IP glucose tolerance test performed on F/F and KO mice after 4 weeks of HFD feeding. *p < 0.05, **p < 0.01. n = 5 per group, 14-week old female mice.

(F) Insulin tolerance test performed on F/F and KO mice after 10 weeks of HFD feeding. *p < 0.05, **p < 0.01. n = 5 per group, 20 week-old female mice.

(G) Relative gene expression in iWAT, BAT, and skeletal muscle from F/F and KO mice after 10 weeks on HFD determined by real-time PCR. n = 8 per group, 20-week old female mice.

Figure 7.3 Energy expenditure of adipose-specific *Pspc1* KO mice.

(A) Expression of Pspc1 mRNA in WAT and BAT from *Pspc*$1^{F/F}$ (F/F) and *Pscp1*$^{F/F}$ *Cre*+ (KO) mice. n = 8 per group, female mice.

(B) Serum triglyceride and serum cholesterol in F/F and KO mice after 10 weeks on HFD. n = 8 per group, female mice.

(C) Energy expenditure rate (kCal/hr), VO_2 (ml/kg/hr), and VCO_2 of F/F and KO mice in metabolic chamber after 4 weeks on HFD.12 hr light/dark cycles, 66hr total duration. n = 8 per group, female mice.

(D) Activity of F/F and KO mice in metabolic chamber after 4 weeks on HFD.12 hr light/dark cycles, 66hr total duration, each light/dark bar represents 12hr duration. *n* = 8 per group, female mice.

Table 1 Candidate Pspc1-interacting Proteins from IP-mass spec.

Table 2 qPCR primers used.

Figure 1.1

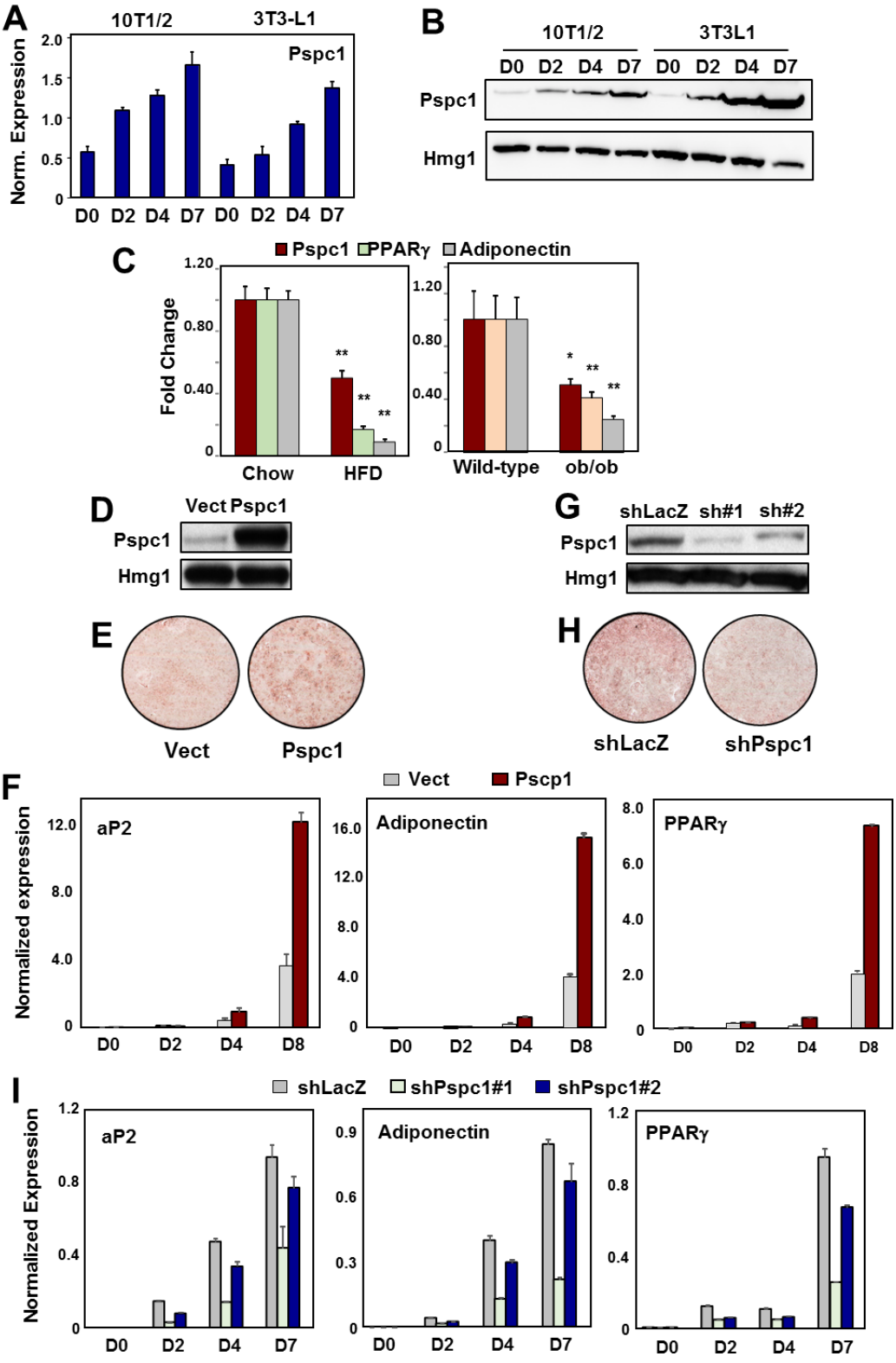

A
10T1/2
3T3-L1
Pspc1
Norm. Expression
D0 D2 D4 D7 D0 D2 D4 D7
B
10T1/2
3T3L1
D0 D2 D4 D7 D0 D2 D4 D7
Pspc1
Hmg1
C
Pspc1 PPARγ Adiponectin
Fold Change
Chow
HFD
Wild-type
ob/ob
D
Vect Pspc1
Pspc1
Hmg1
G
shLacZ sh#1 sh#2
Pspc1
Hmg1
E
Vect
Pspc1
H
shLacZ
shPspc1
F
Vect
Pscp1
Normalized expression
aP2
Adiponectin
PPARγ
D0 D2 D4 D8
I
shLacZ
shPspc1#1
shPspc1#2
Normalized Expression
aP2
Adiponectin
PPARγ
D0 D2 D4 D7

Figure 1.2

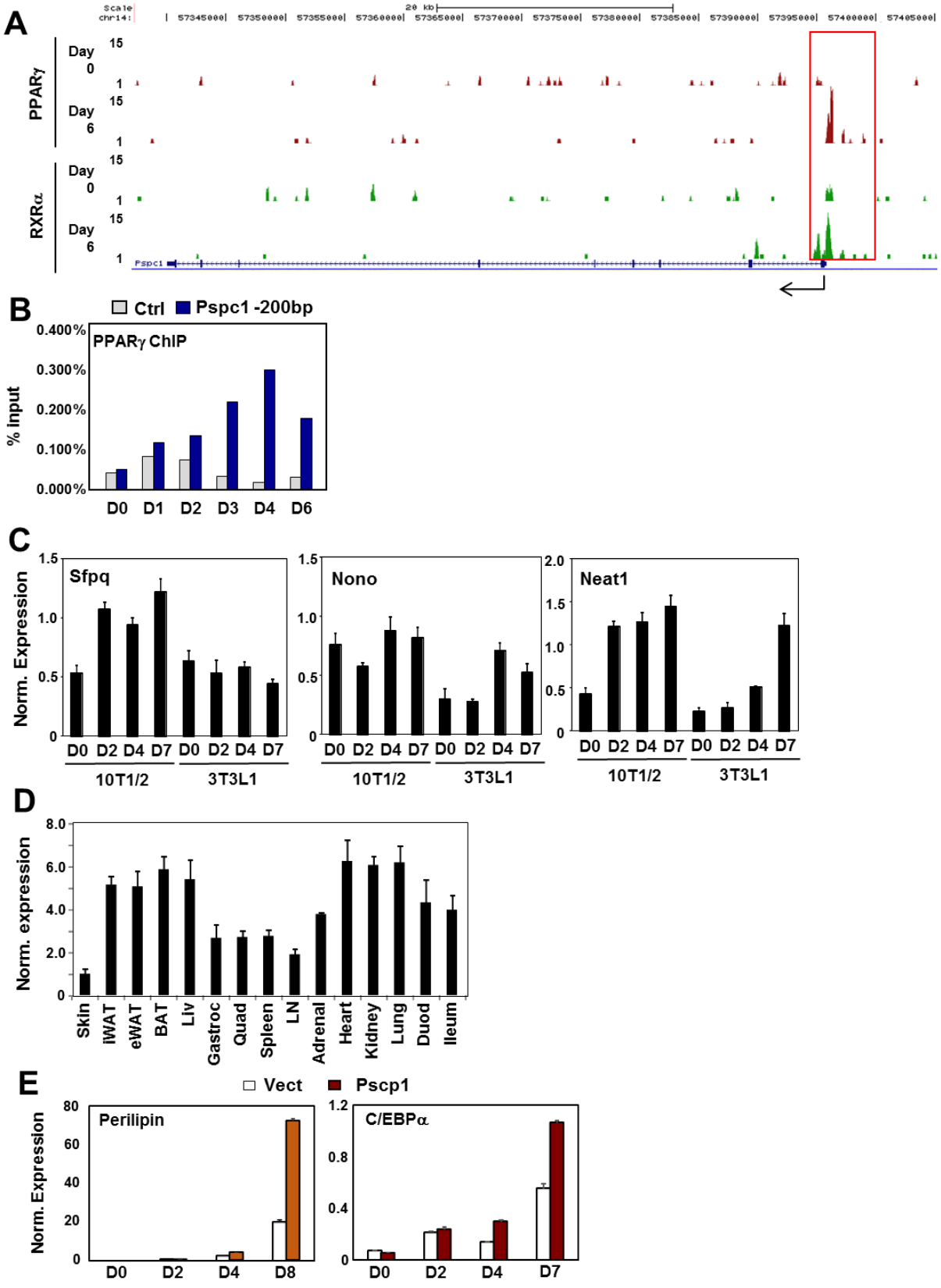

A
PPARγ
RXRα
Day 0
Day 6
Pspc1
B
Ctrl
Pspc1 -200bp
PPARγ ChIP
% Input
D0 D1 D2 D3 D4 D6
C
Sfpq
Nono
Neat1
Norm. Expression
D0 D2 D4 D7 D0 D2 D4 D7
10T1/2
3T3L1
D
Norm. expression
Skin
iWAT
eWAT
BAT
Liv
Gastroc
Quad
Spleen
LN
Adrenal
Heart
Kidney
Lung
Duod
Ileum
E
Vect
Pscp1
Perilipin
C/EBPα
Norm. Expression
D0 D2 D4 D8
D0 D2 D4 D7

Figure 1.3

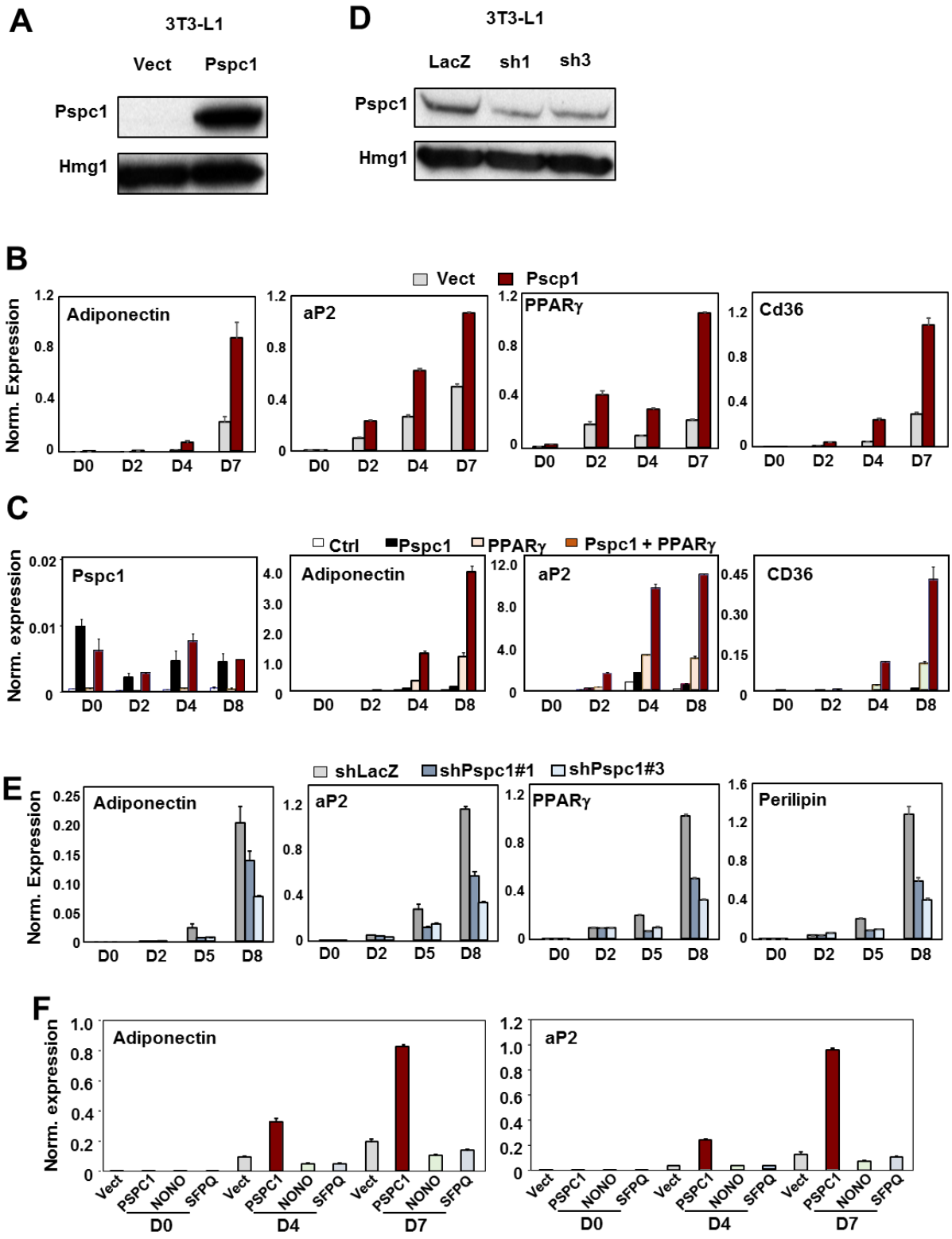
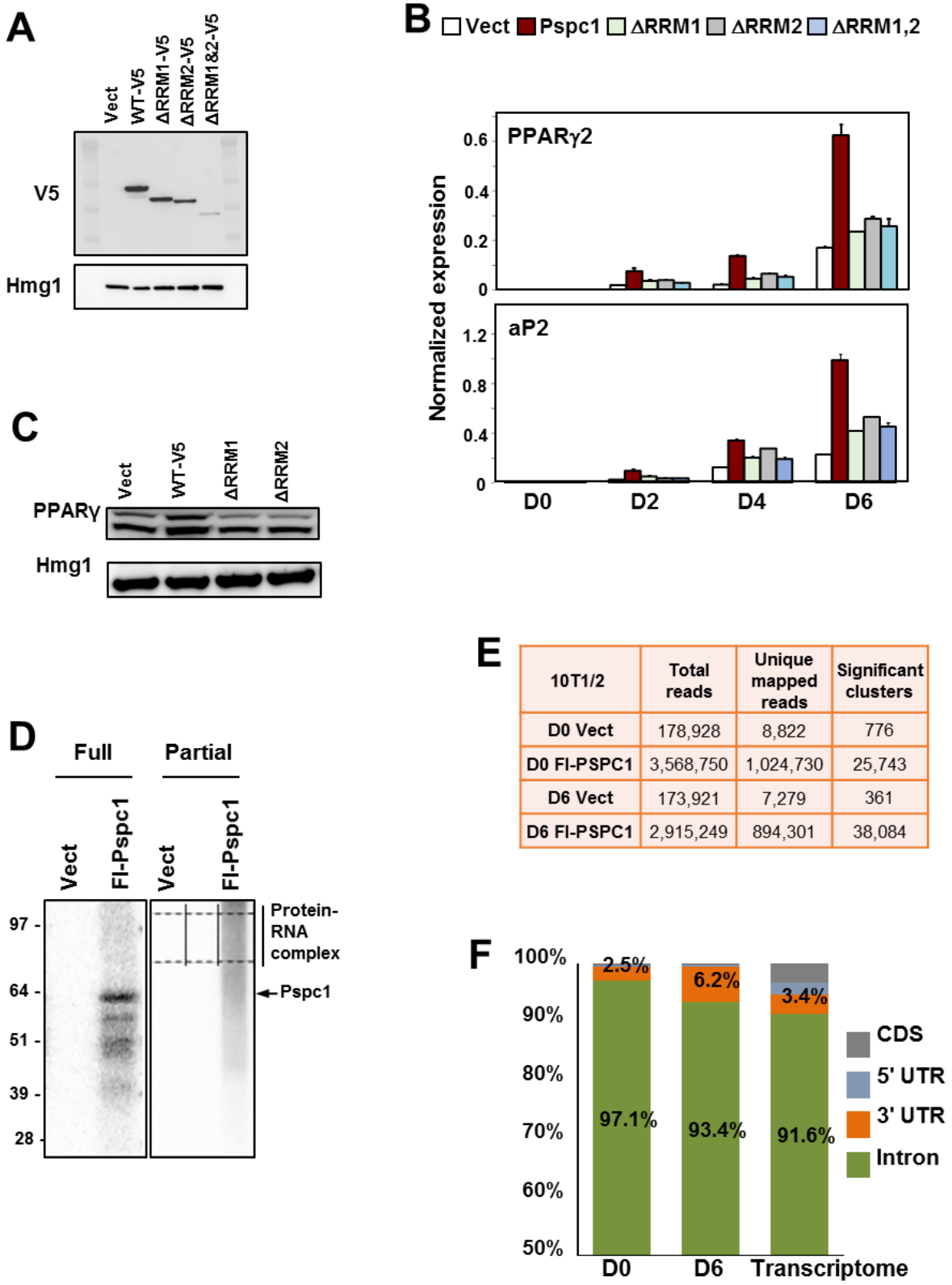

A
3T3-L1
Vect
Pspc1
Pspc1
Hmg1
D
3T3-L1
LacZ
sh1
sh3
Pspc1
Hmg1
B
Vect
Pscp1
Norm. Expression
Adiponectin
aP2
PPARγ
Cd36
D0
D2
D4
D7
C
Ctrl
Pspc1
PPARγ
Pspc1 + PPARγ
Norm. expression
Pspc1
Adiponectin
aP2
CD36
D0
D2
D4
D8
E
shLacZ
shPspc1#1
shPspc1#3
Norm. Expression
Adiponectin
aP2
PPARγ
Perilipin
D0
D2
D5
D8
F
Norm. expression
Adiponectin
aP2
Vect
PSPC1
NONO
SFPQ
D0
D4
D7

Figure 2.1



10T1/2	Total reads	Unique mapped reads	Significant clusters
D0 Vect	178,928	8,822	776
D0 Fl-PSPC1	3,568,750	1,024,730	25,743
D6 Vect	173,921	7,279	361
D6 Fl-PSPC1	2,915,249	894,301	38,084

Figure 2.2

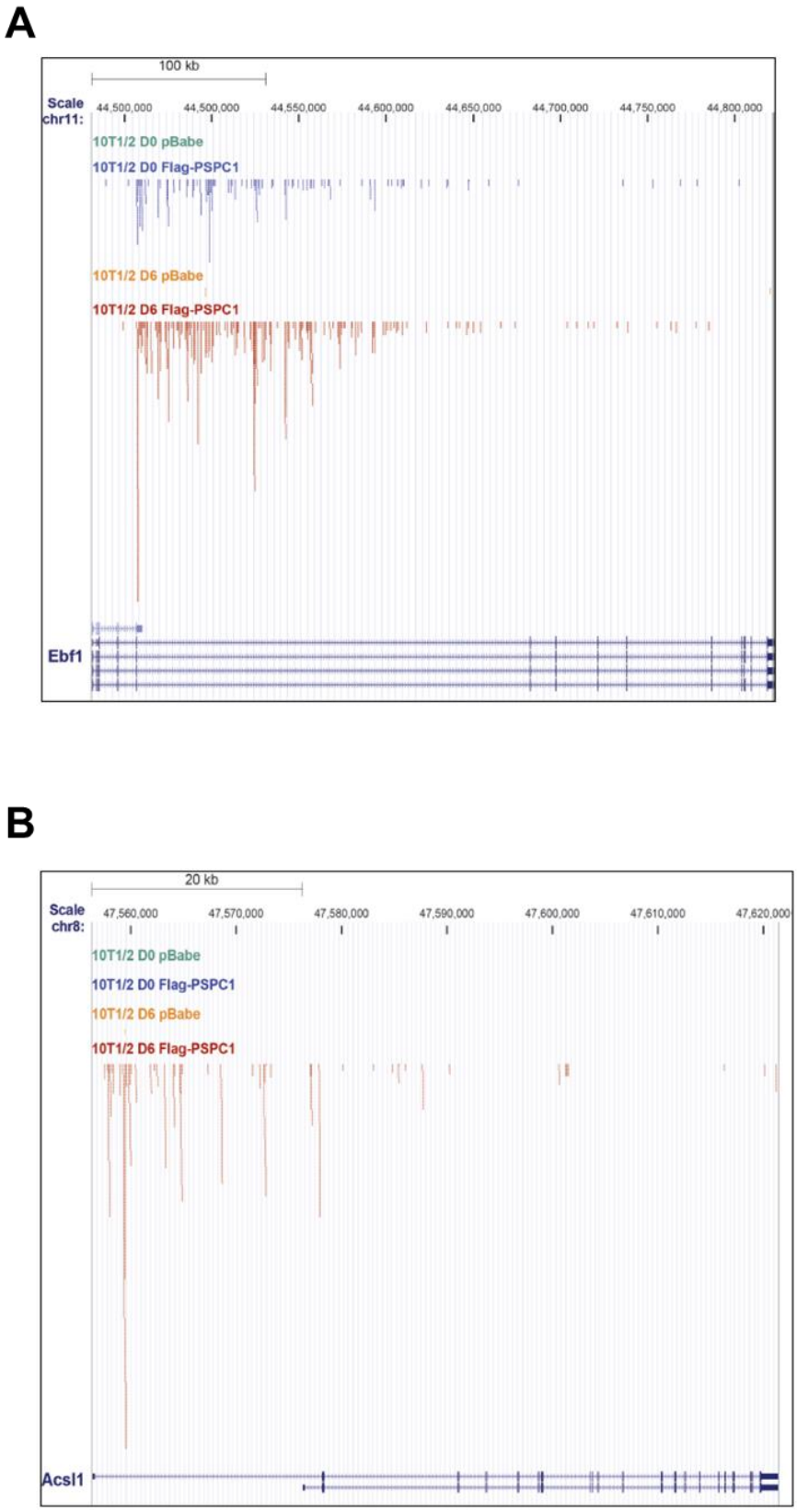

A
100 kb
Scale
chr11:
44,500,000
44,500,000
44,550,000
44,600,000
44,650,000
44,700,000
44,750,000
44,800,000
10T1/2 D0 pBabe
10T1/2 D0 Flag-PSPC1
10T1/2 D6 pBabe
10T1/2 D6 Flag-PSPC1
Ebf1
B
20 kb
Scale
chr8:
47,560,000
47,570,000
47,580,000
47,590,000
47,600,000
47,610,000
47,620,000
10T1/2 D0 pBabe
10T1/2 D0 Flag-PSPC1
10T1/2 D6 pBabe
10T1/2 D6 Flag-PSPC1
Acsl1

Figure 2.3

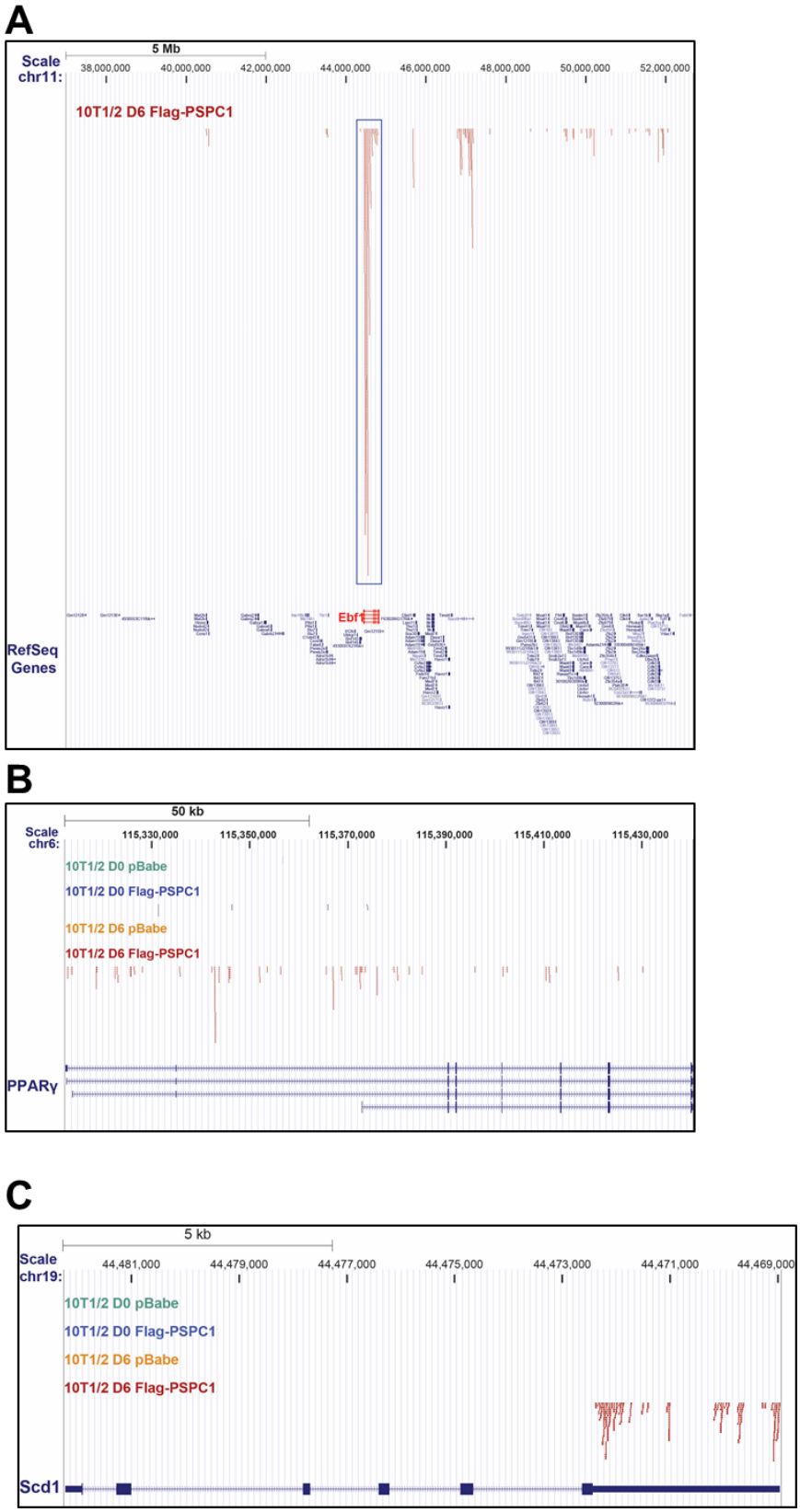

A
Scale
chr11:
5 Mb
38,000,000
40,000,000
42,000,000
44,000,000
46,000,000
48,000,000
50,000,000
52,000,000
10T1/2 D6 Flag-PSPC1
Ebf1
RefSeq
Genes
B
Scale
chr6:
50 kb
115,330,000
115,350,000
115,370,000
115,390,000
115,410,000
115,430,000
10T1/2 D0 pBabe
10T1/2 D0 Flag-PSPC1
10T1/2 D6 pBabe
10T1/2 D6 Flag-PSPC1
PPARγ
C
Scale
chr19:
5 kb
44,481,000
44,479,000
44,477,000
44,475,000
44,473,000
44,471,000
44,469,000
10T1/2 D0 pBabe
10T1/2 D0 Flag-PSPC1
10T1/2 D6 pBabe
10T1/2 D6 Flag-PSPC1
Scd1

Figure 2.4

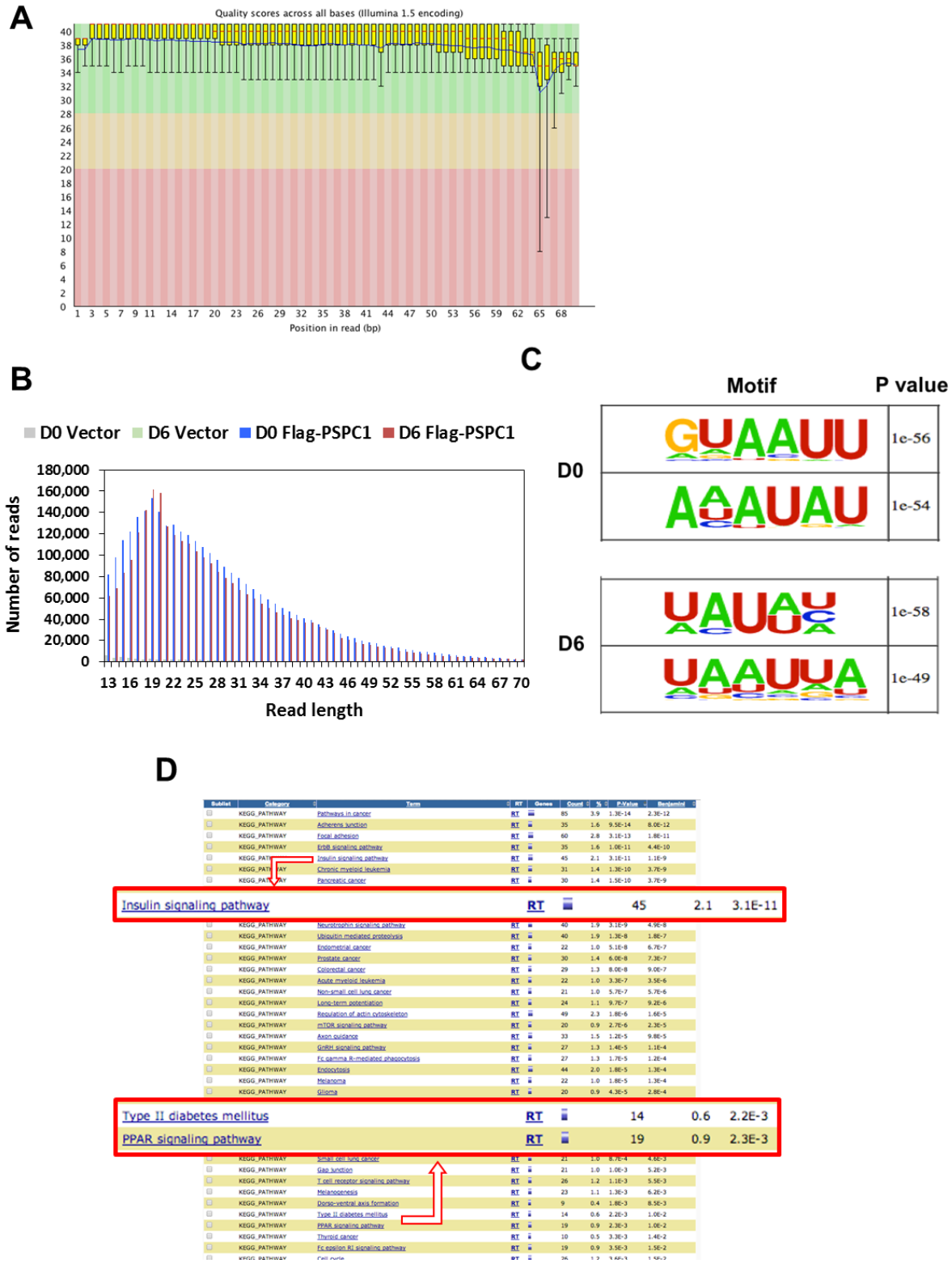

A
Quality scores across all bases (Illumina 1.5 encoding)
Position in read (bp)
B
D0 Vector
D6 Vector
D0 Flag-PSPC1
D6 Flag-PSPC1
Number of reads
Read length
C
Motif
P value
D0
1e-56
1e-54
D6
1e-58
1e-49
D
Insulin signaling pathway RT 45 2.1 3.1E-11
Type II diabetes mellitus RT 14 0.6 2.2E-3
PPAR signaling pathway RT 19 0.9 2.3E-3

Figure 3

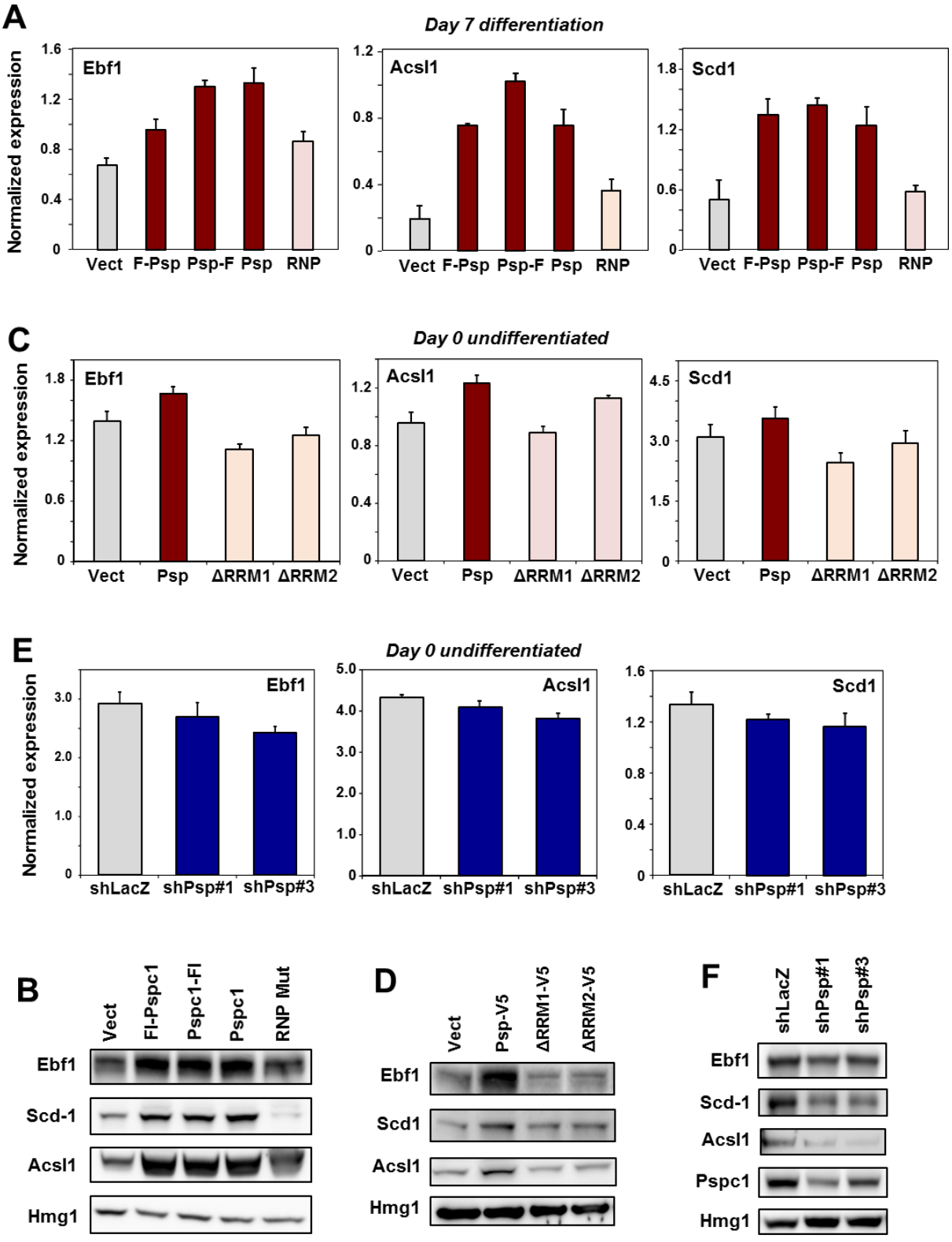

A
Day 7 differentiation
Normalized expression
Ebf1
Acsl1
Scd1
Vect F-Psp Psp-F Psp RNP
C
Day 0 undifferentiated
Vect Psp ΔRRM1 ΔRRM2
E
Day 0 undifferentiated
shLacZ shPsp#1 shPsp#3
B
Vect Fl-Pspc1 Pspc1-Fl Pspc1 RNP Mut
Ebf1
Scd-1
Acsl1
Hmg1
D
Vect Psp-V5 ΔRRM1-V5 ΔRRM2-V5
Ebf1
Scd1
Acsl1
Hmg1
F
shLacZ shPsp#1 shPsp#3
Ebf1
Scd-1
Acsl1
Pspc1
Hmg1

Figure 4

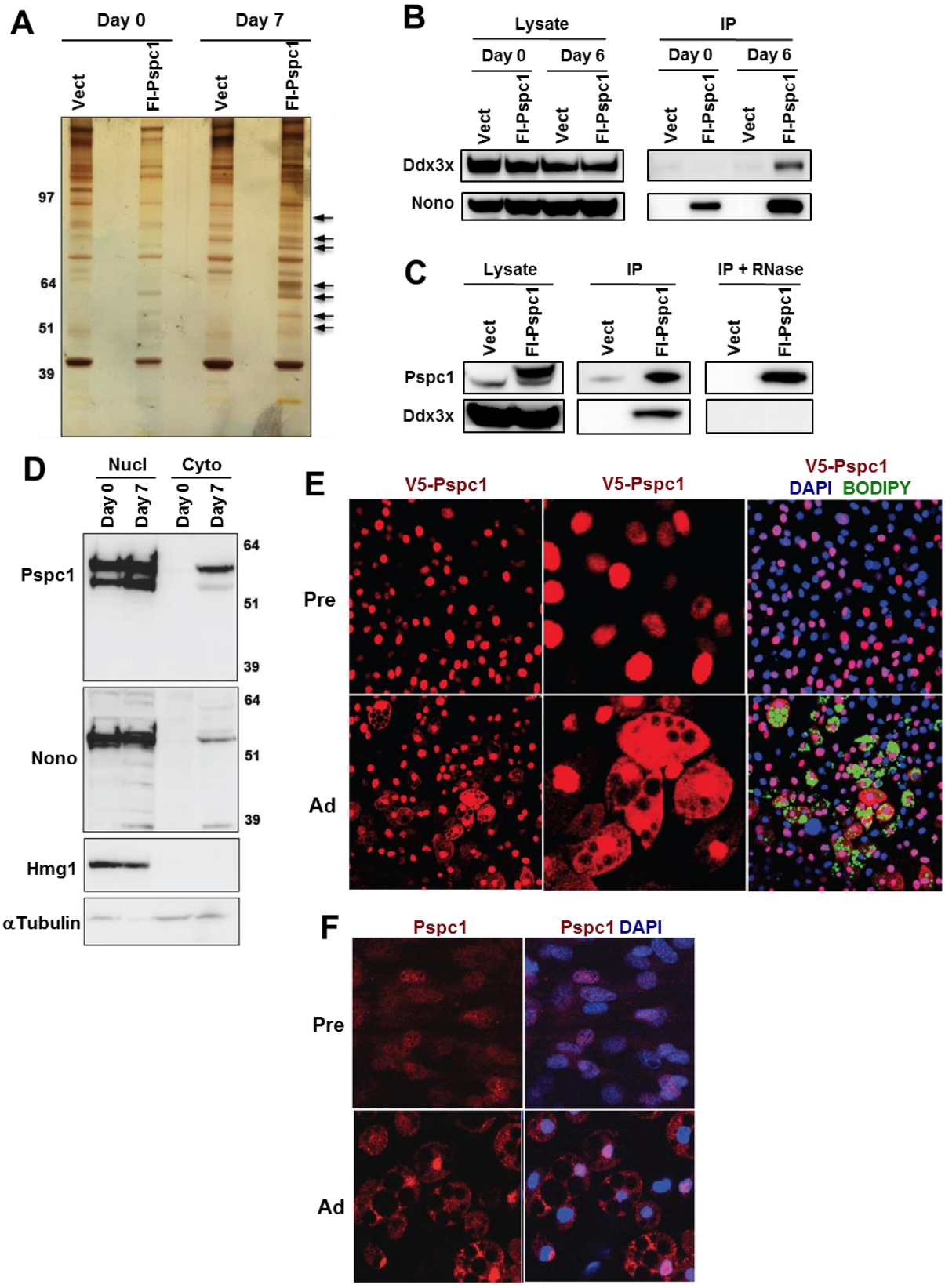

A
Day 0
Day 7
Vect
Fl-Pspc1
Vect
Fl-Pspc1
97
64
51
39
B
Lysate
IP
Day 0
Day 6
Day 0
Day 6
Vect
Fl-Pspc1
Vect
Fl-Pspc1
Vect
Fl-Pspc1
Vect
Fl-Pspc1
Ddx3x
Nono
C
Lysate
IP
IP + RNase
Vect
Fl-Pspc1
Vect
Fl-Pspc1
Vect
Fl-Pspc1
Pspc1
Ddx3x
D
Nucl
Cyto
Day 0
Day 7
Day 0
Day 7
Pspc1
Nono
Hmg1
αTubulin
64
51
39
64
51
39
E
V5-Pspc1
V5-Pspc1
V5-Pspc1
DAPI BODIPY
Pre
Ad
F
Pspc1
Pspc1 DAPI
Pre
Ad

Figure 5.1

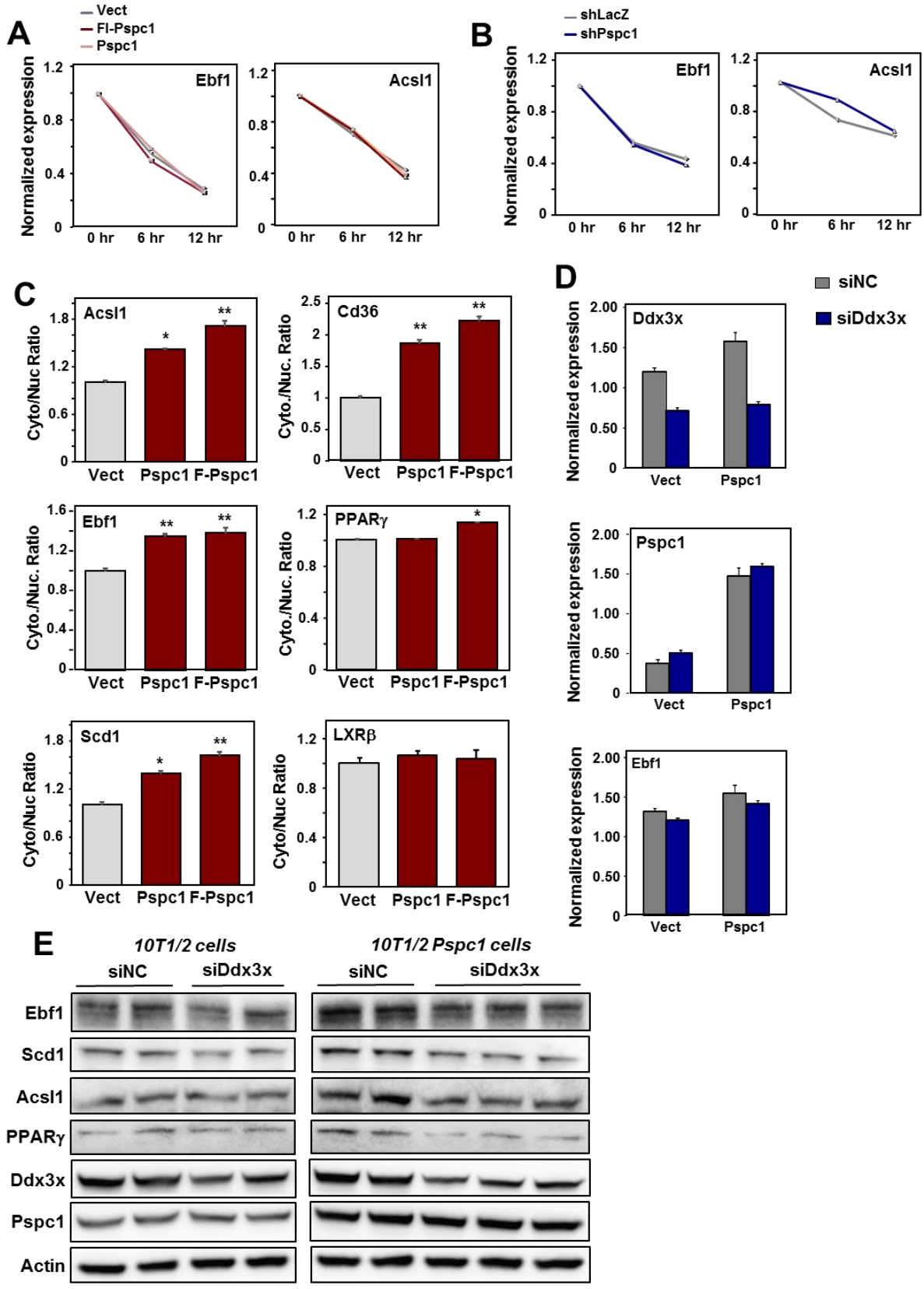

A
Vect
Fl-Pspc1
Pspc1
Normalized expression
Ebf1
Acsl1
0 hr
6 hr
12 hr
B
shLacZ
shPspc1
C
Cyto/Nuc Ratio
Cyto./Nuc. Ratio
Acsl1
Cd36
Ebf1
PPARγ
Scd1
LXRβ
Vect
Pspc1
F-Pspc1
D
siNC
siDdx3x
Ddx3x
Pspc1
Ebf1
E
10T1/2 cells
10T1/2 Pspc1 cells
siNC
siDdx3x
Ebf1
Scd1
Acsl1
PPARγ
Ddx3x
Pspc1
Actin

Figure 5.2

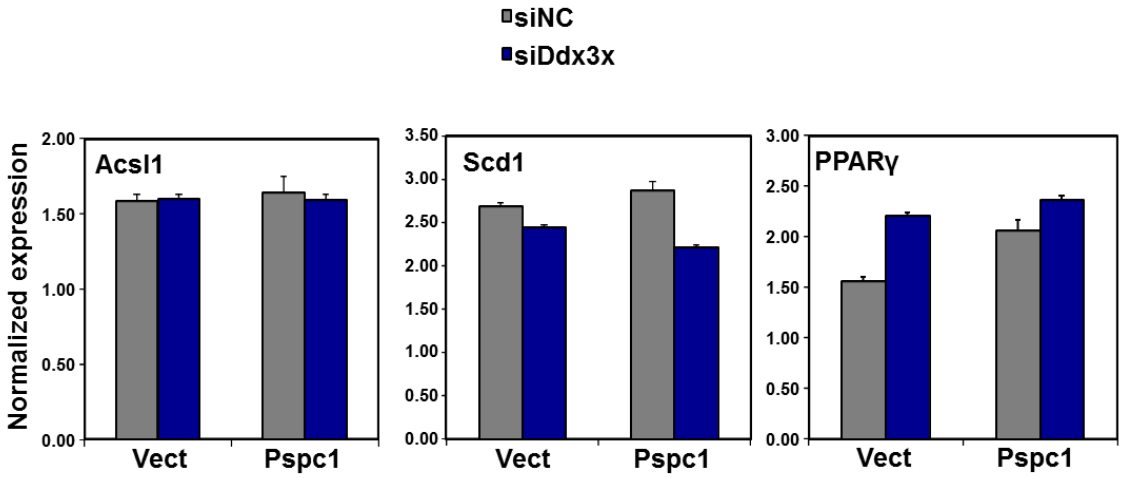

siNC
siDdx3x
Normalized expression
Acsl1
Scd1
PPARγ
Vect
Pspc1
Vect
Pspc1
Vect
Pspc1

Figure 6.1

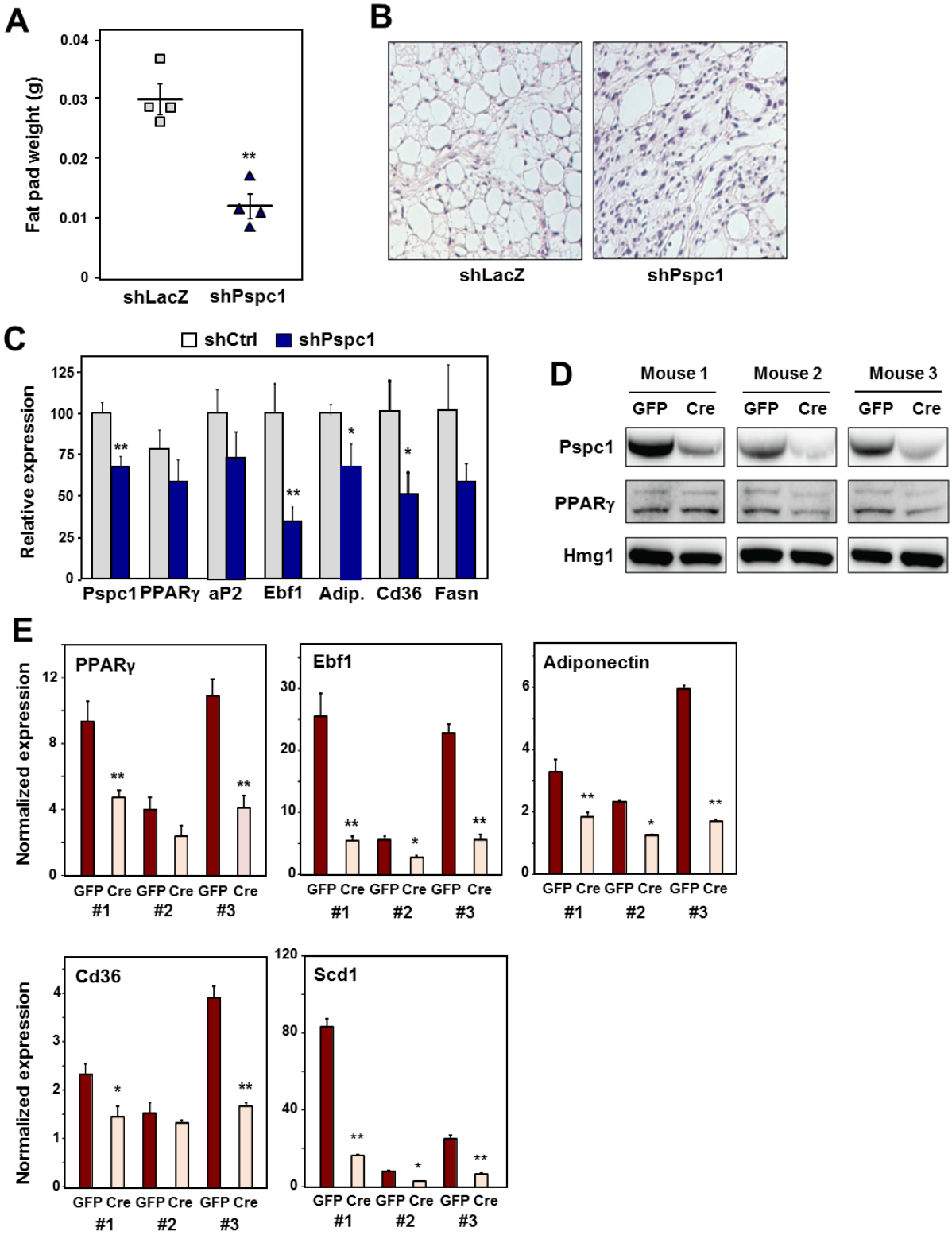

A
Fat pad weight (g)
0.04
0.03
0.02
0.01
0
**
shLacZ
shPspc1
B
shLacZ
shPspc1
C
shCtrl
shPspc1
Relative expression
125
100
75
50
25
0
Pspc1
PPARγ
aP2
Ebf1
Adip.
Cd36
Fasn
D
Mouse 1
Mouse 2
Mouse 3
GFP
Cre
Pspc1
PPARγ
Hmg1
E
PPARγ
Ebf1
Adiponectin
Cd36
Scd1
Normalized expression
GFP Cre GFP Cre GFP Cre
#1
#2
#3

Figure 6.2

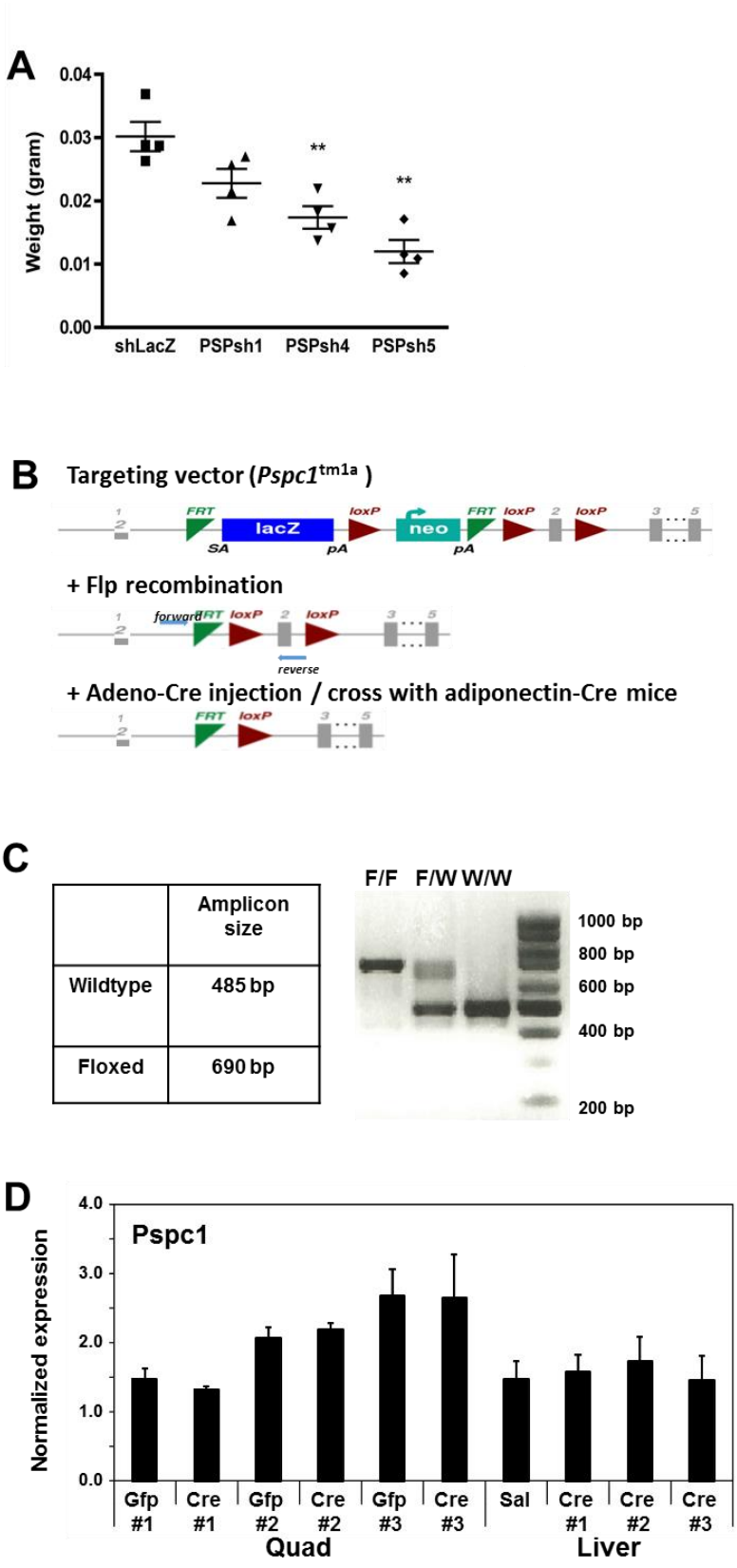

A
Weight (gram)
0.04
0.03
0.02
0.01
0.00
**
**
shLacZ
PSPsh1
PSPsh4
PSPsh5
B
Targeting vector (Pspc1tm1a)
FRT
lacZ
loxP
neo
FRT
loxP
loxP
SA
pA
pA
+ Flp recombination
forward
reverse
+ Adeno-Cre injection / cross with adiponectin-Cre mice
C
Amplicon size
Wildtype
485 bp
Floxed
690 bp
F/F
F/W
W/W
1000 bp
800 bp
600 bp
400 bp
200 bp
D
Pspc1
Normalized expression
4.0
3.0
2.0
1.0
0.0
Gfp #1
Cre #1
Gfp #2
Cre #2
Gfp #3
Cre #3
Sal
Cre #1
Cre #2
Cre #3
Quad
Liver

Figure 7.1

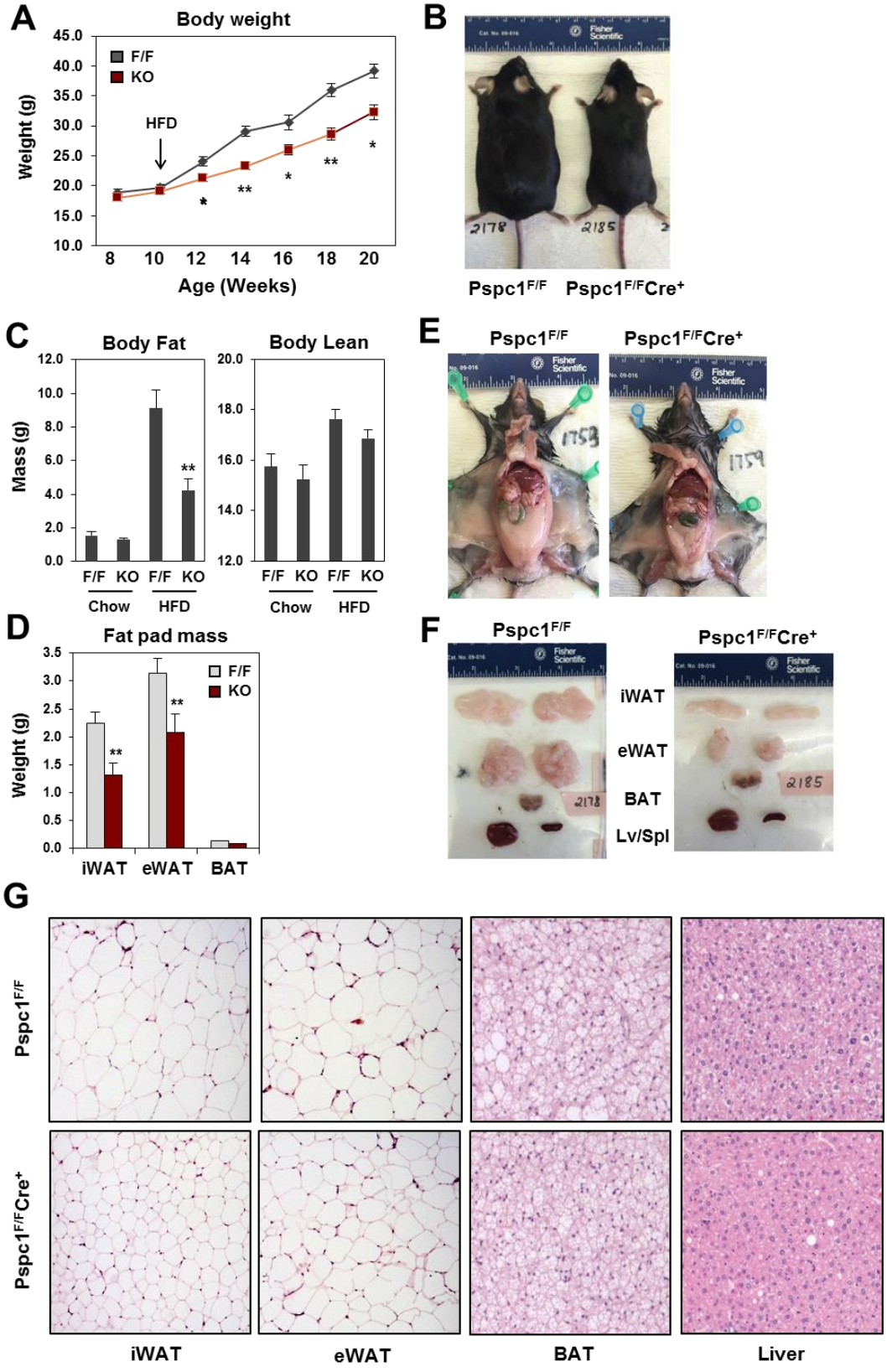

A
Body weight
F/F
KO
HFD
Weight (g)
Age (Weeks)
B
Pspc1F/F
Pspc1F/FCre+
C
Body Fat
Body Lean
Mass (g)
F/F KO F/F KO
Chow
HFD
D
Fat pad mass
Weight (g)
iWAT
eWAT
BAT
E
Pspc1F/F
Pspc1F/FCre+
F
Pspc1F/F
Pspc1F/FCre+
iWAT
eWAT
BAT
Lv/Spl
G
Pspc1F/F
Pspc1F/FCre+
iWAT
eWAT
BAT
Liver

Figure 7.2

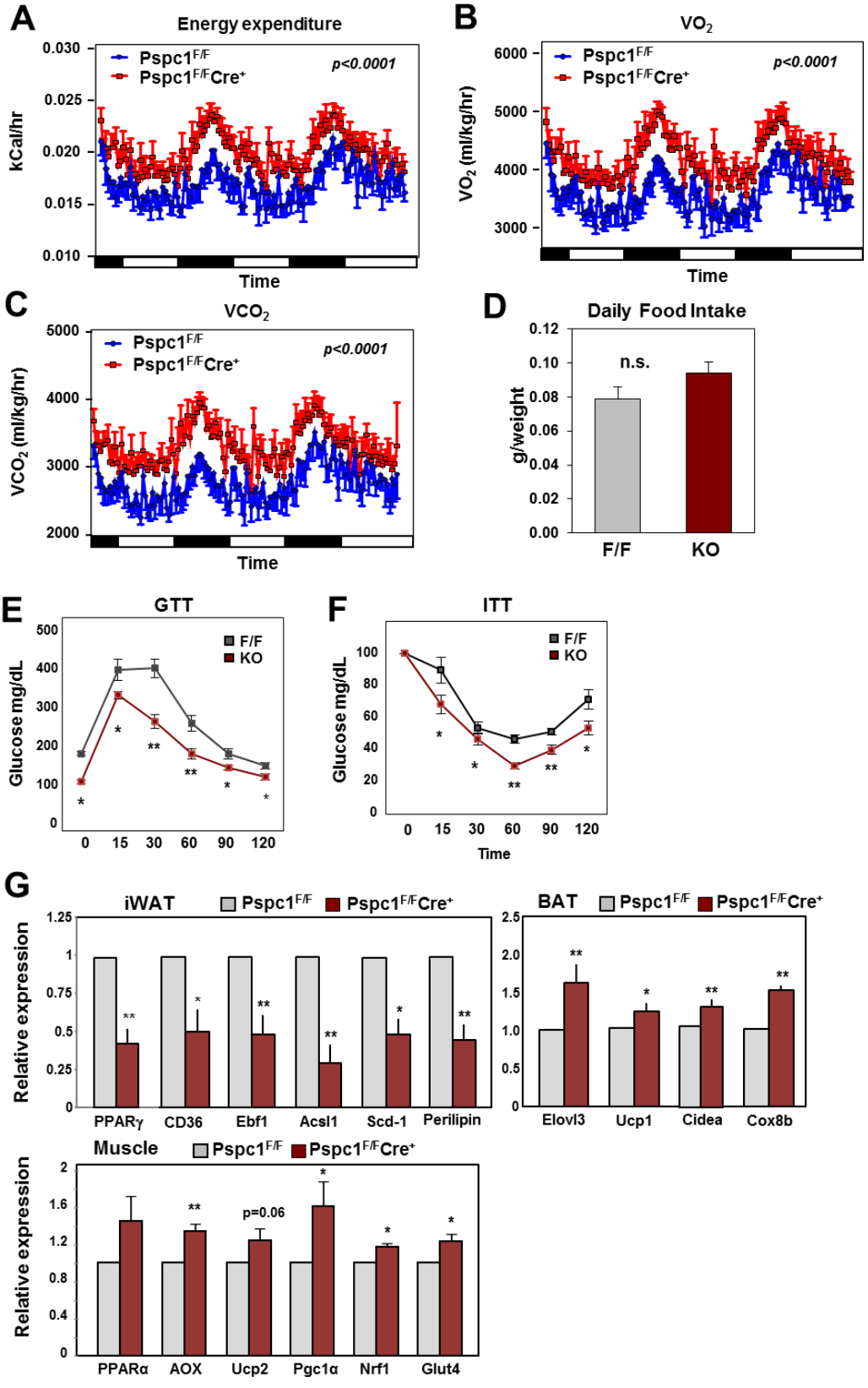

A
Energy expenditure
Pspc1F/F
Pspc1F/FCre+
p<0.0001
kCal/hr
Time
B
VO2
VO2 (ml/kg/hr)
C
VCO2
VCO2 (ml/kg/hr)
D
Daily Food Intake
n.s.
g/weight
F/F
KO
E
GTT
Glucose mg/dL
F
ITT
G
iWAT
BAT
Muscle
Relative expression
PPARγ
CD36
Ebf1
Acsl1
Scd-1
Perilipin
Elovl3
Ucp1
Cidea
Cox8b
PPARα
AOX
Ucp2
Pgc1α
Nrf1
Glut4
p=0.06

Figure 7.3

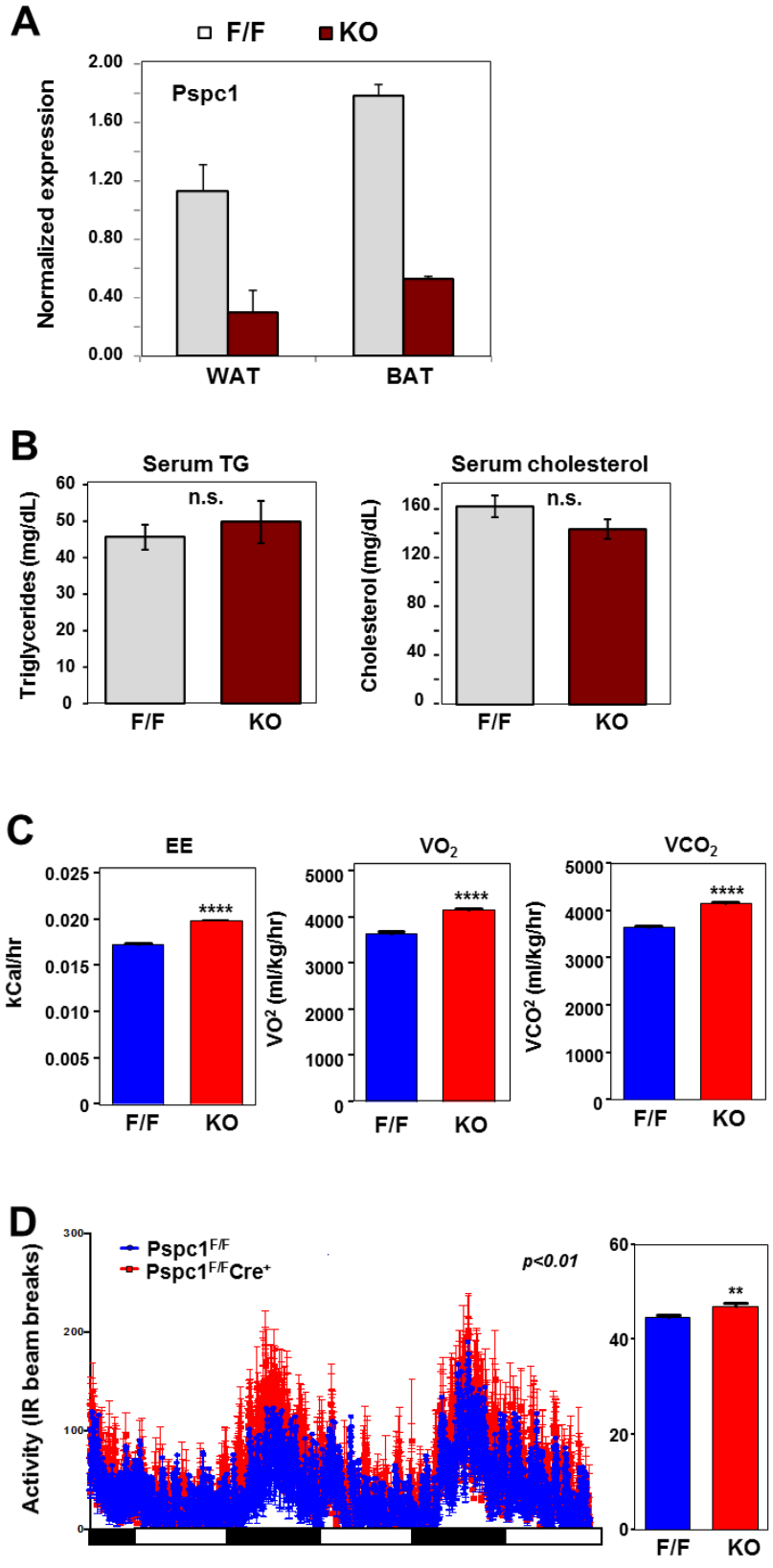

A
F/F
KO
Pspc1
Normalized expression
2.00
1.60
1.20
0.80
0.40
0.00
WAT
BAT
B
Serum TG
n.s.
Triglycerides (mg/dL)
60
50
40
30
20
10
0
F/F
KO
Serum cholesterol
n.s.
Cholesterol (mg/dL)
160
120
80
40
0
F/F
KO
C
EE
kCal/hr
0.025
0.020
0.015
0.010
0.005
0
****
F/F
KO
VO2
VO2 (ml/kg/hr)
5000
4000
3000
2000
1000
0
****
F/F
KO
VCO2
VCO2 (ml/kg/hr)
5000
4000
3000
2000
1000
0
****
F/F
KO
D
Activity (IR beam breaks)
300
200
100
0
Pspc1F/F
Pspc1F/FCre+
p<0.01
60
40
20
0
**
F/F
KO

Table 1

Function/Type (number)	Protein Name
Protein synthesis (5)	Eif2ak3, ribosomal protein L9 (RPL9), RPL13, RPL12, RPL4
RNA transport (2)	Ddx3x, Purb
preRNA processing (2)	Ptbp1, hnRNPh2
Other RNA associated (6)	SFPQ, NONO, Pabpc4, Ybx1, Igf2bp1, Igf2bp2

Table 2

Pspc1	F	ATGCAGAAAACTCAACAGTACCAT
	R	AATGTCCCAGGTTGAGCAAA
36B4	F	AGATGCAGCAGATCCGCAT
	R	GTTCTTGCCCATCAGCACC
aP2	F	CACCGCAGACGACAGGAAG
	R	GCACCTGCACCAGGGC
Adiponectin	F	CCGGAACCCCTGGCAG
	R	CTGAACGCTGAGCGATACACA
CD36	F	TTGAAAAGTCTCGGACATTGAG
	R	TCAGATCCCAACACAGCGTA
PPARγ	F	AACTCTGGGAGATTCTCCTGTTGA
	R	TGGTAATTTCTTGTGAAGTGCTCATA
Perilipin	F	CCATCTCTACCCGCCTTCG
	R	CTTGTCAGAGGTGCTTGCAATG
C/EBPα	F	GCGGGCAAAGCCAAGAA
	R	GCGTTCCCGCCGTACC
Nono	F	CCCCACCAATACCTGCAA
	R	TTCAGGTCAATAGTCAAGCCTTC
Sfpq	F	TGGTGGCATAGGTTATGAAGC
	R	CCAAAGCGCTCAGTACGC
Neat1	F	ACCCTTTTTCATGGGGGTAG
	R	GCTGGATGGAGGCTTGTTTA
Glut4	F	ATGAGAAACGGAAGTTGGAGAGA
	R	GTGGGTGCGGCTGCC
Pgc1α	F	GAAAAGGCCAAACAGAGAGA
	R	GTAAATCACACGGCGCTCTT

Table 2 Continued

Acsl1	F	CCACCATCTTCCCTGTGG
	R	GGAAGTGTTTGCTTGTCCAAA
Scd1	F	TTCCCTCCTGCAAGCTCTAC
	R	CAGAGCGCTGGTCATGTAGT
Ebf1	F	GGGATGATGGGTGTGAACTC
	R	GAGTTGCGGGTGAAACCTT
Lpl	F	TTTGTGAAATGCCATGACAAG
	R	CAGATGCTTTCTTCTCTTGTTTGT
Fasn	F	TGCTCCCAGCTGCAGGC
	R	GCCCGGTAGCTCTGGGTGTA
Ucp1	F	GGCCTCTACGACTCAGTCCA
	R	TAAGCCGGCTGAGATCTTGT
MyoD1	F	AGCACTACAGTGGCGACTCA
	R	GGCCGCTGTAATCCATCAT
LXRβ	F	CAGGAGATTGTGGACTTTGC
	R	TTGTAGCGTCTGGCTGTTTC
Ddx3x	F	GGAAGTGGATCAAGGGGAAG
	R	CAAATTTGCCAAAGCCACTT
PPARα	F	CCGAGGGCTCTGTCATCA
	R	GGGCAGCTGACTGAGGAA
AOX	F	TGGCCAAGGCGACCTG
	R	AAGCCTTCAGCCCAGCTGT
Ucp2	F	CCCTAATGGCTGCCTACCAA
	R	GGGTCCAGGTCAGCATGG
Nrf1	F	GCAGCACCTTTGGAGAATGTG
	R	GCCAGAGCAGACTCGAGGTC

Materials and Methods

Reagents and Plasmids—Dexamethasone (D2915), 3-isobutyl-1-methylxanthine (IBMX, I7018), PPARγ agonist GW1929 (G5668), and actinomycin D (A1410) were from Sigma-Aldrich. Insulin (12585-014) was from Gibco. Pspc1 shRNA sequences were designed using BLOCK-iT RNAi designer tool (Invitrogen). Sense and antisense oligos were annealed and cloned into pENTR/U6 plasmid (Invitrogen). Using LR recombination (Invitrogen), shRNA constructs were subcloned into a Gateway-adapted pBabe-Puro plasmid. The following shRNA oligos were used: lacZ shRNA CACCGGGCCAGCTGTATAGACATCTCGAAAGATGTCTATACAGCTGGCCC; Pspc1 shRNA1 CACCGGTTGTTTCCAATGAGCTTCTCGAAAGAAGCTCATTGGAAACAACC; Pspc1 shRNA2 CACCGCGGCTTTAAACCAAACTATACGAATATAGTTTGGTTTAAAGCCGC; Pspc1 and shRNA3 CACCGCAAATATGGGAACTCCAATGCGAACATTGGAGTTCCCATATTTGC. Only sense strands are shown here. ON-TARGETplus mouse Ddx3x siRNA SMARTpool (L-043597) and Non-targeting Pool (D-001810) were from Dharmacon. Adenovirus was amplified, purified and tittered by Viraquest Inc.

Cell Culture—Murine preadipocyte cell lines 3T3-L1 and 3T3-F442A, and murine fibroblast cell line NIH-3T3 were cultured in DMEM supplemented with 10% bovine calf serum (BCS). 10T1/2 preadipocytes were cultured in DMEM with 10% fetal bovine serum (FBS). For *in vitro* differentiation, preadipocytes were grown to confluence in DMEM with 10% FBS plus insulin (5 μg/ml). Confluent cells were induced to differentiate with dexamethasone (1 μM), IBMX (0.5

μM), insulin (5 μg/ml), and GW1929 for 2 days, followed by insulin and GW1929 alone. Growth media was exchanged every 2 days during the course of differentiation. All stable cells were generated using the pBabe retroviral system [24]. Retrovirus was obtained by transfection of Phoenix E cells with the pBabe vector and harvest of growth media 72 h later. Preadipocytes were transduced with retrovirus overnight and selected with particular antibiotics. For RNA stability studies, differentiated adipocytes were treated with actinomycin D (4 μg/ml). RNA samples were collected before and at multiple time points after the treatment.

Gene Expression Analysis—Total RNA was isolated using TRIzol reagent (Invitrogen) and reverse transcribed with the iScript cDNA synthesis kit (Biorad). cDNA was quantified by real-time PCR using SYBR Green Master Mix (Diagenode) on an ABI 7900 instrument. Gene expression levels were determined by using a standard curve. Each gene was normalized to the housekeeping gene 36B4 and was analyzed in duplicate. Primers used for real-time PCR are listed in Table 2.

Protein Analysis—Whole cell lysate was extracted using RIPA lysis buffer (Boston Bioproducts) supplemented with complete protease inhibitor cocktail (Roche). Proteins were diluted in Nupage loading dye (Invitrogen), heated at 95°C for 5 min, and run on 4–12% NuPAGE Bis-Tris Gel (Invitrogen). Proteins were transferred to hybond ECL membrane (GE Healthcare) and blotted with Pspc1 (ab115184, Abcam), PPARγ (81B8, Cell Signaling), Ebf1 (ab108369, Abcam), Scd1 (sc14719, Santa Cruz), Acsl1 (4047S, Cell Signaling), Nono (N8789, Sigma), Ddx3x (ab37160, Abcam), Ppm1b (A300-887A, Bethyl Labs), V5 (R960-25,

Invitrogen), Hmg1 (ab18256, Abcam), actin (A2066, Sigma), αTubulin (CP06, Calbiochem) antibodies.

Chromatin Immunoprecipitation (ChIP) —ChIP assays were performed according to a standard protocol [4]. Briefly, following formaldehyde cross-linking, cells were lysed and sonicated using Bioruptor (Diagenode) according to the manufacturer's protocol. Chromatin was immunoprecipitated with antibodies against PPARγ (sc7196, Santa Cruz) and RXR (sc774, Santa Cruz) overnight at 4°C in the presence of Protein A/G PLUS agarose beads (Santa Cruz). After reversal of cross-linking, DNA was extracted and DNA enrichment was quantified by real-time PCR. Primers used for this study are as follows: Pspc1 –0.2kb forward TGG AGG AGG GGG TTG TTT TG, Pspc1 –0.2kb reverse CCG GAG GGT CGA AAG CTA AG; βGlobin forward TGG TAG CCT CAG GAG CTT GC, βGlobin reverse ATC CAA GAT GGG ACC AAG CTG. Occupancy was quantified using a standard curve and normalized to input DNA.

Individual Nucleotide Resolution Cross-linking and Immunoprecipitation (iCLIP) and High-throughput Sequencing—iCLIP assays were performed according to a modified iCLIP protocol [12, 25]. Briefly, 10T1/2 cells expressing Flag-Pspc1 were irradiated with 254nm UV-C light at 800 mJ/cm^2 on ice to covalently cross-link proteins to nucleic acids. Upon cell lysis, Protein–RNA complexes were immunoprecipitated with anti-Flag M2 antibody (F1804, Sigma) immobilized on Dynabeads Protein G (10003D, Novex) overnight. After high-salt stringent washing, RNAs on beads were partially fragmented using low concentrations of micrococcal nuclease (M0247S, NEB), ligated to an RNA adaptor at the 3′ end, and radioactively labeled on the 5′ end. Protein-RNA complexes were eluted using 3X Flag peptides (F4799, Sigma) and then

run on 4–12% NuPAGE Bis-Tris Gel (Invitrogen). After transfer to a nitrocellulose membrane, protein–RNA complexes in the range of 20–40 kDa above Flag-Pspc1 were recovered and digested with proteinase K to isolate RNA. Reverse transcription was done with SuperScript III Reverse Transcriptase (18080044, Invitrogen), using primers containing two inversely oriented adaptor regions separated by a *Bam*HI site as well as a 3-nt barcode to mark individual cDNA molecules. cDNAs were size-purified using denaturing gel electrophoresis, circularized by CircLigase II ssDNA ligase (CL9021K, Epicentre), and linearized by FastDigest *Bam*HI (FD0054, Thermo Scientific). Linearized cDNAs were then PCR-amplified and subjected to high-throughput sequencing (single end 100 nt) using Illumina HiSeq2000 at UCLA Broad Stem Cell Research Center High Throughput Sequencing Core.

iCLIP-seq Data Analysis—CLIP-seq reads were trimmed to remove adaptor sequences and categorized according to different barcodes. To eliminate redundancies created by PCR duplicates, all reads with identical adaptor sequence were considered a single read. Quality control check was applied to all the trimmed reads using the FastQC tool from Babraham Bioinformatics. CLIP-seq reads were mapped to the mouse genome (NCBI37/mm9) using the TopHat alignment pipeline on UCLA Galaxy platform with parameters set to search for unique alignment, with < 2 mismatches, with no indels. Mapped reads were then subjected to the CLIP-seq cluster finding algorithm, CLIPper, to call significant (FDR < 0.05, P < 0.05) clusters [14]. Significant clusters were uploaded onto UCSC genome browser as custom annotation tracks. Read distribution over the genome was analyzed using the RSeQC tool [26]. De novo motif search was performed using the Homer's findMotifsGenome program with parameters -rna -S 10 -len 4,5,6 -size given -h -nlen 0 –noweight. Background sequences were from CLIP-seq reads of

the experimental control library [15]. Pathway analysis on CLIP-identified Pspc1 target genes was done using the DAVID Bioinformatics Database v6.7 [27].

Co-immunoprecipitation (Co-IP) and Mass Spectrometry—Cells expressing Flag-Pspc1 were lysed with ice-cold lysis buffer containing 50 mM Tris-HCl pH 7.5, 150 mM NaCl, 0.6% Triton X-100, plus complete protease inhibitor (Roche). Cell lysates were pre-cleared with empty Protein A/G PLUS agarose beads (Santa Cruz) and then immunoprecipitated with beads prelinked with anti-Flag M2 antibody (F1804, Sigma) overnight at 4°C. Beads were washed with 50 mM Tris-HCl pH 7.5, 150 mM NaCl, and 0.1% Triton X-100, then eluted with 3X Flag peptides (F4799, Sigma). In specific experiments, RNase cocktail enzyme (AM2286, Ambion) was used to treat cell lysates before immunoprecipitation. IP Eluents from Flag-Pspc1 cells and control cells were processed by UCLA Pasarow Mass Spectrometry Laboratory. Nano-liquid chromatography with data-dependent tandem mass spectrometry was performed on an orbitrap mass spectrometer as described [28]. Results were analyzed using the Mascot software Matrix Sciences.

Subcellular Fractionation—Cells were washed with 1× PBS and incubated with TEN-buffer (10 mM Tris-HCl pH 7.5, 100 mM NaCl, 1 mM EDTA pH 8.0). Cells were allowed to swell on ice for 15 min in 10 mM HEPES, 10mM KCl, 0.1 mM EGTA, 0.1 mM EDTA, 1 mM DTT, plus complete protease inhibitor (Roche). Cells were then mixed with NP-40 alternative (Calbiochem) to a final concentration of 0.4%, incubated for 5 min, and centrifuged at 12,000 × *g* for 5 min. Supernatant was collected as the cytoplasmic fraction. Nuclear pellet was resuspended in 20 mM HEPES, 420 mM NaCl, 1.5 mM $MgCl_2$, 0.2 mM EDTA, 25% glycerol, 1 mM DTT, plus

complete protease inhibitor. After a 15-min incubation, nuclear extracts were spun at 12,000 × *g* for 5 min and the supernatant was saved for future analysis. For RNA analysis, all the buffers above were supplemented with 10 mM ribonucleoside-vanadyl complex (NEB) to inhibit ribonucleases. RNA was extracted from the nuclear and cytoplasmic fraction using Purelink RNA mini kit (Ambion).

Immunofluorescence—10T1/2 Cells were plated in gelatin-coated glass-bottom dishes (Mas Tek). At day 0 and day 6 of differentiation, cells were fixed with 4% paraformaldehyde in PBS. Cells were permeabilized with 0.1% Triton and treated with NH_4Cl to quench free aldehyde groups. Cells were then blocked with 5% normal goat serum (Vector Labs) and 1% bovine serum albumin (Sigma) in PBS for 30 min. Cells were incubated with V5 (R960-25, Invitrogen) or Psps1 (sc374181, Santa Cruz) antibody in blocking buffer overnight at 4°C. After washes, cells were incubated with Alexa Fluor 594–conjugated secondary antibody (A-21125, Invitrogen) for 1 h at room temperature and washed. Cells were stained with BODIPY 493/503 (Invitrogen) and/or DAPI (Invitrogen). Cells were visualized with LSM510 confocal laser scanning microscope (Carl Zeiss).

Animal Studies—For the preadipocyte transplantation study, 6-week old male NCr nude mice were acquired from Taconic. Mice were anesthetized using 2–3% isoflurane in O_2. 2×10^7 3T3-F442A preadipocytes were injected subcutaneously over the sternum, using an insulin syringe attached to a 28-gauge needle. The injection site was chosen due to the absence of endogenous subcutaneous fat. 5 weeks after the transplantation, newly formed subcutaneous fat pads were dissected, weighed, and processed for histological and gene expression analysis. A conditional-

potential knockout allele for *Pspc1* was generated using a "targeted trapping/conditional-ready" gene-targeting vector (*Pspc1*^{tm1a}) (Figure S6B). The targeting vector was electroporated into C57BL/6N ES cell line JM8.N4. Out of 12 validated targeted ES cell clones, a euploid clone (clone A11) was selected for *in vitro* Flp recombination. Flp recombinase excised the gene-trapping cassette within intron 1 of *Pspc1*, producing a conditional knockout allele containing a *loxP* site in intron 1 and a *loxP* site in intron 2. Genotyping was completed by amplification of the genomic region flanking loxP sites using the following primer pairs: forward acg tag ccc agg tag gta ttt cag g and reverse tgt aac aag atc tga tgt cct ctt ctg g (Figure S6C). 11 clones passed Flp testing, and clone A11_flp_A09 was selected and injected into Balb/c blastocysts to generate chimeric mice. High-percentage male chimeras were obtained, and were crossed to C57BL/6N mice to establish germline transmission. Homozygous *Pspc1*-floxed mice carrying the conditional-ready knockout allele were used for Adenovirus-Cre injection studies. For the adeno-Cre delivery to fat pads, 2×10^9 PFU of adenovirus was percutaneously injected into each inguinal fat depot of *Pspc1*$^{F/F}$ mice at 8 weeks of age. In each mouse, Ad-Cre was injected into iWAT on one side, and Ad-GFP was injected into the contralateral side as a control. 7 days after the injection, iWAT were resected for histological and gene expression analysis. Homozygous *Pspc1*-floxed mice were crossed with adiponectin-*Cre* mice to generate adipose-specific Pspc1-deficient mice. At 10 weeks of age, *Pspc1*$^{F/F}$ *Cre*+ mice and their *Pspc1*$^{F/F}$ littermates were fed a 60% high-fat diet (Research Diets, New Brunswick, NJ) for the indicated times. For glucose tolerance tests, mice were fasted for 6 hr and challenged with an i.p. injection of glucose (2 g/kg). For insulin tolerance tests, mice were fasted for 6 hr and given an i.p. injection of insulin (1 U/kg). Blood glucose levels were monitored using the ACCU-CHEK active glucometer (Roche). Body composition was determined by EchoMRI analysis. Indirect calorimetry was

performed using a Columbus Instruments Comprehensive Lab Animal Monitoring System (CLAMS, Columbus Instruments, Columbus, OH). Animals were placed individually in chambers for 3 consecutive days at ambient temperature (26.5°C) with 12 hr light/dark cycles. Animals had free access to food and water. Respiratory measurements were made in 20 min intervals after initial 6 hr acclimation period. Energy expenditure was calculated from VO_2 and RER using the Lusk equation, EE in cal/min = $(3.815 + 1.232 \times \text{RER}) \times VO_2$ in ml/min. Statistical significance for EE measurements was determined by using two-way ANOVA. Serum triglyceride and cholesterol were measured using Wako L-Type TG M test and Wako Cholesterol E test. Animal experiments were conducted in accordance with the UCLA Institutional Animal Care and Research Advisory Committee.

References

1. Waki, H., et al., *The small molecule harmine is an antidiabetic cell-type-specific regulator of PPAR gamma expression.* Cell Metabolism, 2007. **5**(5): p. 357-370.
2. Villanueva, C.J., et al., *TLE3 is a dual-function transcriptional coregulator of adipogenesis.* Cell Metab, 2011. **13**(4): p. 413-27.
3. Villanueva, C.J., et al., *Adipose Subtype-Selective Recruitment of TLE3 or Prdm16 by PPAR gamma Specifies Lipid Storage versus Thermogenic Gene Programs.* Cell Metabolism, 2013. **17**(3): p. 423-435.
4. Nielsen, R., et al., *Genome-wide profiling of PPARgamma:RXR and RNA polymerase II occupancy reveals temporal activation of distinct metabolic pathways and changes in RXR dimer composition during adipogenesis.* Genes Dev, 2008. **22**(21): p. 2953-67.
5. Fox, A.H., C.S. Bond, and A.I. Lamond, *P54nrb forms a heterodimer with PSP1 that localizes to paraspeckles in an RNA-dependent manner.* Mol Biol Cell, 2005. **16**(11): p. 5304-15.
6. Gernapudi, R., et al., *MicroRNA 140 Promotes Expression of Long Noncoding RNA NEAT1 in Adipogenesis.* Mol Cell Biol, 2015. **36**(1): p. 30-8.
7. Tontonoz, P., E.D. Hu, and B.M. Spiegelman, *Stimulation of Adipogenesis in Fibroblasts by Ppar-Gamma-2, a Lipid-Activated Transcription Factor.* Cell, 1994. **79**(7): p. 1147-1156.
8. Bond, C.S. and A.H. Fox, *Paraspeckles: nuclear bodies built on long noncoding RNA.* Journal of Cell Biology, 2009. **186**(5): p. 637-644.

9. Maris, C., C. Dominguez, and F.H.T. Allain, *The RNA recognition motif, a plastic RNA-binding platform to regulate post-transcriptional gene expression.* Febs Journal, 2005. **272**(9): p. 2118-2131.

10. Bandziulis, R.J., M.S. Swanson, and G. Dreyfuss, *Rna-Binding Proteins as Developmental Regulators.* Genes & Development, 1989. **3**(4): p. 431-437.

11. Konig, J., et al., *iCLIP - Transcriptome-wide Mapping of Protein-RNA Interactions with Individual Nucleotide Resolution.* Jove-Journal of Visualized Experiments, 2011(50).

12. Damianov, A., et al., *Rbfox Proteins Regulate Splicing as Part of a Large Multiprotein Complex LASR.* Cell, 2016. **165**(3): p. 606-19.

13. Trapnell, C., L. Pachter, and S.L. Salzberg, *TopHat: discovering splice junctions with RNA-Seq.* Bioinformatics, 2009. **25**(9): p. 1105-1111.

14. Lovci, M.T., et al., *Rbfox proteins regulate alternative mRNA splicing through evolutionarily conserved RNA bridges.* Nature Structural & Molecular Biology, 2013. **20**(12): p. 1434-1442.

15. Heinz, S., et al., *Simple Combinations of Lineage-Determining Transcription Factors Prime cis-Regulatory Elements Required for Macrophage and B Cell Identities.* Molecular Cell, 2010. **38**(4): p. 576-589.

16. Rocak, S. and P. Linder, *DEAD-box proteins: the driving forces behind RNA metabolism.* Nat Rev Mol Cell Biol, 2004. **5**(3): p. 232-41.

17. Jarmoskaite, I. and R. Russell, *RNA helicase proteins as chaperones and remodelers.* Annu Rev Biochem, 2014. **83**: p. 697-725.

18. Sharma, D. and E. Jankowsky, *The Ded1/DDX3 subfamily of DEAD-box RNA helicases.* Crit Rev Biochem Mol Biol, 2014. **49**(4): p. 343-60.

19. Soto-Rifo, R. and T. Ohlmann, *The role of the DEAD-box RNA helicase DDX3 in mRNA metabolism.* Wiley Interdiscip Rev RNA, 2013. **4**(4): p. 369-85.

20. Lai, M.C., Y.H.W. Lee, and W.Y. Tarn, *The DEAD-box RNA helicase DDX3 associates with export messenger ribonucleoproteins as well as tip-associated protein and participates in translational control.* Molecular Biology of the Cell, 2008. **19**(9): p. 3847-3858.

21. Yedavalli, V.S., et al., *Requirement of DDX3 DEAD box RNA helicase for HIV-1 Rev-RRE export function.* Cell, 2004. **119**(3): p. 381-92.

22. Sharma, D. and J. Bhattacharya, *Evolutionary constraints acting on DDX3X protein potentially interferes with Rev-mediated nuclear export of HIV-1 RNA.* PLoS One, 2010. **5**(3): p. e9613.

23. Tran, T.T. and C.R. Kahn, *Transplantation of adipose tissue and stem cells: role in metabolism and disease.* Nature Reviews Endocrinology, 2010. **6**(4): p. 195-213.

24. Hummasti, S. and P. Tontonoz, *The peroxisome proliferator-activated receptor N-terminal domain controls isotype-selective gene expression and adipogenesis.* Mol Endocrinol, 2006. **20**(6): p. 1261-75.

25. Konig, J., et al., *iCLIP reveals the function of hnRNP particles in splicing at individual nucleotide resolution.* Nat Struct Mol Biol, 2010. **17**(7): p. 909-15.

26. Wang, L.G., S.Q. Wang, and W. Li, *RSeQC: quality control of RNA-seq experiments.* Bioinformatics, 2012. **28**(16): p. 2184-2185.

27. Huang, D.W., B.T. Sherman, and R.A. Lempicki, *Systematic and integrative analysis of large gene lists using DAVID bioinformatics resources.* Nature Protocols, 2009. **4**(1): p. 44-57.

28. Patananan, A.N., et al., *Non-repair pathways for minimizing protein isoaspartyl damage in the yeast Saccharomyces cerevisiae.* J Biol Chem, 2014. **289**(24): p. 16936-53.

Chapter 3

Discussion

Adipogenesis involves different levels of regulation, with the majority of known control factors exerting their effects at the transcriptional level. In the present study, we delineated a role for the RNA-binding protein Pspc1 in adipocyte differentiation. Pspc1 is a direct target of the master regulator PPARγ, and its expression is induced during differentiation. Complementary *in vitro* and *in vivo* analyses demonstrated that Pspc1 expression facilitates adipocyte-specific protein expression and adipogenesis. Deletion of Pspc1 in mature fat *in vivo* impairs adipocyte-specific gene expression and reduces adipose tissue mass and adipocyte size. Mechanistically, we showed that Pspc1 binds directly to a battery of adipose-specific mRNA transcripts *via* its two RRM domains. Pspc1 interacts with the RNA export factor Ddx3x and translocates from the nucleus to the cytoplasm during the course of differentiation, thereby enhancing the nuclear export of its target transcripts. Loss of Pspc1 expression in adipose tissue in vivo compromises adipocyte development and lipid storage and affects the development of diet-induced obesity and insulin resistance.

Pspc1 initially emerged as the defining protein for paraspeckles, which are one of the most newly identified subnuclear bodies located in the interchromatin space. They are RNA-protein structures composed of a long noncoding RNA Neat1 and three core protein components from the DBHS protein family: Pspc1, Nono, and Sfpq[1]. Numerous studies had been done on Nono and Sfpq long before the identification of paraspeckle. Both of them are involved in many aspects of RNA production and processing including transcription initiation, transcriptional termination and splicing[2-6]. However, very little is known about the cellular function of Pspc1 except for its implicated role in coactivating androgen receptor during the process of spermatogenesis[7, 8]. Whether Pspc1 exhibits similar functions as its family members is also largely unknown. In the present study, we uncovered the least characterized paraspeckle

component Pspc1 to be a bona fide RNA binding protein that directly interacts and regulates a number of adipose-specific genes via a nuclear export mechanism. This provides new insights and deeper understanding of molecular function of this protein and its relation to biological processes.

Previous work has linked a small number of RNA-binding proteins to adipocyte differentiation, most of which appear to be involved in adipocyte-specific RNA splicing events. Alternatively spliced isoforms of the insulin receptor, lipin, nuclear receptor co-repressor 1, and preadipocyte factor 1 have all been associated with differentiation [9-12]. More recently, the alternative splicing factor Sam68 was found to regulate adipogenesis by modulating intron 5 retention in *mTOR* transcripts and isoform switching of ribosomal S6 kinase [13, 14]. The RNA-binding motif protein 4 (RBM4) has also been reported to regulate the splicing of several adipocyte-specific genes, including the insulin receptor, PPARγ, and Pref-1, thereby facilitating the development of the brown adipocyte lineage [15]. Apart from pre-mRNA splicing, whether other aspects of post-transcriptional RNA processing, such as mRNA export from the nucleus, mRNA turnover, and translation initiation are also regulated during adipogenesis has been unclear [16-18]. Furthermore, the importance of RNA processing factors for the development and function of adipose tissue *in vivo* has not been tested. Our data identify Pspc1-dependent maturation of adipocyte mRNAs a new control point in the differentiation process and show that this sequence-specific RNA-binding protein is critical for adipocyte gene expression in mice.

One function previously assigned to paraspeckles is the nuclear retention of hyperedited RNA transcripts that contain double-stranded regions formed by inverted repeat elements (Alu repeats). dsRNA structures are generally subject to adenosine-to-inosine (A-to-I) editing and retained within paraspeckles in the nucleus, rather than being exported to the cytoplasm for

translation [19]. Despite being discovered as an antiviral mechanism, A-to-I RNA editing is revealed to be a widespread phenomenon in the human transcriptome, affecting thousands of genes[20]. More recent work found that the hyperedited region in the transcript of a mouse gene Slc7a2 is post-transcriptionally cleaved upon stress, enabling the release of the mRNA to cytoplasm followed by translation[21]. Another bioinformatic analysis identified hundreds of putative cleavage loci in the A-to-I edited repeats of human and mouse transcripts [22]. However, the biological impact and significance of this widespread phenomenon is still elusive. One study reported a link between paraspeckle function and cellular differentiation, showing that paraspeckle formation increases during human embryonic stem cell differentiation and modulates nuclear RNA retention [23]. Here we showed that Pspc1 facilitates the nuclear export of its target mRNA transcripts during the course of adipocyte differentiation. As a core component of paraspeckles, Pspc1 may participate in the nuclear retention of particular RNA transcripts and their subsequent release in response to the appropriate cellular cues. One possibility is that in the preadipocyte state certain adipose-specific hyperedited transcripts are retained within paraspeckles in the nucleus, as they are not yet functionally needed for the cell. Upon induction to differentiate, Pspc1 is responsible for the release and accelerated export of these retained transcripts from the nucleus, allowing for their entry into cytoplasm followed by translation. This proposes a new paradigm for the role of RNA nuclear retention and release in regulating gene expression in a physiologically relevant context.

In an effort to better understand how paraspeckle complexes may contribute to adipogenesis, we purified Pscp1-containing complexes from preadipocytes and adipocytes. IP-mass spectrometry analysis identified a number of adipocyte-specific Pspc1 interaction partners, including Ddx3x. These findings imply that under specific cellular contexts, the core paraspeckle

components may recruit different interaction proteins to the complex to accomplish tissue-specific functions. Ddx3x belongs to the DEAD-box RNA helicase family, which has been implicated in many aspects of RNA metabolism, including transcription, mRNA splicing, and RNA export [24]. Recent studies have highlighted the ability of Ddx3x to shuttle between nucleus and cytoplasm and pointed to a role for Ddx3x in the RNA nuclear export pathway [25-27]. However, previous work did not address the possibility that Ddx3x might facilitate export of a specific subset of messenger ribonucleoproteins. In the present study, we demonstrated that Pspc1 interacts with Ddx3x in adipocytes but not in preadipocytes, and that this is associated with the maturation of a subset of adipocyte mRNAs. Knocking down Ddx3x expression blunted the ability of Pspc1 to increase protein levels of its targets, strongly suggesting that Ddx3x is an important effector of Pscp1's actions in adipogenesis.

Although DBHS proteins have been characterized as nuclear proteins, some evidence points to potential roles for them in the cytoplasm. For example Pspc1, Nono, and Sfpq were isolated as part of an RNA-transporting granule in dendrites, suggesting a possible function in RNA transport in the cytoplasm. Interestingly, Ddx3x was also purified from this granule, supporting our finding of Ddx3x as an interaction partner of Pspc1 [28]. Another study showed that Nono shuttles to the cytoplasm during cell fusion [29]. In agreement with this work, we showed here that Pspc1 traffics from the nucleus to the cytoplasm during adipocyte differentiation using biochemical and cell biological approaches. Moreover, the translocation of Pspc1 to the cytoplasm was linked to the increased expression of a battery of adipose-specific proteins, including the key transcription factor Ebf-1. These results not only outline a new function for Pspc1, but also highlight an additional layer of regulatory complexity in the process of adipocyte development.

Reciprocal interactions exist between members of the DBHS protein family, and they have been found to form homo- and heterodimers *in vivo* [19]. Their interaction and common location in paraspeckles raise the question as to whether Pspc1 acts independently or in a complex with the other paraspeckle components in adipogenesis. Our immunoprecipitation studies indicated that Pspc1 indeed forms heterodimers with Nono and Sfpq during adipogenesis, with a stronger interaction observed in mature adipocytes than in preadipocytes (Figure 4B). Furthermore, we observed translocation of Nono along with Pspc1 to the cytoplasm upon adipocyte differentiation (Figure 4D), consistent with the possibility that paraspeckle proteins may function together in promoting mRNA maturation. However, ectopic expression of neither Nono nor Sfpq alone was able to facilitate adipocyte differentiation, suggesting that either Pspc1 may act independently of Nono and Sfpq, or that levels of Pspc1 may be limiting during differentiation. The question of whether Pspc1 acts in concert with Nono and Sfpq or with the noncoding RNA Neat1 in adipocyte development remains to be addressed. Additional studies will also be required to dissect the precise molecular function(s) of Pspc1 in RNA maturation.

Adipose tissue plays a fundamental role in maintaining systemic metabolic homeostasis. To assess how loss of Pspc1 in fat might affect metabolic health we generated preadipcoytes and mice lacking *Pspc1*. Consistent with our *in vitro* data, we observed impaired adipose tissue development *in vivo* when preadipocytes expressed reduced amount of Pspc1 (Figure 6.1). Adipose Pspc1-deficient mice did not present with lipodystrophy on normal chow diet, indicating that Pspc1 function is not absolutely required for adipose tissue lipid storage. However, the mice were markedly resistant to high-fat diet-induced obesity, with diminished mass of both subcutaneous and visceral WAT (Figure 7.1). Histology revealed reduced adipocyte size, similar to that observed in heterozygous *PPARγ*-deficient mice [30]. Furthermore, despite their apparent

reduced adipose tissue lipid storage capacity, adipose Pspc1-deficient mice did not show expected systemic consequences of profound lipodystrophy; rather, loss of adipose Pspc1 in a high-fat diet fed state resulted in improved glucose tolerance and insulin sensitivity.

Previous studies have found that impairment of mature adipocyte function, including alterations in lipogenesis and lipolysis, can provoke compensatory responses in other metabolic tissues [31, 32]. For example, such compensatory effects have been observed with PPARγ hypomorphic mice. Despite being lipodystrophic, these mice exhibit relatively benign metabolic consequences due to induction of a gene expression program in muscle that enables efficient oxidation of excess lipids [33]. A second aP2-Cre driven PPARγ knockout model also demonstrated improved glucose tolerance on high-fat diet, possibly due to a compensatory increase in hepatic glucose disposal [34]. Consistent with these findings, we observed that loss of Pspc1 expression in fat led to an increase in genes linked to thermogenesis in BAT and fatty acid utilization in skeletal muscle. Increased expression of skeletal muscle Glut4 further suggests that enhanced muscle glucose uptake is likely to contribute to improved glucose tolerance and insulin sensitivity.

References

1. Fox, A.H., et al., *Paraspeckles: A novel nuclear domain.* Current Biology, 2002. **12**(1): p. 13-25.
2. Patton, J.G., et al., *Cloning and characterization of PSF, a novel pre-mRNA splicing factor.* Genes Dev, 1993. **7**(3): p. 393-406.
3. Yang, Y.S., et al., *NonO, a non-POU-domain-containing, octamer-binding protein, is the mammalian homolog of Drosophila nonAdiss.* Mol Cell Biol, 1993. **13**(9): p. 5593-603.
4. Peng, R., et al., *PSF and p54nrb bind a conserved stem in U5 snRNA.* RNA, 2002. **8**(10): p. 1334-47.
5. Kaneko, S., et al., *The multifunctional protein p54nrb/PSF recruits the exonuclease XRN2 to facilitate pre-mRNA 3' processing and transcription termination.* Genes Dev, 2007. **21**(14): p. 1779-89.
6. Kameoka, S., P. Duque, and M.M. Konarska, *p54(nrb) associates with the 5' splice site within large transcription/splicing complexes.* EMBO J, 2004. **23**(8): p. 1782-91.
7. Kuwahara, S., et al., *PSPC1, NONO, and SFPQ are expressed in mouse Sertoli cells and may function as coregulators of androgen receptor-mediated transcription.* Biol Reprod, 2006. **75**(3): p. 352-9.
8. Myojin, R., et al., *Expression and functional significance of mouse paraspeckle protein 1 on spermatogenesis.* Biol Reprod, 2004. **71**(3): p. 926-32.
9. Entingh, A.J., C.M. Taniguchi, and C.R. Kahn, *Bi-directional regulation of brown fat adipogenesis by the insulin receptor.* Journal of Biological Chemistry, 2003. **278**(35): p. 33377-33383.

10. Peterfy, M., J. Phan, and K. Reue, *Alternatively spliced lipin isoforms exhibit distinct expression pattern, subcellular localization, and role in adipogenesis.* Journal of Biological Chemistry, 2005. **280**(38): p. 32883-32889.

11. Goodson, M.L., et al., *Alternative mRNA Splicing of Corepressors Generates Variants That Play Opposing Roles in Adipocyte Differentiation.* Journal of Biological Chemistry, 2011. **286**(52): p. 44988-44999.

12. Mei, B.S., et al., *Only the large soluble form of preadipocyte factor-1 (Pref-1), but not the small soluble and membrane forms, inhibits adipocyte differentiation: role of alternative splicing.* Biochemical Journal, 2002. **364**: p. 137-144.

13. Huot, M.E., et al., *The Sam68 STAR RNA-binding protein regulates mTOR alternative splicing during adipogenesis.* Mol Cell, 2012. **46**(2): p. 187-99.

14. Song, J. and S. Richard, *Sam68 Regulates S6K1 Alternative Splicing during Adipogenesis.* Mol Cell Biol, 2015. **35**(11): p. 1926-39.

15. Lin, J.C., W.Y. Tarn, and W.K. Hsieh, *Emerging role for RNA binding motif protein 4 in the development of brown adipocytes.* Biochimica Et Biophysica Acta-Molecular Cell Research, 2014. **1843**(4): p. 769-779.

16. Hu, Y.J., et al., *Transcriptional and post-transcriptional control of adipocyte differentiation by Jumonji domain-containing protein 6.* Nucleic Acids Research, 2015. **43**(16): p. 7790-7804.

17. Yu, H.Y., et al., *Stk40 represses adipogenesis through translational control of CCAAT/enhancer-binding proteins.* Journal of Cell Science, 2015. **128**(15): p. 2881-2890.

18. Cho, H., et al., *Staufen1-Mediated mRNA Decay Functions in Adipogenesis.* Molecular Cell, 2012. **46**(4): p. 495-506.

19. Fox, A.H. and A.I. Lamond, *Paraspeckles.* Cold Spring Harbor Perspectives in Biology, 2010. **2**(7).

20. Levanon, E.Y., et al., *Systematic identification of abundant A-to-I editing sites in the human transcriptome.* Nat Biotechnol, 2004. **22**(8): p. 1001-5.

21. Prasanth, K.V., et al., *Egulating gene expression through RNA nuclear retention.* Cell, 2005. **123**(2): p. 249-263.

22. Osenberg, S., et al., *Widespread cleavage of A-to-I hyperediting substrates.* RNA, 2009. **15**(9): p. 1632-9.

23. Chen, L.L. and G.G. Carmichael, *Altered nuclear retention of mRNAs containing inverted repeats in human embryonic stem cells: functional role of a nuclear noncoding RNA.* Mol Cell, 2009. **35**(4): p. 467-78.

24. Rocak, S. and P. Linder, *DEAD-box proteins: the driving forces behind RNA metabolism.* Nat Rev Mol Cell Biol, 2004. **5**(3): p. 232-41.

25. Lai, M.C., Y.H.W. Lee, and W.Y. Tarn, *The DEAD-box RNA helicase DDX3 associates with export messenger ribonucleoproteins as well as tip-associated protein and participates in translational control.* Molecular Biology of the Cell, 2008. **19**(9): p. 3847-3858.

26. Yedavalli, V.S., et al., *Requirement of DDX3 DEAD box RNA helicase for HIV-1 Rev-RRE export function.* Cell, 2004. **119**(3): p. 381-92.

27. Sharma, D. and J. Bhattacharya, *Evolutionary constraints acting on DDX3X protein potentially interferes with Rev-mediated nuclear export of HIV-1 RNA.* PLoS One, 2010. **5**(3): p. e9613.

28. Kanai, Y., N. Dohmae, and N. Hirokawa, *Kinesin transports RNA: isolation and characterization of an RNA-transporting granule.* Neuron, 2004. **43**(4): p. 513-25.

29. Zolotukhin, A.S., et al., *PSF acts through the human immunodeficiency virus type 1 mRNA instability elements to regulate virus expression.* Mol Cell Biol, 2003. **23**(18): p. 6618-30.

30. Kubota, N., et al., *PPAR gamma mediates high-fat diet-induced adipocyte hypertrophy and insulin resistance.* Mol Cell, 1999. **4**(4): p. 597-609.

31. Lodhi, I.J., et al., *Inhibiting adipose tissue lipogenesis reprograms thermogenesis and PPARgamma activation to decrease diet-induced obesity.* Cell Metab, 2012. **16**(2): p. 189-201.

32. Polak, P., et al., *Adipose-specific knockout of raptor results in lean mice with enhanced mitochondrial respiration.* Cell Metab, 2008. **8**(5): p. 399-410.

33. Koutnikova, H., et al., *Compensation by the muscle limits the metabolic consequences of lipodystrophy in PPAR gamma hypomorphic mice.* Proc Natl Acad Sci U S A, 2003. **100**(24): p. 14457-62.

34. Jones, J.R., et al., *Deletion of PPARgamma in adipose tissues of mice protects against high fat diet-induced obesity and insulin resistance.* Proc Natl Acad Sci U S A, 2005. **102**(17): p. 6207-12.

Appendix

Adipose subtype–selective recruitment of TLE3 or Prdm16 by PPARγ specifies lipid-storage *versus* thermogenic gene programs

Claudio J. Villanueva[1,2,9], Laurent Vergnes[3], Jiexin Wang[1,2], Brian G. Drew[4,5], Cynthia Hong[1,2], Yiping Tu[4,6], Yan Hu[4,6], Xu Peng[7], Feng Xu[7], Enrique Saez[8], Kevin Wroblewski[1,2], Andrea L. Hevener[4,5], Karen Reue[3], Loren G. Fong[4,6], Stephen G. Young[3,4,6], and Peter Tontonoz[1,2]

[1]Howard Hughes Medical Institute and Departments of [2]Pathology and Laboratory Medicine, [3]Human Genetics and [4]Medicine, and Divisions of [5]Endocrinology and [6]Cardiology, University of California, Los Angeles, CA 90095, USA

[7]Growth, Development and Metabolism Programme, Brenner Center for Molecular Medicine, National University of Singapore, 30 Medical Drive, Singapore, 117609

[8]Department of Chemical Physiology, The Skaggs Institute for Chemical Biology, The Scripps Research Institute, La Jolla, CA 92037

[9]Current Address: Department of Biochemistry, University of Utah School of Medicine, Salt Lake City, UT, 84112-5650, USA.

Abstract

Transcriptional effectors of white adipocyte-selective gene expression have not been described. Here we show that TLE3 is a white-selective cofactor that acts reciprocally with the brown adipocyte-selective cofactor Prdm16 to specify lipid storage and thermogenic gene programs. Occupancy of TLE3 and Prdm16 on certain adipocyte promoters is mutually exclusive, due to the ability of TLE3 to disrupt the physical interaction between Prdm16 and PPARγ. When expressed at elevated levels in brown fat, TLE3 counters Prdm16, suppressing brown-selective genes and inducing white-selective genes, resulting in impaired fatty acid oxidation and adaptive thermogenesis. Conversely, mice lacking TLE3 selectively in adipose tissue show enhanced thermogenesis in inguinal white adipose depots and are protected from age-dependent deterioration of brown adipose tissue function. Our results suggest that the establishment of distinct adipocyte phenotypes with different capacities for thermogenesis and lipid storage is accomplished in part through the cell type–selective recruitment of TLE3 or Prdm16 to key adipocyte target genes.

Introduction

White and brown adipocytes are specialized for distinct functions. White adipocytes are optimized to store energy as triglycerides in large unilocular lipid droplets. In times of metabolic need, white adipocytes mobilize energy through hydrolysis of triglycerides and release of free fatty acids into the circulation (Zechner et al., 2009). White adipocytes express a battery of genes involved in lipid handling, triglyceride biosynthesis, triglyceride mobilization, and endocrine signaling (Coleman and Bell, 1980; Cook et al., 1987; Halaas et al., 1995; Kawamura et al., 1981). The importance of white adipose tissue function for systemic energy metabolism is highlighted by human and mouse models of lipodystrophy, which develop severe insulin resistance and hepatic steatosis (Chao et al., 2000; Reitman et al., 2000; Reue and Peterfy, 2000). These metabolic derangements are largely due to the inability to store lipid and the failure to secrete adipokines important for lipid and carbohydrate homeostasis, such as leptin and adiponectin (Shimomura et al., 1999; Yamauchi et al., 2001).

Brown adipocytes derive their color from their high mitochondrial content. Unlike white adipocytes, brown adipocytes store energy primarily to provide an intracellular fuel source for thermogenesis (Smith and Roberts, 1964). Brown adipose tissue is found predominantly in the interscapular region in mice and is highly vascularized and innervated (Cannon and Nedergaard, 2004; Rauch and Hayward, 1969). Although human infants have long been recognized to have significant brown adipose tissue depots, it has been debated whether adults have brown adipose tissue and whether it plays a role in thermogenesis (Lean et al., 1986). Recent studies using 2-fluorodeoxyfluoroglucose coupled with PET scanning have shown that humans have substantial brown adipose tissue in supraclavicular and paraspinal depots (Cypess et al., 2009; Mirbolooki et al., 2012; van Marken Lichtenbelt et al., 2009; Virtanen et al., 2009). During cold exposure,

brown adipose tissue executes a transcriptional program that promotes energy expenditure and thermogenesis. Induction of the mitochondrial uncoupling protein, UCP1, is critical for brown fat thermogenesis (Bouillaud et al., 1985; Jacobsson et al., 1985; Matthias et al., 2000).

Lineage-tracing studies suggest that subscapular brown adipose tissue and white adipose tissue are derived from distinct precursors (Atit et al., 2006; Seale et al., 2008). However, it has recently become clear that certain white adipose tissue depots exhibit plasticity with respect to their thermogenic capacity. Mice exposed to cold, β-adrenergic agonists, or thiazolidinediones adapt by increasing the expression of UCP1, Elovl3, Dio2, Cidea, and other brown adipocyte-selective factors in "brite" or "beige" cells, a discrete subpopulation of cells found in the white adipose tissue depots (Cousin et al., 1992; Ohno et al., 2012; Young et al., 1984). Understanding the processes involved in the adaptive reprogramming of white adipocytes to brown adipocytes has the potential to provide new therapeutic strategies to combat obesity and metabolic disease.

The transcriptional determinants of the white and brown adipocyte gene programs are incompletely understood. PPARγ is the master transcriptional regulator of white and brown fat differentiation, and mice deficient in PPARγ lack both types of adipose tissue (Barak et al., 1999; Rosen et al., 1999; Tontonoz et al., 1994a; Tontonoz et al., 1994b). Seminal studies by Spiegelman and colleagues identified the transcriptional cofactor Prdm16 as a key factor driving brown adipocyte lineage development (Kajimura et al., 2008; Seale et al., 2007). Prdm16 acts in concert with PPARγ and C/EBPs to promote the expression of brown-selective factors such as UCP-1, Cidea, Elovl3, and Dio2 (Kajimura et al., 2009; Seale et al., 2008). Another cofactor, PGC-1α is also preferentially expressed in brown adipose tissue and is highly induced in response to cold exposure (Puigserver et al., 1998). PGC-1α is particularly important for UCP-1 expression and mitochondrial oxidative metabolism in brown fat (Wu et al., 1999).

Relatively little is known about factors that specify white adipocyte-selective gene expression. In particular, it has been unclear whether white fat is a "default" transcriptional program that is executed by PPARγ in the absence of Prdm16 and PGC-1α, or whether there are white fat-selective counterparts to these brown-selective cofactors. Previously, we identified the groucho family member TLE3 as an adipogenic coregulator (Villanueva et al., 2011). Here we demonstrate that TLE3 is a white-selective PPARγ cofactor that enforces an opposing transcriptional program to Prdm16. TLE3 counters the brown fat program and promotes lipid storage by blocking the interaction of Prdm16 with PPARγ, thereby reducing the occupancy of Prdm16 on brown fat-selective genes. Mice expressing elevated levels of TLE3 in brown adipose tissue exhibit a phenotypic switch from brown to white, and mice deficient in TLE3 in adipose tissue show enhanced thermogenic capacity. Our results suggest that the brown and white fat phenotypes are accomplished in part through the cell type-selective recruitment of TLE3 or Prdm16 to key adipocyte target genes.

Results

Transient Expression of TLE3 During Brown Fat Differentiation

Previously, we identified TLE3 as cofactor for PPARγ that promotes the differentiation of white adipocytes (Villanueva et al., 2011). To investigate a potential role for TLE3 in brown adipose tissue gene expression, we analyzed protein expression during the differentiation of immortalized brown adipocytes. As expected, mRNA encoding PPARγ was induced during the first 2-days of differentiation, while that encoding UCP1 was induced later. TLE3 protein expression peaked on the first day of differentiation, but eventually declined as differentiation proceeded (Fig. 1A). The induction of TLE3 protein expression coincided with induction of the mRNA encoding aP2, an adipocyte marker highly induced in both white and brown fat differentiation (Fig. 1B). By contrast, mRNA encoding the brown adipocyte marker Cidea was induced later during the course of differentiation. As we had previously observed in 3T3-L1 white preadipocytes (Villanueva et al., 2011), *Tle3* expression was also induced by the PPARγ agonist rosiglitazone in brown preadipocytes. Stimulators of brown fat-selective gene expression such as norepinephrine (NE), thyroid hormone (T3), bezafibrate (PPARα agonist), and (β-adrenergic agonists (CL-316,243, isoproterenol) did not alter TLE3 mRNA or protein expression (Fig. S1A,B). Interestingly, TLE3 protein expression in mice was markedly higher in white adipose tissue (WAT) than in brown adipose tissue (BAT) (Fig. 1C).

Forced TLE3 Expression in Brown Preadipocytes Promotes Differentiation and Lipid storage

To examine the role of TLE3 in brown fat cell differentiation, we generated stable cell pools by retroviral expression (Fig. 1D). Western blot analysis of brown preadipocytes confirmed overexpression of TLE3 protein (Fig. 1D). Forced expression of TLE3 in brown

preadipocytes increased lipid storage as measured by Oil-Red-O (ORO) and BODIPY staining (Fig. 1E). Gene-expression analysis revealed that mRNAs encoding PPARγ and its downstream targets aP2, CD36, and perilipin were upregulated in TLE3-expressing cells, consistent with enhanced differentiation (Fig. 1F). Unexpectedly, however, the overall gene expression profile of TLE3-expressing brown adipocytes was more reminiscent of white adipocytes, with decreased expression of multiple brown fat-selective markers, including *Dio2* and *Cldn1* (Fig. 1F).

TLE3 Expression Promotes a Brown-to-White Phenotypic Switch

To test whether TLE3 expression might alter the brown adipose gene-expression program *in vivo*, we analyzed transgenic mice that selectively express TLE3 in adipose tissue (Villanueva et al., 2011). The level of TLE3 protein in the BAT of aP2-TLE3 Tg mice was substantially elevated, but comparable to the level normally observed in WAT (Fig. 2A). Interestingly, UCP-1 protein expression was correspondingly reduced in BAT from aP2-TLE3 Tg mice. Analysis of subscapular brown adipose tissue revealed a marked phenotypic change in the BAT from aP2-TLE3 Tg mice (Fig. 2B). Grossly, the tissue was paler than that from WT animals, suggesting higher lipid content (Fig. 2B). Histologically, BAT from aP2-TLE3 Tg mice showed increased numbers of cells with large unilocular lipid droplets, a feature more characteristic of WAT (Fig. 2B). We speculated that the increased lipid storage in BAT of aP2-TLE3 Tg mice might negatively impact thermogenic capacity. Indeed, BAT expressing WAT levels of TLE3 exhibited reduced rates of fatty acid oxidation, despite preserved rates of fatty acid uptake compared to controls (Fig. 2C). To determine whether cellular energetics were altered, we performed real time respirometry (using the Seahorse extracellular flux analyzer). Retroviral expression of TLE3 in brown preadipocytes led to a reduced rate of oxygen consumption and

there was a trend towards a reduced rate of extracellular acidification (Fig. 2D). In accordance with these *in vitro* results, aP2-TLE3 Tg mice exhibited reduced energy expenditure when housed in metabolic cages (Fig. 2E). They also showed increased activity and reduced food intake (Fig. S2). To further test the functional consequences of the changes in BAT phenotype in aP2-TLE3 Tg mice, we challenged them with cold exposure at 4°C. aP2-TLE3 Tg mice had an impaired ability to respond to cold exposure compared to littermate control mice, as evidence by a marked drop in core body temperature (Fig. 2F). It is possible that the increased activity of the aP2-TLE3 mice may be a compensatory response to reduced thermogenesis.

Transcriptional Reprogramming of BAT by TLE3

The blunted thermogenic response of aP2-TLE3 Tg mice led us to hypothesize that TLE3 might be altering the BAT transcriptional response to cold exposure. We performed transcriptional profiling using Affymetrix GeneChip Mouse Gene 1.0 ST Arrays with BAT RNA isolated from control and aP2-TLE3 Tg mice at ambient temperature or after 5 h at 4^{o}C. Remarkably, as depicted by the Venn Diagram in Fig. 3A, 47% of the transcripts changed by more than twofold in response to TLE3 expression (aP2-TLE3 Tg versus WT) were also altered during cold exposure (WT RT versus WT 4 ^{o}C). Hierarchical clustering on entities revealed several classes of genes differentially expressed in BAT from aP2-TLE3 Tg and control mice (Fig. 3B; a high resolution image of the clustering results is provided in Fig. S3). Group 1 included genes minimally changed in WT mice in response to cold, but increased basally in aP2-TLE3 Tg mice. Group 2 included genes slightly upregulated in WT mice in response to cold in WT mice but strikingly upregulated in aP2-TLE3 Tg mice in response to cold. Groups 3 and 4 included genes upregulated by cold in WT mice that failed to be upregulated in aP2-TLE3 Tg

mice. Overall, these data are consistent with a markedly altered gene-expression response to thermal challenge in aP2-TLE3 Tg mice.

Subsequent validation of these results focused primarily on brown fat-selective genes implicated in thermogenesis, many of which were represented in Groups 3 and 4. Real-time PCR showed that mRNAs encoding Elovl3 and Dio2, enzymes involved in fatty acid elongation and thyroid hormone (T3) synthesis, respectively, failed to be induced in aP2-TLE3 Tg mice in response to cold challenge (Fig. 3C). We also identified a number of genes with no previous link to thermogenesis such as *Cldn1* and *Dhrs9* that were highly induced during cold exposure in WT mice but showed diminished response in the setting of TLE3 expression. Notably, however, not all thermogenic genes were altered between the genotypes; WT and aP2-TLE3 Tg mice exhibited similar levels of mRNA encoding PGC-1α at room temperature and during cold exposure (Fig. 3C).

We also validated a number of genes from Group 1 whose expression was unresponsive to cold, but generally increased in aP2-TLE3 Tg mice (Fig. 3D). Interestingly, many of these genes are known to be preferentially expressed in WAT compared to BAT, including resistin, *Gsta3, Lyz2, Ephx1,* and *Pltp* (Siersbaek et al., 2012). In fact, many of the genes most differentially regulated between WT and aP2-TLE3 Tg mice are also differentially expressed in WAT and BAT (Fig. 3E and data not shown). In general, WAT-selective transcripts were upregulated in BAT of aP2-TLE3 mice, whereas BAT-selective transcripts (e.g., *Elovl3*, *Cldn1,* and *Dhrs9*) were reduced.

Finally, analysis of genes in Group 2 (genes strongly upregulated by TLE3 in the setting of cold exposure) revealed multiple targets of PPARα and PPARδ, such as *Cyp4b1*, *Egr1, Cyp4a32, Cyp4a14,* and *Cyp4a10* (Table S1). These findings are consistent with our previous

observation that TLE3 may co-activate PPARα and PPARδ as well as PPARγ (Villanueva et al., 2011). Overall, these data suggest that the expression of TLE3 in BAT affects transcriptional reprogramming towards a gene-expression profile that is more consistent with the lipid storage function of WAT rather than the thermogenic function of BAT.

Conditional Deletion of TLE3 in Adipose Tissue Improves Thermogenic Response

To further examine the role of TLE3 in brown adipose tissue biology, we generated adipose tissue-selective TLE3 KO (Ad-TLE3 KO) mice by crossing *Tle3*$^{fl/fl}$ mice (Fig. S3; see Experimental Procedures) with adiponectin-Cre transgenic mice (Eguchi et al., 2011). In BAT, *Tle3*$^{fl/fl}$ mice expressing adiponectin-Cre had markedly diminished levels of TLE3 protein compared to Cre-negative littermate controls (Fig. 4A). Adiponectin is expressed only in mature adipocytes, and the residual expression observed in unfractionated adipose tissue is due to TLE3 expression in stromal cells (data not shown). As mice age, the thermogenic capacity of their BAT deteriorates and the tissue acquires WAT-like characteristics, including unilocular lipid droplets and reduced mitochondrial content. To test whether deletion of TLE3 could prevent the age-dependent whitening of brown adipose tissue, we examined brown adipose tissue at 1.5 yrs of age. BAT from Ad-TLE3 KO mice was obviously browner in color compared to BAT from control animals (Fig. 4B). Furthermore, histological analysis revealed that, whereas BAT from control mice was composed primarily of cells with large unilocular lipid droplets, BAT from Ad-TLE3 KO mice contained more cells with multilocular lipid droplets characteristic of young brown adipose tissue (Fig. 4C).

These morphological changes translated to altered thermogenic capacity when mice were challenged with cold exposure at 4°C. Ad-TLE3 KO mice showed an improved thermogenic

response when compared to controls, as evidenced by a better ability to maintain core body temperature during cold exposure (Fig. 4D). Consistent with these results, Ad-TLE3 KO mice showed increased energy expenditure when housed in metabolic cages (Fig. 4E). Body weight and adipose tissue mass determined by MRI were similar between groups (Fig. S5A). Although the difference did not reach statistical significance, there was a trend towards decreased activity in Ad-TLE3 KO mice (Fig. S5B). Food intake was not different between control and Ad-TLE3 KO mice in these metabolic cage studies (Fig. S5C).

To determine the transcriptional basis for this improved BAT function we analyzed gene expression. Ad-TLE3 KO mice exhibited increased basal expression of multiple genes characteristic of BAT, including Cidea, Elovl3, Cldn1 and FGF-21 (Fig. 4F). Furthermore, the expression of cold-responsive genes, including UCP-1, Elovl3, Dhrs9, and Cldn1 was enhanced.

Recent studies have reported that mice exposed to cold, β-adrenergic agonists, or thiozolidinediones, induce the expression of UCP-1, Elovl3, Dio2, Cidea, and other BAT-selective proteins in a subpopulation of cells present in inguinal WAT depots termed “brite” or “beige” cells (Cousin et al., 1992; Ohno et al., 2012; Wu et al., 2012; Young et al., 1984). Given the suppressive effect of TLE3 on BAT-selective gene expression, we hypothesized that TLE3 deficiency might affect BAT-selective gene expression in WAT depots. Interestingly, the expression of TLE3 protein was higher in epididymal fat compared to inguinal fat (Fig. 5A). Furthermore, inguinal adipose depots of Ad-TLE3 KO mice showed evidence of browning by histology, with increased numbers of cells with multilocular lipid droplets characteristic of thermogenic beige adipocytes (Fig. 5B). Furthermore, the expression of UCP1, FGF-21, and Cidea was elevated in inguinal WAT compared to littermate controls (Fig. 5C). However, we

observed no induction of these genes in epididymal WAT from Ad-TLE3 KO mice, indicating that the consequences of TLE3 loss are depot-specific.

We also analyzed the effect of transgenic TLE3 expression on the histology and gene expression of inguinal WAT. Since WT C57Bl/6 mice contain few beige cells at baseline, we treated aP2-TLE3 Tg and littermate control mice with the β3-adrenergic agonist CL-316,243 (CL) to induce browning(Seale et al., 2011). As expected, CL treatment had a striking effect on inguinal WAT histology (Fig. 5D). We did not appreciate a consistent morphological difference between control and aP2-TLE3 Tg mice (Fig. 5D); however, the gene expression profile of the adipocytes in this depot was clearly different, despite the comparable morphology. The expression of genes linked to thermogenesis, including Dio2, UCP-1, Pgc1a and Elovl3, was decreased in aP2-TLE3 Tg mice compared to controls (Fig. 5E). As expected the degree of induction of brown adipocyte genes by CL was lower in epididymal fat compared to inguinal fat (Fig. 5E). We did not observe a significant effect of transgenic TLE3 expression on the induction of these genes in epididymal fat. Collectively, the observations that similar target genes are dysregulated in both aP2-TLE3 Tg mice and Ad-TLE3 KO mice, and that these changes correlate with altered thermogenesis, implicate TLE3 as a physiological modulator of thermogenic gene expression.

Reciprocal Roles for Prdm16 and TLE3 in WAT- and BAT-Selective Gene Expression

Prdm16 is a transcriptional coregulator that drives the brown adipocyte gene program (Seale et al., 2007). Transgenic overexpression of Prdm16 in WAT leads to the browning of white adipocytes (Seale et al., 2011). Interestingly, many of the genes whose expression was most strongly affected by gain or loss of TLE3 expression in BAT in our studies (e.g., UCP1,

Elovl3, Eva1, and Dio2) were previously reported to be responsive to Prdm16 (Seale et al., 2007). We therefore hypothesized that Prdm16 and TLE3 might be mechanistically linked through differential interactions with PPARγ on the promoters of common adipose target genes. To test this hypothesis we employed viral vectors to express TLE3 and/or Prdm16 in 10T1/2 preadipocytes, differentiated the cells with a brown fat-permissive cocktail, and analyzed the impact on differentiation-dependent gene expression (Fig. 6A). Expression of TLE3 alone induced the level of representative WAT-selective transcripts including *Serpina3K* and *Lyz2*, whereas expression of Prdm16 alone had no effect on these transcripts (Fig. 6B). Expression of these genes was prominent on Day 3 of differentiation, but declined by the time they were differentiated on Day12. Coexpression of Prdm16 blunted the induction of WAT-selective genes by TLE3. By contrast, expression of Prdm16, but not TLE3, potently induced the expression of BAT genes, including mRNAs encoding Cidea, Otop-1, Eva1 and PGC-1α, consistent with prior reports (Seale et al., 2011). Furthermore, co-expression of TLE3 antagonized the Prdm16-mediated induction of the brown fat program at both Day 3 and Day 12 of differentiation (Fig. 6B). In addition, TLE3 expression inhibited the ability of the β-adrenergic agonist isoproterenol to induce *Elovl3, Dio2, Cldn1,* and *Ucp1* expression in fully differentiated Prdm16-expressing cells (Fig. 6C). Other PPAR-responsive transcripts, such as the mRNAs encoding aP2 and Ear2, did not show reciprocal regulation by TLE3 and Prdm16, emphasizing the gene-specific nature of the crosstalk between these factors (Fig. 6C). Together with the results of Figs 2 and 3, our data indicate that these two PPARγ cofactors, TLE3 and Prdm16, promote distinct adipocyte gene programs *in vitro* and *in vivo*.

To determine whether the reciprocal effects of TLE3 and Prdm16 on adipocyte genes are due to their interactions with adipocyte gene promoters, we analyzed the occupancy of TLE3,

PPARγ, and Flag-tagged Prdm16 on the regulatory regions of BAT- and WAT-selective genes. ChIP qPCR revealed that TLE3, Prdm16, and PPARγ occupied the promoters of *Dhrs9, Cldn1, Ephx1, aP2, perilipin, Adrp, Agpat2,* and *Acsl1* in differentiated 10T1/2 cells (Fig. 7A and data not shown). We hypothesized that the differential effects of TLE3 and Prdm16 on the expression of certain adipocyte genes might be due to their mutually-exclusive occupancy at PPARγ binding sites. In support of this idea, we found that expression of TLE3 reduced the occupancy of Prdm16 on the *aP2, Dhrs9,* and *Ephx1* promoters (Fig. 7B). Since Prdm16 interacts directly with PPARγ and because TLE3 is also present in PPARγ-containing complexes (Seale et al., 2008; Villanueva et al., 2011), we hypothesized that the interaction of Prdm16 and TLE3 with PPARγ might be mutually exclusive. To test this idea, we immunoprecipitated V5-Prdm16 from cells in the presence or absence of TLE3 and then immunoblotted for PPARγ. Remarkably, TLE3 expression disrupted the interaction of PPARγ with Prdm16 (Fig. 7C). This was most likely due to competitive physical interaction of Prdm16 with TLE3, as Prdm16 and TLE3 coimmunoprecipated (Fig. 7C). Prdm16 has also been reported to interact with C/EBPβ to regulate BAT gene expression(Kajimura et al., 2009). In our system we observed weak interaction between Prdm16 with C/EBPβ and this was not affected by the presence of TLE3 (Fig. 7D). Together, our results demonstrate that direct mechanistic interactions between TLE3 and Prdm16 on adipocyte promoters dictate differential adipocyte gene expression programs.

Discussion

White and brown adipocytes have shared but distinct transcriptional programs that facilitate long-term lipid storage and thermogenesis, respectively. The transcriptional determinants that specify white versus brown fat-selective gene expression are incompletely understood. We have shown here that adipose subtype-selective gene expression is accomplished in part through differential recruitment of the PPARγ cofactors TLE3 and Prdm16. TLE3, which is preferentially expressed in white fat, inhibits the expression of brown-selective Prdm16 target genes while promoting the expression of white-selective genes. Expression of TLE3 *in vivo* favors the "whitening" of brown adipose tissue and the suppression of adaptive thermogenesis, whereas the loss of TLE3 leads to the "browning" of inguinal WAT. The interaction of Prdm16 with TLE3 and PPARγ is mutually exclusive and TLE3 antagonizes thermogenic gene expression by inhibiting the co-occupancy of Prdm16 and PPARγ on adipocyte promoters. Although PPARγ is well known to interact with a variety of cofactors, to our knowledge this is the first study to directly correlate differential promoter occupancy of PPARγ coactivators with cell type-selective gene expression.

Although the vast majority of adipocyte genes are expressed at similar levels in brown and white adipocytes, a subset is preferentially expressed in one adipocyte type or the other. PPARγ drives a transcriptional cascade common to both white and brown adipocytes, regulating the expression of shared markers of the differentiated phenotype, for example aP2, CD36, Plin, and adiponectin (Tontonoz and Spiegelman, 2008). But PPARγ also promotes the expression of brown-selective markers such as UCP1 and Elovl3, and white-selective markers such as Ephx1. The mechanistic basis for the tissue-selective actions of PPARγ on brown and white adipocyte promoters is still unclear.

Several auxiliary factors have been identified that work in concert with PPARγ to facilitate brown fat-selective gene expression. The first to be characterized was PGC-1α, a cold-inducible coactivator of PPARγ that drives the expression of UCP1 in brown adipose tissue (Puigserver et al., 1998). PGC-1α promotes the expression of cold-inducible genes and those linked to mitochondrial oxidative metabolism, but has little effect on the expression of a number of other BAT-selective genes (Uldry et al., 2006). In addition to promoting adaptive thermogenesis, PGC-1α also plays important roles in oxidative metabolism and mitochondrial biogenesis in heart and skeletal muscle (Lehman et al., 2000; Wu et al., 1999). More recently, Prdm16 was identified as a critical factor that drives the entire brown fat-selective transcriptional program through direct interaction with PPARγ (Seale et al., 2008). Prdm16 is highly enriched in BAT and its forced expression in white preadipocytes or myoblasts promotes a lineage switch to brown fat (Seale et al., 2008; Seale et al., 2007). Mice overexpressing Prdm16 in adipose tissue show increased expression of BAT-selective transcripts in certain white adipose tissue depots, such as inguinal WAT (Seale et al., 2011), and Prdm16 also suppresses the expression of certain WAT-selective transcripts (Kajimura et al., 2008).

By comparison, relatively little is known about factors that specify white adipocyte-selective gene expression. It has been unclear whether white fat is simply a "default" transcriptional program that is executed by PPARγ in the absence of Prdm16 and PGC-1α, or whether there are white fat-selective counterparts to these brown-selective cofactors. Our data suggest that TLE3 is one such factor, enforcing an opposing transcriptional program to Prdm16.

We initially identified TLE3 as an adipogenic coregulator in a high-throughput cDNA screen (Villanueva et al., 2011). TLE3 is induced early in the course of adipocyte differentiation and its expression is directly regulated by PPARγ. TLE3 and PPARγ act synergistically to drive

adipocyte gene expression and differentiation, and colocalize on PPAR response elements within adipogenic promoters. PPARγ likely employs some common cofactors to promote gene expression common to both WAT and BAT, perhaps including p300, SRCs and mediator complex, and we initially suspected that TLE3 would promote the expression of all PPARγ target genes equally. Unexpectedly, however, we found that TLE3 exerts differential effects on BAT- and WAT-selective gene expression. Brown adipose tissue from aP2-TLE3 Tg mice showed histological features of white fat and impaired adaptive thermogenesis, and these changes correlated with an impaired capacity to induce thermogenic gene expression during cold challenge. Conversely, mice lacking TLE3 showed enhanced expression of thermogenic genes in both WAT and BAT and improved cold-tolerance. These findings suggest that TLE3 plays a specific role in helping to define the differential brown, white and perhaps beige adipocyte gene programs.

During brown preadipocyte differentiation, the induction of genes involved in lipid biosynthesis and lipid droplet formation occurs prior to the induction of most BAT-selective transcripts such as UCP-1. TLE3 is also induced early during the course of brown adipocyte differentiation, suggesting that TLE3 may be help to establish the lipid-storage and lipid-synthesis capacity common to all adipocytes, and may prevent the induction in brown fat transcripts during early differentiation. During the later stages of brown preadipocyte differentiation, TLE3 expression declines, allowing the brown fat program to proceed. This observation is consistent with the relatively low level of expression of TLE3 in mature BAT compared to mature WAT.

Together with earlier work (Kajimura et al., 2008), our data suggest that the mechanistic basis for the differential actions of PPARγ in the WAT and BAT gene expression programs

involves the formation of cell-type selective transcriptional complexes on the promoters of key adipocyte genes. Prdm16 binds directly to PPARγ, and studies have established that the ability of Prdm16 to interact with PPARγ and C/EBPβ is critical for its ability to drive BAT development (Kajimura et al., 2009; Seale et al., 2008). TLE3 is also present in PPARγ-containing transcriptional complexes and can be localized to PPREs by ChIP, although the two proteins do not appear to interact directly (Villanueva et al., 2011). We have shown that the choice of PPARγ to form complexes with Prdm16 and TLE3 is mutually exclusive. Prdm16 binds to TLE3, and TLE3 competes for the interaction between Prdm16 and PPARγ. Elevated TLE3 expression antagonizes thermogenic gene expression by inhibiting the co-occupancy of Prdm16 and PPARγ on adipocyte promoters. Conversely, the loss of TLE3 expression in BAT provides a more permissive context for the actions of Prdm16.

Overall, these studies highlight an intricate balance between overlapping transcriptional programs that specifies adipose cell-type specific gene expression. Ultimately, a better understanding of the mechanisms by which PPARγ controls the lipid storage and thermogenic gene programs may aid in the development of pharmacologic modulators of adipocyte phenotype. Optimization of PPARγ agonists for the their ability to affect the balance between TLE3 and Prdm16 recruitment may facilitate the therapeutic manipulation of thermogenic gene expression and energy expenditure in humans.

Acknowledgements

We thank members of our laboratories for discussions and technical support. P.T. is an investigator of the Howard Hughes Medical Institute. This work was supported by NIH grants HL-090553, S10RR026744 and DK063491 and by a UCLA Jonsson Comprehensive Cancer

Center Fellowship. The authors have no financial interests related to this work.

EXPERIMENTAL PROCEDURES

Cell Culture

10T1/2 cells and brown preadipocytes were plated in DMEM containing 10% FBS, 20 nM insulin, and 1 nM T3. After confluence cells were stimulated to differentiate with DMEM, 10% FBS, 20 nM insulin, 1 nM T3, 0.5 mM isobutylmethylxanthine, 0.5 μM dexamethasone, and 0.125 mM indomethacin for 2 days, followed by DMEM containing 10% FBS, 20 nM insulin, and 1 nM T3. Brown preadipocytes were isolated as previously described (Rodriguez-Cuenca et al., 2007); cells were immortalized by retroviral expression of the SV40 Large T-antigen using a hygromycin selection marker. Gain of function studies for 10T1/2 cells or brown preadipocytes were completed using the pBabe expression system for TLE3 (puromycin), V5-Prdm16 (puromycin) or Flag-Prdm16 (puromycin). Acute overexpression studies were completed using adenoviral expression system using pAd gateway destination vectors (Invitrogen) and adenovirus was amplified using 293 cells. Adenovirus was purified by CsCl gradients and titered for potency (Viraquest Inc., North Liberty, IA). Cells were infected using MOI 50, unless otherwise stated.

Gene Expression and Microarray Analysis

Total RNA was isolated using Trizol reagents (Invitrogen) and reverse transcribed using iScript cDNA synthesis kit (Bio-Rad, Hercules, CA). Gene expression was quantified by real-time PCR using SYBR Green (Diagenode, Denville, NJ) and an ABI 7900 instrument. Primer pairs were designed using the Universal Probe Library (Roche). A standard curve was generated for each primer pair to quantify gene expression and a list of primer pairs is included in Table S1. For microarray experiments of brown adipose tissue, RNA was pooled from four separate mice and

processed by the UCLA microarray core facility using Gene-Chip Mouse Gene 1.0 ST Arrays (Affymetrix, Santa Clara, CA). The results were analyzed using Genespring GX (Agilent, Santa Clara).

Protein Analysis

Cells were homogenized using RIPA buffer plus proteinase inhibitor and sonicated for 10 s using Bioruptor. Brown adipose tissue was homogenized using RIPA buffer plus proteinase inhibitor using dounce (Perkin Elmer) and placed on nutator for 30 min. Cell or tissue homogenate was spun at 12,000g for 10 min at 4 C, supernatant was saved and protein was quantified using a BCA protein assay (Piercenet). Proteins were diluted using Nupage loading dye and heated at 70 C for 20 min and run on 4-12% Bis-Tris Nupage Gels (Invitrogen). Proteins were transferred to hybond ECL(GE Healthcare) and blotted using TLE3 antibody (Proteintech), Hmg1 (Abcam), UCP1 (Abcam), PPARγ (Cell Signaling), or V5 antibody (Invitrogen).

Coimmunoprecipitation

293 cells were transfected using BioT (Bioland Scientific) transfection reagent in 10 cm dish when cells were 80% confluent. Cells were transfected with expression plasmids of V5-Prdm16, Flag-TLE3, Flag-PPARg2 or Myc-CEBPβ (gift from Stephen R. Farmer) as indicated in the legend. 2-days post transfection cells were lysed with RIPA buffer plus proteinase inhibitor (Roche) as described above. Lysate was incubated with V5 (Abcam) followed by protein A beads. Lysate was allowed to incubate overnight at 4C. Agarose beads were washed with RIPA buffer and with PBS for the final wash. Proteins were eluted with Nupage loading dye

(Invitrogen) and were immunoblotted using M2 Flag (Sigma Aldrich), V5(Invitrogen), or Myc (Covance Research Products) antibodies as described above.

Chromatin Immunoprecipitation

ChIP studies were completed as described previously (Villanueva et al., 2011). Briefly, 10T1/2 cells were washed with PBS and fixed with 1% formaldehyde for 10 min. Lysed cells were sonicated with Bioruptor using 30 cycles of 30 s ON/OFF. Chromatin was spun at 12,000 g for 10 min and supernatant was precleared with ProteinA or ProteinG agarose beads. A portion of precleared chromatin was saved for input or incubated with TLE3 (Protein Tech), PPARγ (Santa Cruz) or Flag (Sigma Aldrich) antibodies at 4C overnight. ProteinA agarose beads were incubate for 4 h, spun and washed. Crosslinking was reversed and DNA was purified using columns (Qiagen). DNA enrichment was quantified by real-time PCR using SybrGreen (Diagenode) and ABI 7900. Genomic regions to be tested were determined by mining genomewide PPARγ ChIP seq. experiments available in GEO Datasets (NCBI). Primers were designed using the Universal Probe Library (Roche) and are listed in Table S1. Relative occupancy was quantified by using a standard curve and normalized samples to input.

Animal Studies

Transgenic mice (C57BL6J inbred strain) were generated previously using the -5.4kb aP2 enhancer driving TLE3 cDNA (Villanueva et al., 2011). For cold exposure experiments, control littermates and aP2-TLE3 Tg mice were housed individually without food and bedding immediately before the start of experiments. Mice were allowed free access to water and placed at 4C while core body temperature was monitored every hour using a rectal probe. A conditional

knock-out allele for *Tle3* was generated using a sequence-replacement "targeted trapping/conditional-ready" gene-targeting vector. The targeting vector was electroporated into strain 129/OlaHsd ES cells and G418-resistant targeted clones identified by long-range PCR at both the 5′ and 3′ ends using primers 5′-1033F (tgt gtc tgt gtg gga tga act ttcc) and 5′-4432R (acc gta atg gga tag gtt acg ttg g) for the 5′ end, and primers 3′-71F (gtg gag agg cta ttc ggc tat gact) and 3′-1370R (atc cac tct tcc tga ctg tgg ctt c) for the 3′ end. Nineteen targeted clones (out of 168 G418-resistant clones screened) were identified. Two targeted ES cell clones (#38, #50) were injected into C57BL/6 blastocysts to generate chimeric mice. High-percentage male chimeras were obtained, and resulting chimeras were crossed to C57BL/6J mice to establish germline transmission. Heterozygous mice carrying the conditional-ready knockout allele were mated with mice carrying a *Flp* recombinase deleter transgene. *Flp* recombinase excised the gene-trapping cassette within intron 2 of *Tle3*, producing a conditional knockout allele containing a *lox71* site in intron 2 and a *loxP* site in intron 3. Genotyping was completed by amplification of genomic region flanking loxp sites using the following primer pairs, forward gct ccc ttc ttc agc ttc ct and reverse, gct cca aga ggg att ttt at. $TLE3^{F/F}$ mice were crossed with adiponectin-Cre mice obtained from Evan Rosen. Mice were challenged with cold exposure as described above. Energy expenditure, food intake, and ambulatory activity were determined by using Oxymax Lab Animal Monitoring System: CLAMS (Columbus Instruments) and as described in Villanueva et al, 2011. Mice were treated with 1 mg/kg/day of CL-316,243 for a total of 3-days. The last dose was given 4 h prior to tissue harvest.

Cellular Metabolism

For determination of fatty acid oxidation and uptake, interscapular BAT was excised and immediately placed in warm serum free DMEM containing 1% fatty-acid free BSA and 0.5μM palmitate, with or without nor-adrenaline (10μM). Tissues were allowed to incubate for 1hr at 37 degrees before the addition of 1 μCi/mL of ^{14}C-palmitate (Perkin Elmer) followed by 2 h incubation at 37 degrees. Tissue and media were analyzed for fatty acid oxidation and uptake as previously described (Ribas et al., 2011). Cellular metabolic rates were measured using a XF24 Analyzer (Seahorse Bioscience). Immediately before the measurement, cells were washed with unbuffered DMEM as described (Wu et al., 2007). Plates were placed into the XF24 instrument for measurement of oxygen consumption (OCR) and extracellular acidification (ECAR) rates. Mixing, waiting and measurement times were 4, 2, and 2 min, respectively. The measures were normalized per protein.

REFERENCES

Atit, R., Sgaier, S.K., Mohamed, O.A., Taketo, M.M., Dufort, D., Joyner, A.L., Niswander, L., and Conlon, R.A. (2006). Beta-catenin activation is necessary and sufficient to specify the dorsal dermal fate in the mouse. Dev Biol 296, 164-176.

Barak, Y., Nelson, M.C., Ong, E.S., Jones, Y.Z., Ruiz-Lozano, P., Chien, K.R., Koder, A., and Evans, R.M. (1999). PPAR gamma is required for placental, cardiac, and adipose tissue development. Mol Cell 4, 585-595.

Bouillaud, F., Ricquier, D., Thibault, J., and Weissenbach, J. (1985). Molecular approach to thermogenesis in brown adipose tissue: cDNA cloning of the mitochondrial uncoupling protein. Proc Natl Acad Sci U S A 82, 445-448.

Cannon, B., and Nedergaard, J. (2004). Brown adipose tissue: function and physiological significance. Physiol Rev 84, 277-359.

Chao, L., Marcus-Samuels, B., Mason, M.M., Moitra, J., Vinson, C., Arioglu, E., Gavrilova, O., and Reitman, M.L. (2000). Adipose tissue is required for the antidiabetic, but not for the hypolipidemic, effect of thiazolidinediones. J Clin Invest 106, 1221-1228.

Coleman, R.A., and Bell, R.M. (1980). Selective changes in enzymes of the sn-glycerol 3-phosphate and dihydroxyacetone-phosphate pathways of triacylglycerol biosynthesis during differentiation of 3T3-L1 preadipocytes. J Biol Chem 255, 7681-7687.

Cook, K.S., Min, H.Y., Johnson, D., Chaplinsky, R.J., Flier, J.S., Hunt, C.R., and Spiegelman, B.M. (1987). Adipsin: a circulating serine protease homolog secreted by adipose tissue and sciatic nerve. Science 237, 402-405.

Cousin, B., Cinti, S., Morroni, M., Raimbault, S., Ricquier, D., Penicaud, L., and Casteilla, L. (1992). Occurrence of brown adipocytes in rat white adipose tissue: molecular and morphological characterization. J Cell Sci 103 (Pt 4), 931-942.

Cypess, A.M., Lehman, S., Williams, G., Tal, I., Rodman, D., Goldfine, A.B., Kuo, F.C., Palmer, E.L., Tseng, Y.H., Doria, A., Kolodny, G.M., and Kahn, C.R. (2009). Identification and importance of brown adipose tissue in adult humans. N Engl J Med 360, 1509-1517.

Eguchi, J., Wang, X., Yu, S., Kershaw, E.E., Chiu, P.C., Dushay, J., Estall, J.L., Klein, U., Maratos-Flier, E., and Rosen, E.D. (2011). Transcriptional control of adipose lipid handling by IRF4. Cell Metab 13, 249-259.

Halaas, J.L., Gajiwala, K.S., Maffei, M., Cohen, S.L., Chait, B.T., Rabinowitz, D., Lallone, R.L., Burley, S.K., and Friedman, J.M. (1995). Weight-reducing effects of the plasma protein encoded by the obese gene. Science 269, 543-546.

Jacobsson, A., Stadler, U., Glotzer, M.A., and Kozak, L.P. (1985). Mitochondrial uncoupling protein from mouse brown fat. Molecular cloning, genetic mapping, and mRNA expression. J Biol Chem 260, 16250-16254.

Kajimura, S., Seale, P., Kubota, K., Lunsford, E., Frangioni, J.V., Gygi, S.P., and Spiegelman, B.M. (2009). Initiation of myoblast to brown fat switch by a PRDM16-C/EBP-beta transcriptional complex. Nature 460, 1154-1158.

Kajimura, S., Seale, P., Tomaru, T., Erdjument-Bromage, H., Cooper, M.P., Ruas, J.L., Chin, S., Tempst, P., Lazar, M.A., and Spiegelman, B.M. (2008). Regulation of the brown and white fat gene programs through a PRDM16/CtBP transcriptional complex. Genes Dev 22, 1397-1409.

Kawamura, M., Jensen, D.F., Wancewicz, E.V., Joy, L.L., Khoo, J.C., and Steinberg, D. (1981). Hormone-sensitive lipase in differentiated 3T3-L1 cells and its activation by cyclic AMP-dependent protein kinase. Proc Natl Acad Sci U S A 78, 732-736.

Lean, M.E., James, W.P., Jennings, G., and Trayhurn, P. (1986). Brown adipose tissue uncoupling protein content in human infants, children and adults. Clin Sci (Lond) 71, 291-297.
Lehman, J.J., Barger, P.M., Kovacs, A., Saffitz, J.E., Medeiros, D.M., and Kelly, D.P. (2000). Peroxisome proliferator-activated receptor gamma coactivator-1 promotes cardiac mitochondrial biogenesis. J Clin Invest 106, 847-856.

Matthias, A., Ohlson, K.B., Fredriksson, J.M., Jacobsson, A., Nedergaard, J., and Cannon, B. (2000). Thermogenic responses in brown fat cells are fully UCP1-dependent. UCP2 or UCP3 do not substitute for UCP1 in adrenergically or fatty scid-induced thermogenesis. J Biol Chem 275, 25073-25081.

Mirbolooki, M.R., Constantinescu, C.C., Pan, M.L., and Mukherjee, J. (2012). Quantitative assessment of brown adipose tissue metabolic activity and volume using 18F-FDG PET/CT and Beta3-adrenergic receptor activation. EJNMMI Res 1, 1-11.

Ohno, H., Shinoda, K., Spiegelman, B.M., and Kajimura, S. PPARgamma agonists induce a white-to-brown fat conversion through stabilization of PRDM16 protein. Cell Metab 15, 395-404.

Ohno, H., Shinoda, K., Spiegelman, B.M., and Kajimura, S. (2012). PPARgamma agonists induce a white-to-brown fat conversion through stabilization of PRDM16 protein. Cell Metab 15, 395-404.

Puigserver, P., Wu, Z., Park, C.W., Graves, R., Wright, M., and Spiegelman, B.M. (1998). A cold-inducible coactivator of nuclear receptors linked to adaptive thermogenesis. Cell 92, 829-839.

Rauch, J.C., and Hayward, J.S. (1969). Topography and vascularization of brown fat in a small nonhibernator (deer mouse, Peromyscus maniculatus). Can J Zool 47, 1301-1314.

Reitman, M.L., Arioglu, E., Gavrilova, O., and Taylor, S.I. (2000). Lipoatrophy revisited. Trends Endocrinol Metab 11, 410-416.

Reue, K., and Peterfy, M. (2000). Mouse models of lipodystrophy. Curr Atheroscler Rep 2, 390-396.

Ribas, V., Drew, B.G., Le, J.A., Soleymani, T., Daraei, P., Sitz, D., Mohammad, L., Henstridge, D.C., Febbraio, M.A., Hewitt, S.C., Korach, K.S., Bensinger, S.J., and Hevener, A.L. (2011). Myeloid-specific estrogen receptor alpha deficiency impairs metabolic homeostasis and accelerates atherosclerotic lesion development. Proc Natl Acad Sci U S A 108, 16457-16462.

Rodriguez-Cuenca, S., Monjo, M., Frontera, M., Gianotti, M., Proenza, A.M., and Roca, P. (2007). Sex steroid receptor expression profile in brown adipose tissue. Effects of hormonal status. Cell Physiol Biochem 20, 877-886.

Rosen, E.D., Sarraf, P., Troy, A.E., Bradwin, G., Moore, K., Milstone, D.S., Spiegelman, B.M., and Mortensen, R.M. (1999). PPAR gamma is required for the differentiation of adipose tissue in vivo and in vitro. Mol Cell 4, 611-617.

Seale, P., Bjork, B., Yang, W., Kajimura, S., Chin, S., Kuang, S., Scime, A., Devarakonda, S., Conroe, H.M., Erdjument-Bromage, H., Tempst, P., Rudnicki, M.A., Beier, D.R., and Spiegelman, B.M. (2008). PRDM16 controls a brown fat/skeletal muscle switch. Nature 454, 961-967.

Seale, P., Conroe, H.M., Estall, J., Kajimura, S., Frontini, A., Ishibashi, J., Cohen, P., Cinti, S., and Spiegelman, B.M. (2011). Prdm16 determines the thermogenic program of subcutaneous white adipose tissue in mice. J Clin Invest 121, 96-105.

Seale, P., Kajimura, S., Yang, W., Chin, S., Rohas, L.M., Uldry, M., Tavernier, G., Langin, D., and Spiegelman, B.M. (2007). Transcriptional control of brown fat determination by PRDM16. Cell Metab 6, 38-54.

Shimomura, I., Hammer, R.E., Ikemoto, S., Brown, M.S., and Goldstein, J.L. (1999). Leptin reverses insulin resistance and diabetes mellitus in mice with congenital lipodystrophy. Nature 401, 73-76.

Siersbaek, M.S., Loft, A., Aagaard, M.M., Nielsen, R., Schmidt, S.F., Petrovic, N., Nedergaard, J., and Mandrup, S. (2012). Genome-Wide Profiling of Peroxisome Proliferator-Activated Receptor gamma in Primary Epididymal, Inguinal, and Brown Adipocytes Reveals Depot-Selective Binding Correlated with Gene Expression. Molecular and cellular biology 32, 3452-3463.

Smith, R.E., and Roberts, J.C. (1964). Thermogenesis of Brown Adipose Tissue in Cold-Acclimated Rats. Am J Physiol 206, 143-148.

Tontonoz, P., Hu, E., Graves, R.A., Budavari, A.I., and Spiegelman, B.M. (1994a). mPPAR gamma 2: tissue-specific regulator of an adipocyte enhancer. Genes Dev 8, 1224-1234.

Tontonoz, P., Hu, E., and Spiegelman, B.M. (1994b). Stimulation of adipogenesis in fibroblasts by PPAR gamma 2, a lipid-activated transcription factor. Cell 79, 1147-1156.

Tontonoz, P., and Spiegelman, B.M. (2008). Fat and beyond: the diverse biology of PPARgamma. Annu Rev Biochem 77, 289-312.

Uldry, M., Yang, W., St-Pierre, J., Lin, J., Seale, P., and Spiegelman, B.M. (2006). Complementary action of the PGC-1 coactivators in mitochondrial biogenesis and brown fat differentiation. Cell Metab 3, 333-341.

van Marken Lichtenbelt, W.D., Vanhommerig, J.W., Smulders, N.M., Drossaerts, J.M., Kemerink, G.J., Bouvy, N.D., Schrauwen, P., and Teule, G.J. (2009). Cold-activated brown adipose tissue in healthy men. N Engl J Med 360, 1500-1508.

Villanueva, C.J., Waki, H., Godio, C., Nielsen, R., Chou, W.L., Vargas, L., Wroblewski, K., Schmedt, C., Chao, L.C., Boyadjian, R., Mandrup, S., Hevener, A., Saez, E., and Tontonoz, P. (2011). TLE3 is a dual-function transcriptional coregulator of adipogenesis. Cell Metab 13, 413-427.

Virtanen, K.A., Lidell, M.E., Orava, J., Heglind, M., Westergren, R., Niemi, T., Taittonen, M., Laine, J., Savisto, N.J., Enerback, S., and Nuutila, P. (2009). Functional brown adipose tissue in healthy adults. N Engl J Med 360, 1518-1525.

Wu, J., Bostrom, P., Sparks, L.M., Ye, L., Choi, J.H., Giang, A.H., Khandekar, M., Virtanen, K.A., Nuutila, P., Schaart, G., Huang, K., Tu, H., van Marken Lichtenbelt, W.D., Hoeks, J., Enerback, S., Schrauwen, P., and Spiegelman, B.M. (2012). Beige adipocytes are a distinct type of thermogenic fat cell in mouse and human. Cell 150, 366-376.

Wu, M., Neilson, A., Swift, A.L., Moran, R., Tamagnine, J., Parslow, D., Armistead, S., Lemire, K., Orrell, J., Teich, J., Chomicz, S., and Ferrick, D.A. (2007). Multiparameter metabolic analysis reveals a close link between attenuated mitochondrial bioenergetic function and enhanced glycolysis dependency in human tumor cells. Am. J. Physiol. Cell Physiol. 292, C125-C136.

Wu, Z., Puigserver, P., Andersson, U., Zhang, C., Adelmant, G., Mootha, V., Troy, A., Cinti, S., Lowell, B., Scarpulla, R.C., and Spiegelman, B.M. (1999). Mechanisms controlling mitochondrial biogenesis and respiration through the thermogenic coactivator PGC-1. Cell 98, 115-124.

Yamauchi, T., Kamon, J., Waki, H., Terauchi, Y., Kubota, N., Hara, K., Mori, Y., Ide, T., Murakami, K., Tsuboyama-Kasaoka, N., Ezaki, O., Akanuma, Y., Gavrilova, O., Vinson, C., Reitman, M.L., Kagechika, H., Shudo, K., Yoda, M., Nakano, Y., Tobe, K., Nagai, R., Kimura,

S., Tomita, M., Froguel, P., and Kadowaki, T. (2001). The fat-derived hormone adiponectin reverses insulin resistance associated with both lipoatrophy and obesity. Nat Med 7, 941-946.
Young, P., Arch, J.R., and Ashwell, M. (1984). Brown adipose tissue in the parametrial fat pad of the mouse. FEBS Lett 167, 10-14.

Zechner, R., Kienesberger, P.C., Haemmerle, G., Zimmermann, R., and Lass, A. (2009). Adipose triglyceride lipase and the lipolytic catabolism of cellular fat stores. J Lipid Res 50, 3-21.

Figure Legends

Figure 1. TLE3 modulates the differentiation program of brown preadipocytes. A. Time course of TLE3 protein expression during the differentiation of immortalized primary brown preadipocytes determined by immunoblotting. **B.** Induction of aP2 precedes induction of the brown adipocyte marker Cidea in primary brown adipocytes as determined by realtime PCR. **C.** TLE3 protein expression in mouse tissues determined by immunoblotting. **D**. TLE3 protein expression in brown preadipocytes transduced with control or TLE3-expressing retroviral vectors. **E.** Oil red-O staining (top) and bodipy staining (bottom) of control and TLE3-expressing brown preadipocytes 5 days after induction of differentiation. **F.** Expression of WAT- and BAT-selective target genes in control and TLE3-expressing brown preadipocytes. Similar results were obtained as in E and F with multiple independent control and TLE3-expressing cell pools.

Figure 2. Transgenic TLE3 expression alters brown adipose tissue phenotype and function. **A.** Immunoblot analysis of TLE3 and UCP-1 protein expression in epididymal WAT and subscapular BAT from control and aP2-TLE3 Tg mice. **B.** Gross and histological analysis (H&E staining) of subscapular BAT from control and aP2-TLE3 Tg mice. **C.** Fatty acid uptake and oxidation in primary brown adipose tissue from control and aP2-TLE3 Tg mice was determined as described in Experimental Procedures. **D.** Oxygen consumption rate (OCR) and extracellular acidification rate (ECAR) from vector or TLE3-expressing brown adipocytes were determined with the Seahorse extracellular flux analyzer. *$P < 0.05$ by Student's t-test. **E.** Energy expenditure in control and aP2-TLE3 Tg mice (N=5/group) determined by indirect calorimetry with Oxymax metabolic cages. **F.** Time course of core body temperature of control

(WT) and aP2-TLE3 Tg mice (N=5/group) housed at 4 ^{o}C. Data are presented as mean +/- SEM. Statistical significance was analyzed by repeated measures two-way ANOVA.

Figure 3. Transcriptional reprogramming of the BAT thermogenic gene program by TLE3. A. BAT cDNA from control and aP2-TLE3 Tg mice house at RT or 4 ^{o}C was analyzed by hybridization to Affymetrix GeneChip Mouse Gene 1.0 ST Arrays. Data was processed using GeneSpring software as described in Experimental Procedures. Venn diagram depicting overlap between genes altered greater than 2-fold by TLE3 or cold exposure. **B.** Heat map representation and cluster analysis of genes altered greater than 2-fold between control and aP2-TLE3 Tg BAT as determined by Affymetrix arrays. A complete list of genes in each grouping is provided in Supplemental Table 1. **C.** Realtime PCR analysis of the expression of genes selective for BAT in control and aP2-TLE3 Tg BAT (N=4-7/group). **D.** Realtime PCR analysis of the expression of genes selective for WAT in control and aP2-TLE3 Tg BAT (N=4-7/group). **E.** Realtime PCR analysis of gene expression in WAT and BAT from C57BL/6 mice (N=6-8/group). Data are presented as mean +/- SEM. *$P < 0.05$. Significance was analyzed by two-way ANOVA followed by Bonferroni post-hoc test.

Figure 4. Adipose-specific deletion of TLE3 potentiates BAT thermogenic gene expression and function. A. Immunoblot analysis of TLE3 protein expression in whole brown adipose tissue from floxed TLE3 mice (TLE3$^{F/F}$) mice in the presence or absence of an adiponectin (Adn) Cre transgene. **B.** Gross appearance of BAT from Cre-negative and Cre-positive TLE3$^{F/F}$ mice. **C.** H&E staining of BAT sections from Cre-negative and Cre-positive TLE3$^{F/F}$ mice. **D.** Time course of core body temperature from Cre-negative and Cre-positive TLE3$^{F/F}$ mice (N=4-

7/group) housed at 4 ^{o}C. Statistical significance was analyzed by repeated measures two-way ANOVA. **E.** Energy expenditure in Cre-negative and Cre-positive TLE3$^{F/F}$ mice (N=6-10/group) determined by indirect calorimetry with Oxymax metabolic cages. **F.** Realtime PCR analysis of BAT-selective gene expression from Cre-negative and Cre-positive TLE3$^{F/F}$ mice (N=6-8/group). **G.** Realtime PCR analysis of BAT-selective gene expression in BAT from Cre-negative and Cre-positive TLE3$^{F/F}$ mice housed at RT or 4 ^{o}C for 6 h. N=4-7/group. *P < 0.05. Data are presented as mean +/- SEM.

Figure 5. TLE3 modulates the induction of the thermogenic gene program in inguinal WAT. A. Immunoblot analysis of TLE3 protein levels in various adipose depots from WT C57Bl/6 mice. **B.** H&E staining of representative inguinal WAT sections from Cre-negative and Cre-positive TLE3$^{F/F}$ mice. **C.** Realtime PCR analysis of gene expression in inguinal and epididymal WAT from control and Adn-Cre/TLE3$^{F/F}$ mice fed high-fat diet for 13 wks. N=7-11. **D.** H&E staining of representative inguinal WAT sections from aP2-TLE Tg and littermate controls (N=3-4) treated for 3 days with 1 mg/kg/day CL-316,243 (CL). **E.** Real-time PCR analysis of gene expression from inguinal WAT from aP2-TLE Tg and littermate controls treated for 3 days with 10 μM CL-316,243. *P < 0.05. Data are presented as mean +/- SEM (N=3).

Figure 6. TLE3 and Prdm16 reciprocally regulate the expression of BAT and WAT-selective gene expression. A. Immunoblot analysis of TLE3 and Prdm16 expression in virally transduced 10T1/2-CAR cells. Stable pools of vector or Prdm16-expressing cells were differentiated with BAT-induction cocktail for 9 days and then transduced with control or TLE3 adenoviral vectors for 3 days. Lysates were collected on Day 12. **B**. Realtime PCR analysis of

BAT- and WAT-selective gene expression in virally-transduced 10T1/2-CAR cells on Day 3 and Day 12 after induction with BAT differentiation cocktail. RNA isolated 3-days after transduction with control or TLE3 adenovirus. **C.** Realtime PCR analysis of cold-inducible genes in virally-transduced 10T1/2-CAR cells on Day 10 after induction with BAT differentiation cocktail. Cells were also treated with vehicle or 5 μM isoproterenol for 4 h. RNA was isolated 3-days after adenoviral infection.

Figure 7. TLE3 binds to Prdm16 and competes for its interaction with PPARγ. A. TLE3 and Prdm16 localize to common target genes. ChIP assays were performed on 10T1/2-CAR cells stably transduced with Flag-tagged Prdm16 as described in Experimental Procedures. Cells were crosslinked on Day 4 after induction with BAT differentiation cocktail, and proteins precipitated with control IgG or antibodies to Flag, endogenous PPARγ, and endogenous TLE3 as indicated. A non-specific region of chromosome 15 was used as a negative control for binding. Promoter occupancy was determined by realtime PCR. **B.** Expression of TLE3 displaces Prdm16 from BAT- and WAT-selective gene promoters. Stable 10T1/2-CAR cells expressing vector or Flag-Prdm16 were differentiated for 7 days with BAT induction cocktail and then transduced with control or TLE3-expressing adenoviral vectors for 3-days. ChIP assays were performed using control IgG or an antibody to Flag as in A. **C**. 293 cells were transfected with V5-Prdm16, Flag-PPARγ2 and/or Flag-TLE3. Lysates were immunoprecipitated with anti-V5 antibody, and the precipitates were analyzed by immunoblotting. Similar results were obtained in multiple independent experiments. **D**. 293 cells were transfected with V5-Prdm16, myc-C/EBPβ and/or Flag-TLE3. Lysates were immunoprecipitated with anti-V5 antibody, and

the precipitates were analyzed by immunoblotting. Similar results were obtained in multiple independent experiments.

Supplemental Figure Legends

Figure S1. Induction of TLE3 expression in brown preadipocytes by PPARγ agonists. A. Real-time PCR analysis of TLE3 expression in immortalized primary brown preadipocytes treated with various stimuli. B. Immunoblot analysis of TLE3 protein expression in differentiated brown preadipocytes treated on Day 9 of differentiation with vehicle or 5 μM isoproterenol as indicated.

Figure S2. Physical activity (A) and food intake (B) in aP2-TLE3 Tg and littermate control mice (N=5) determined by housing in Oxymax metabolic cages.

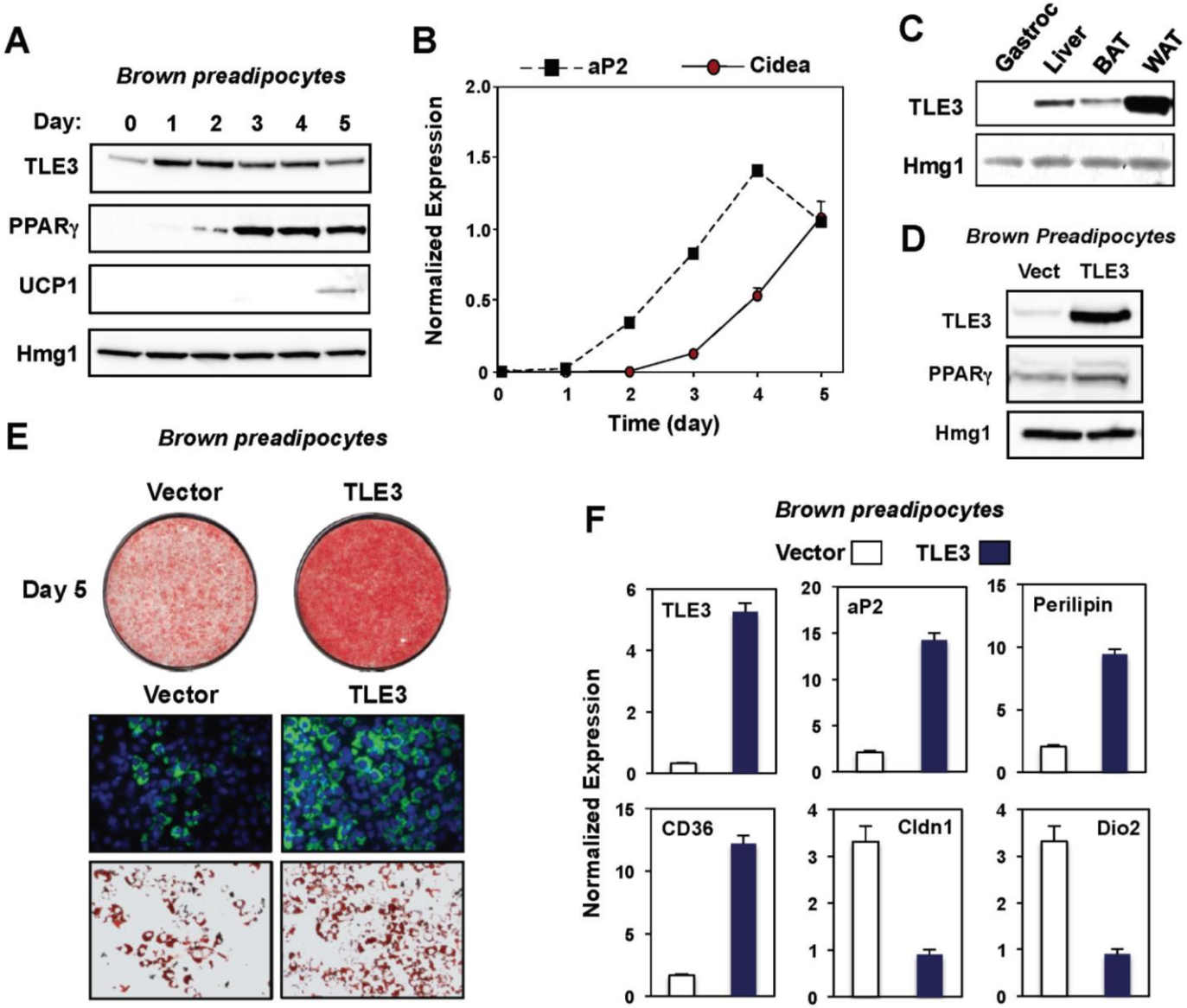
Figure S3. Alteration of the gene expression response to cold exposure in aP2-TLE3 Tg mice. BAT cDNA from control and aP2-TLE3 Tg mice house at RT or 4 ^{o}C was analyzed by hybridization to Affymetrix GeneChip Mouse Gene 1.0 ST Arrays. High resolution heatmap image of the data shown in Fig 3A is shown.

Figure S4. Strategy for the generation of adipose-specific TLE3 knockout mice. A. Schematic of the *Tle3* targeting vector containing a *βgeo* gene-trapping cassette (flanked by Frt sites; green) in intron 2 and a pair of loxP sites (red triangles) flanking exon 3. After recombination with the targeting vector, the targeted allele (*Tle3*$^{-}$) will produce a fusion transcript consisting of exons 1 and 2 of *Tle3* and βgeo. Removal of the *βgeo* gene-trapping cassette with *Flp* recombinase creates a floxed allele (*Tle3*^{F}). *Cre* recombinase removes exon 3 from *Tle3*^{F}, generating a frameshift and creating a delta allele (*Tle3*$^{\Delta}$). Open squares represent exons. LoxP and Frt sites are depicted as red triangles and green squares, respectively. B. Schematic illustration of pCR genotyping strategy. C. PCR analysis of WT and Ad-TLE3 KO

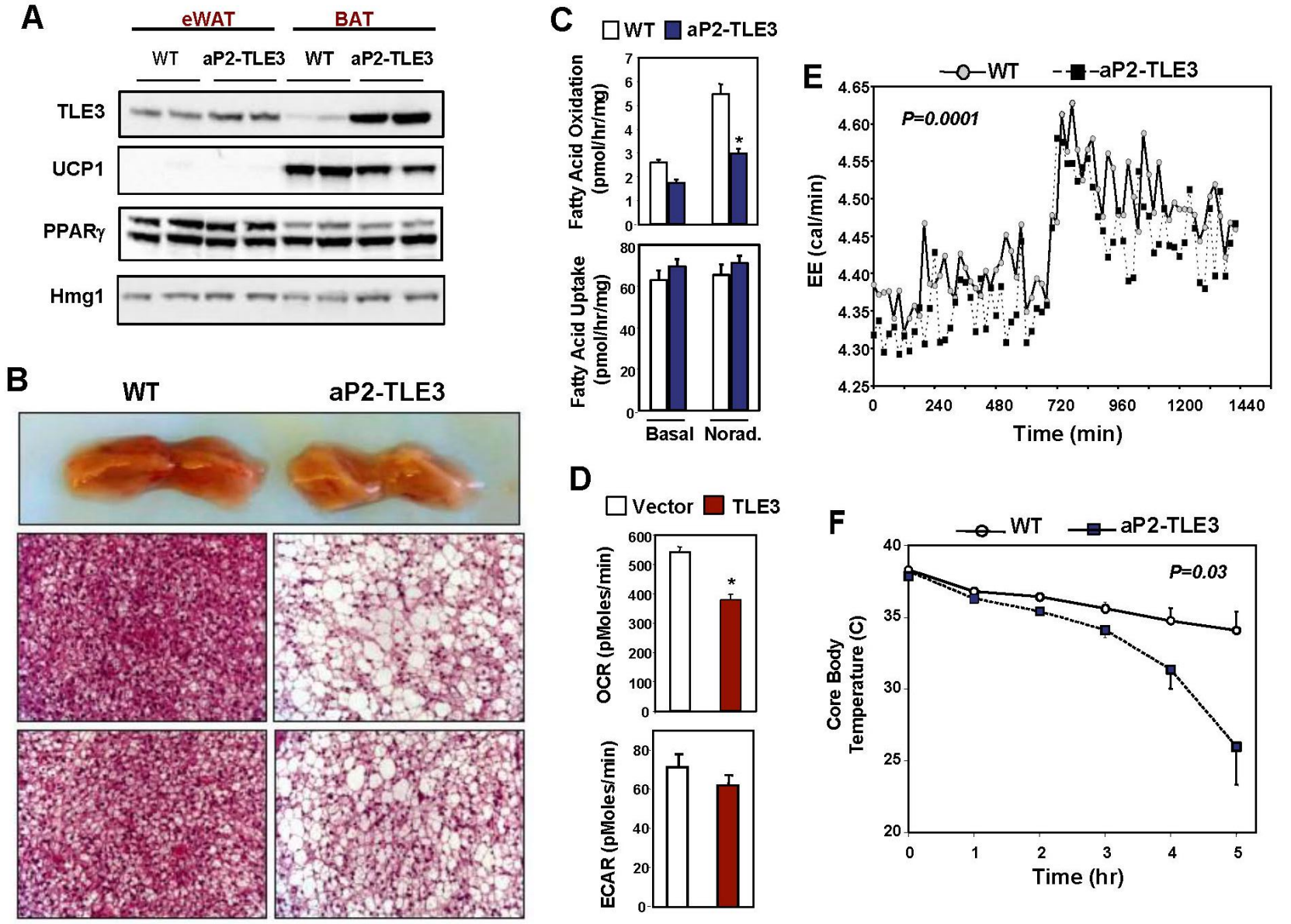
mice. D. TLE3 protein expression in epididymal adipose tissue from WT and Ad-TLE3 KO mice.

Figure S5. Physical activity (A) and food intake (B) in Cre-negative and Cre-positive $TLE3^{F/F}$ mice (N=6-10/group) determined by housing in Oxymax metabolic cages.

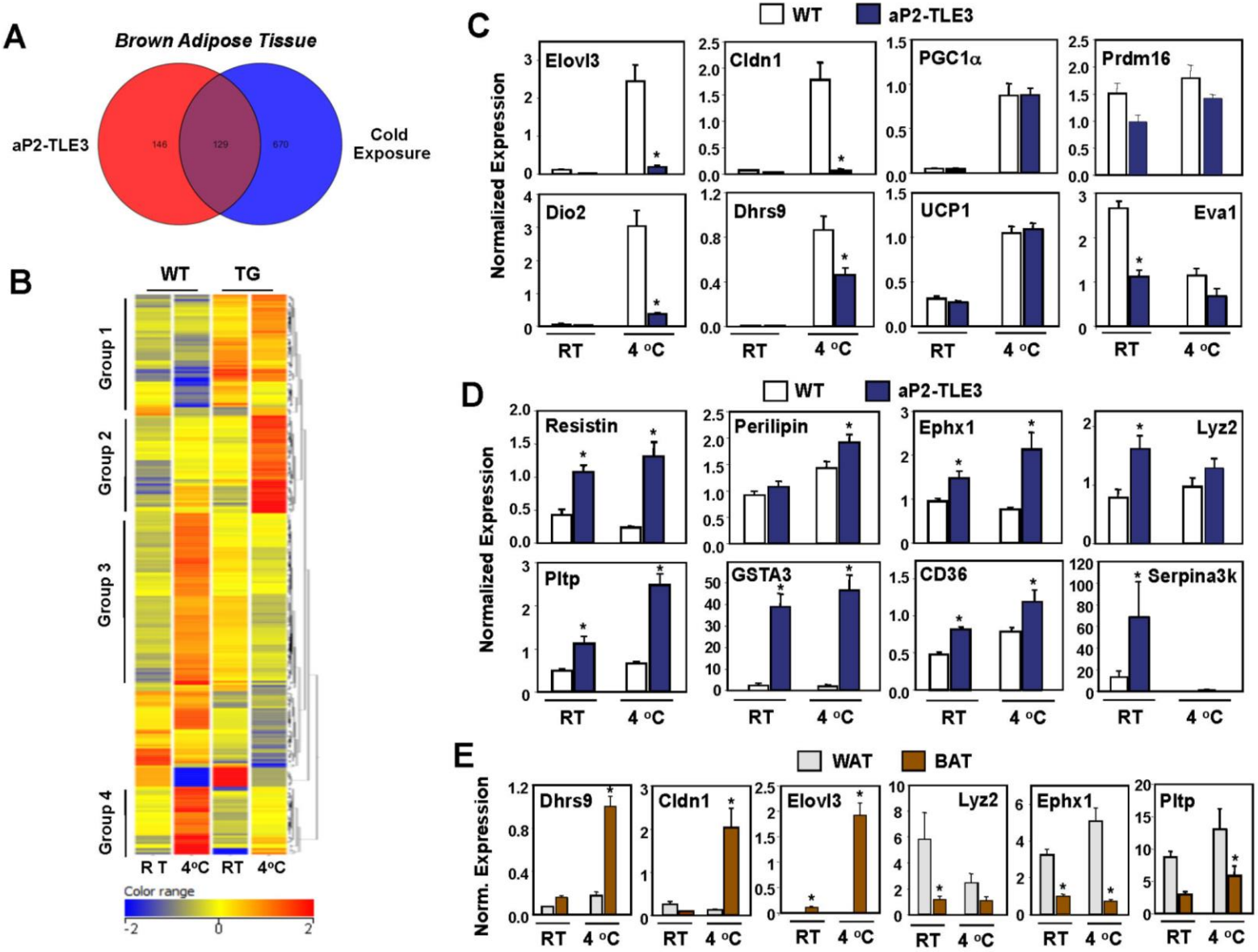
Table S1. Complete list of genes altered more than 2-fold in the microarray studies shown in Fig. 3A.



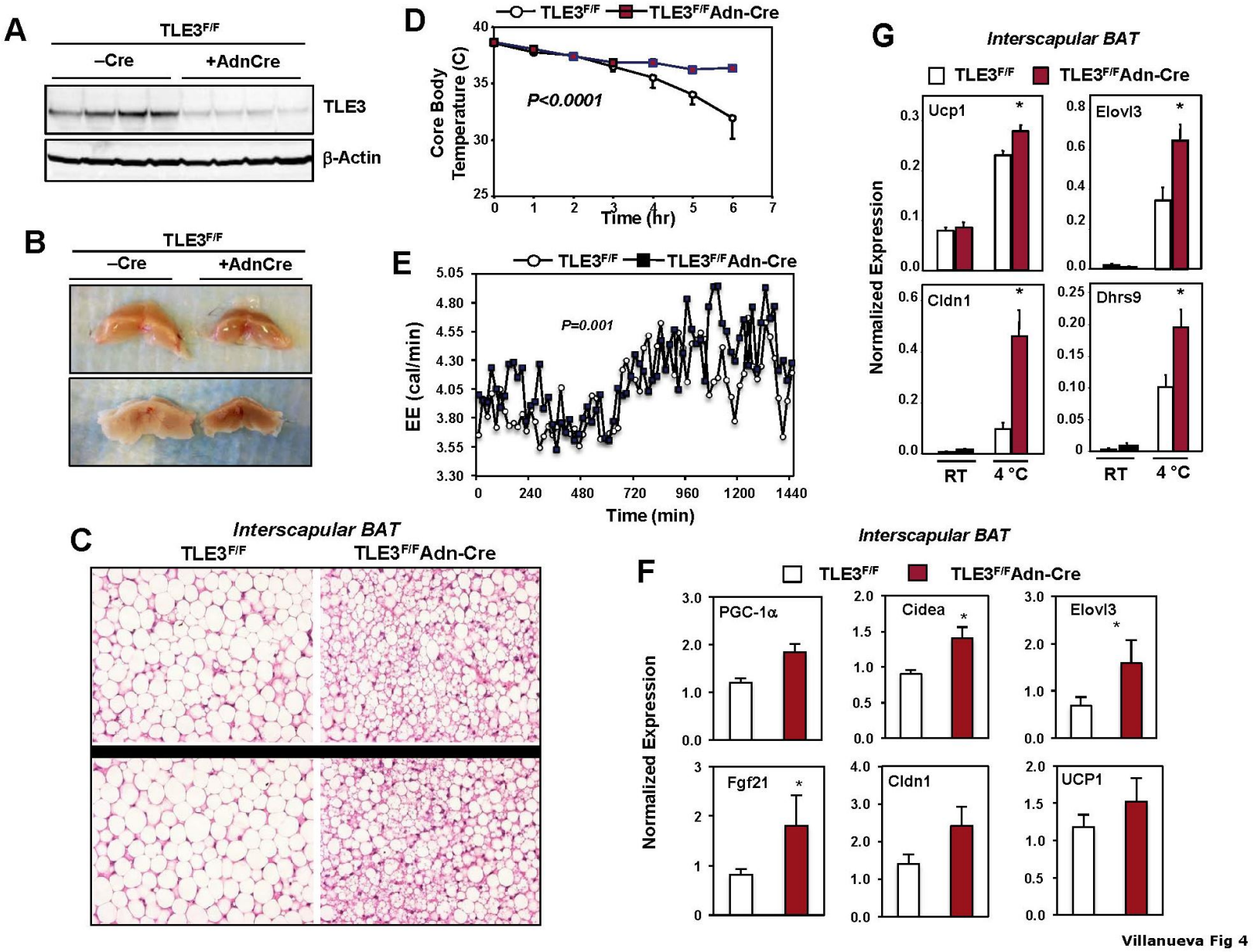
Villanueva Fig 1



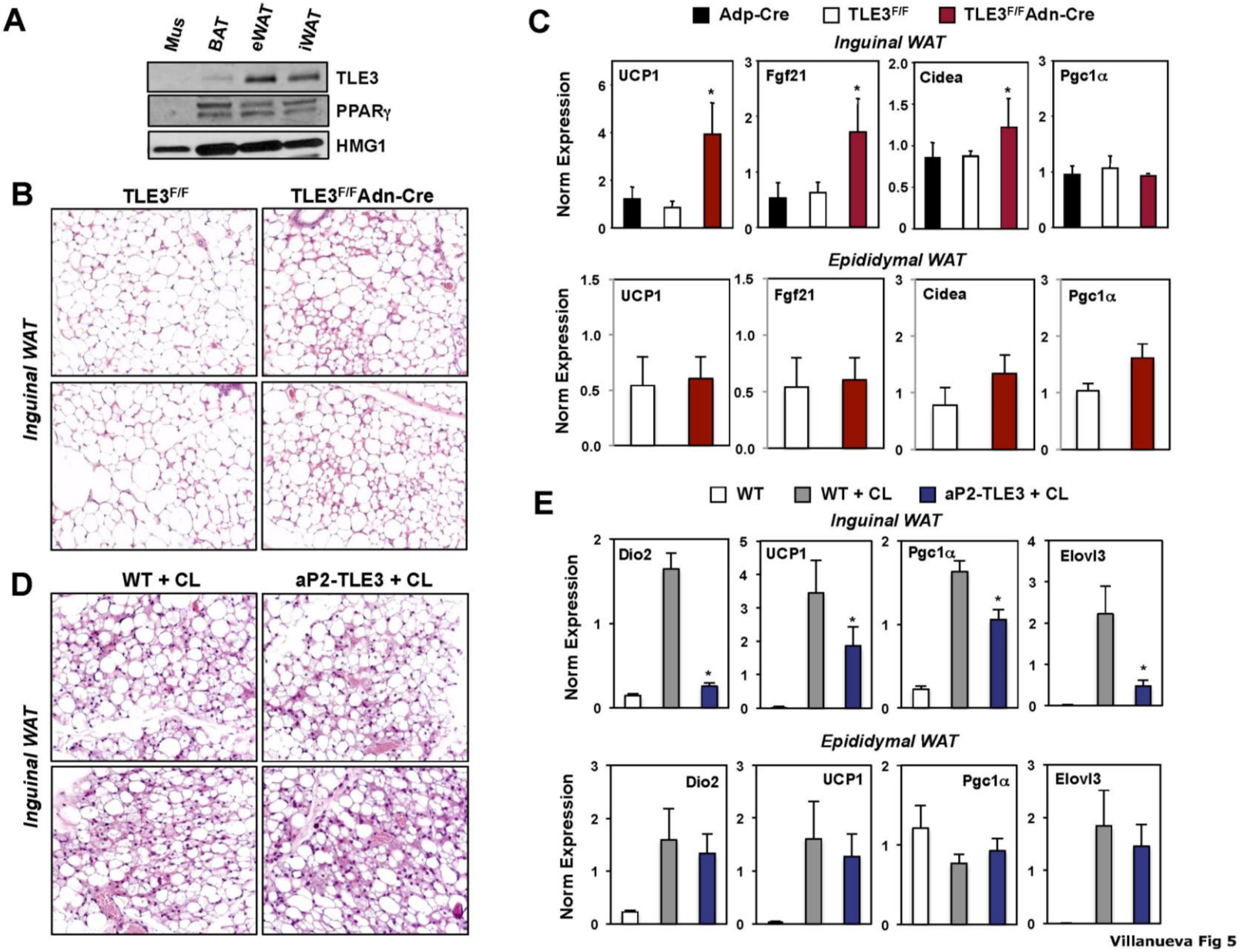
Villanueva Fig 2



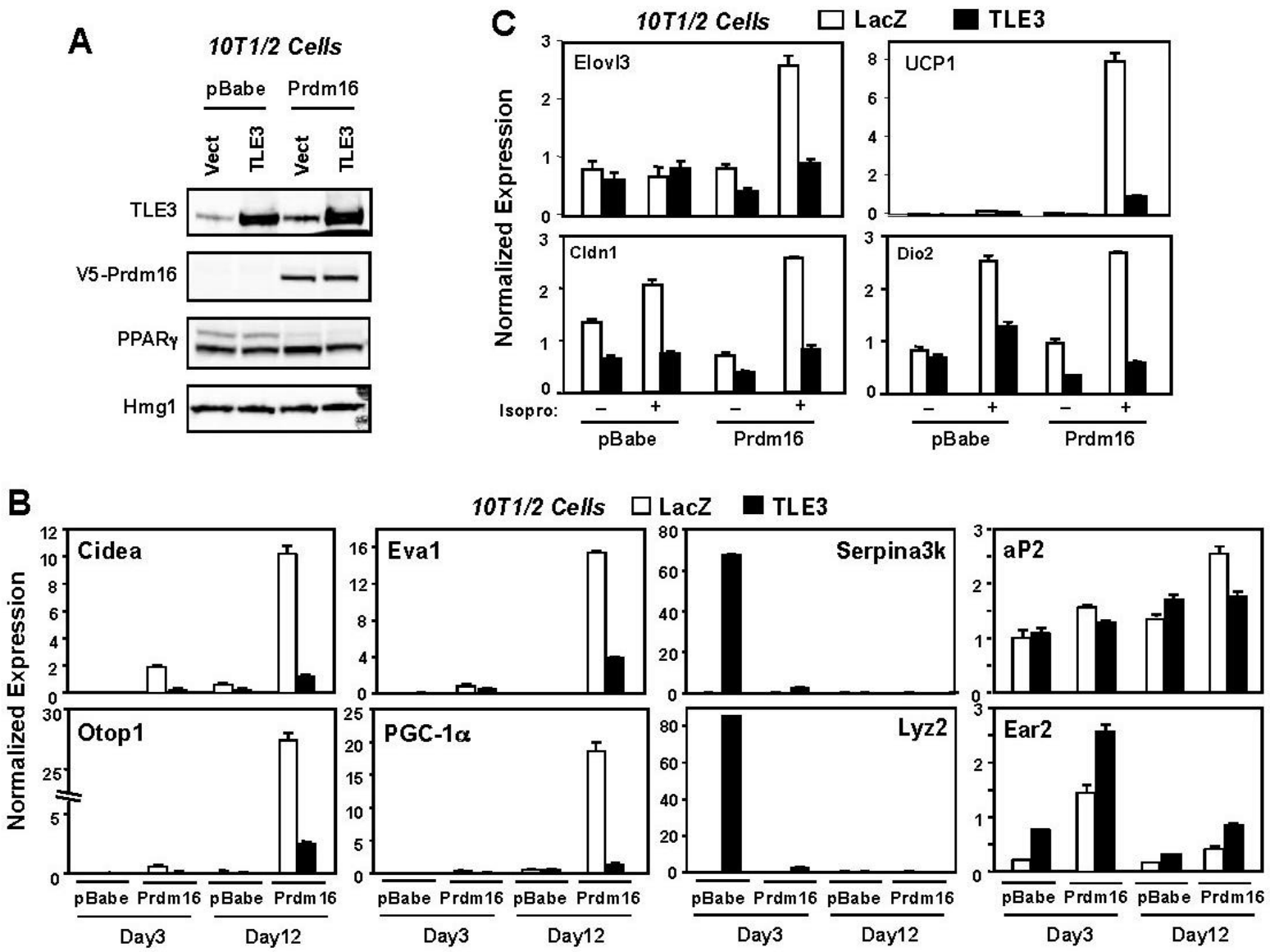
Villanueva Fig 3



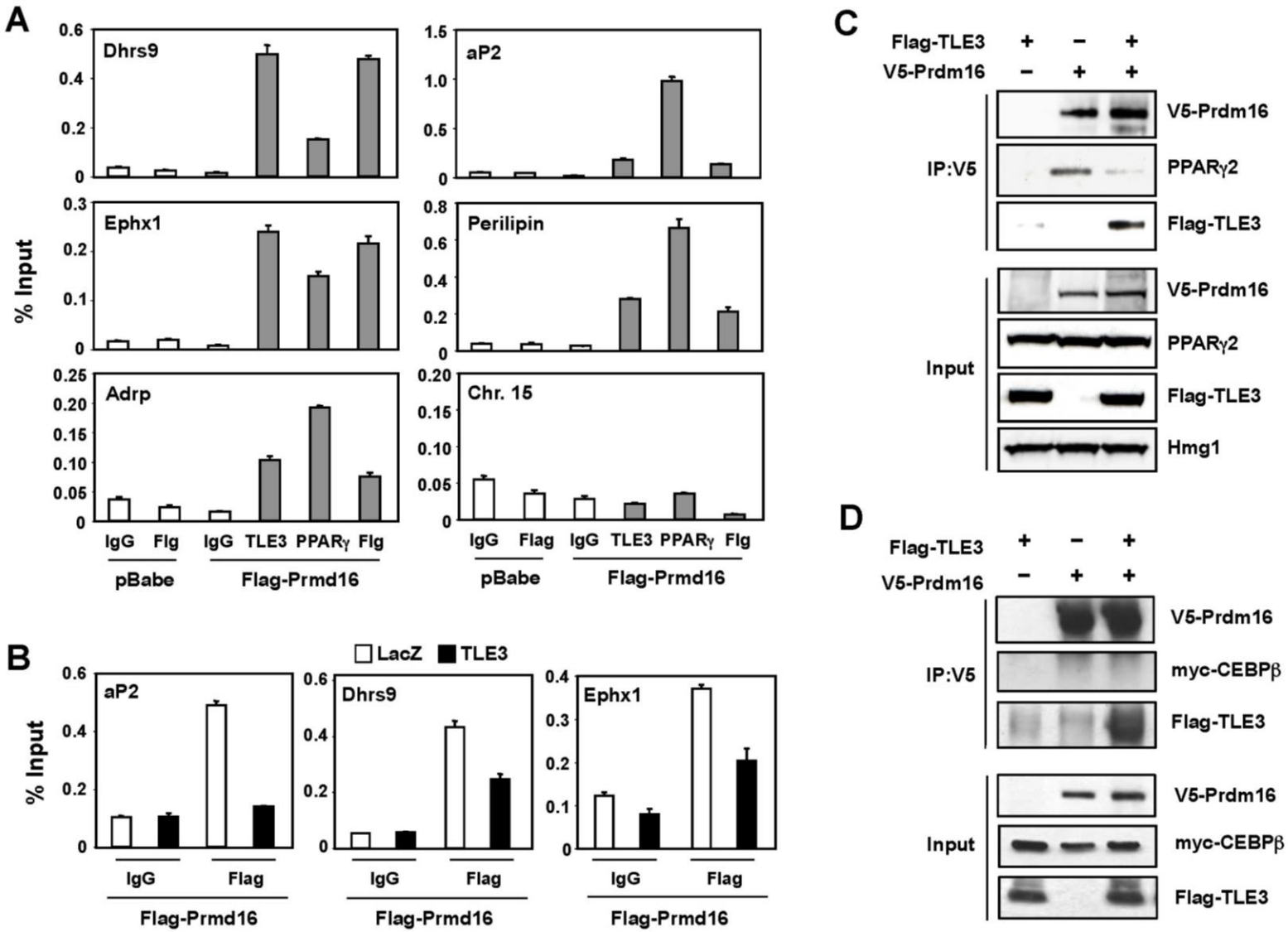
Villanueva Fig 4



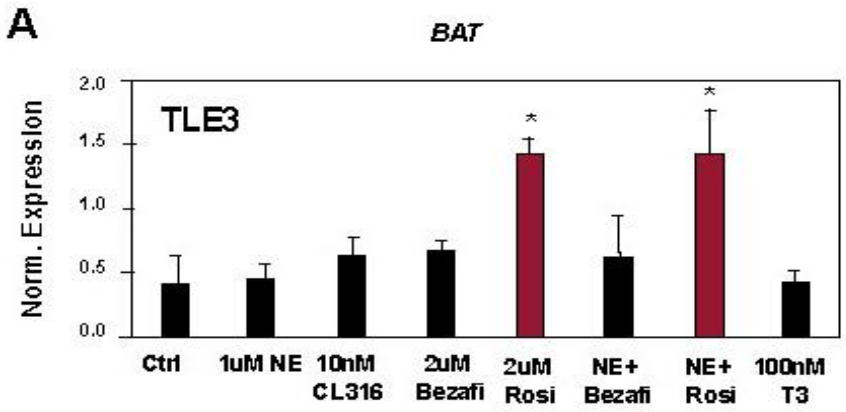
Villanueva Fig 5

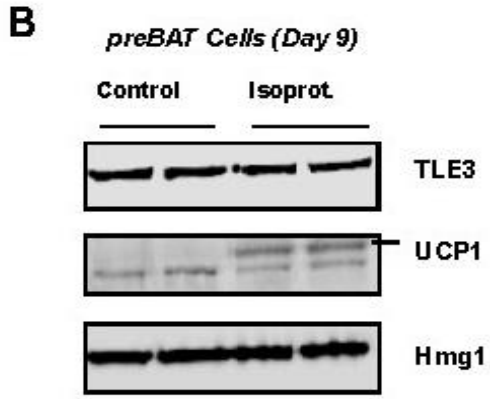


Villanueva Fig 6

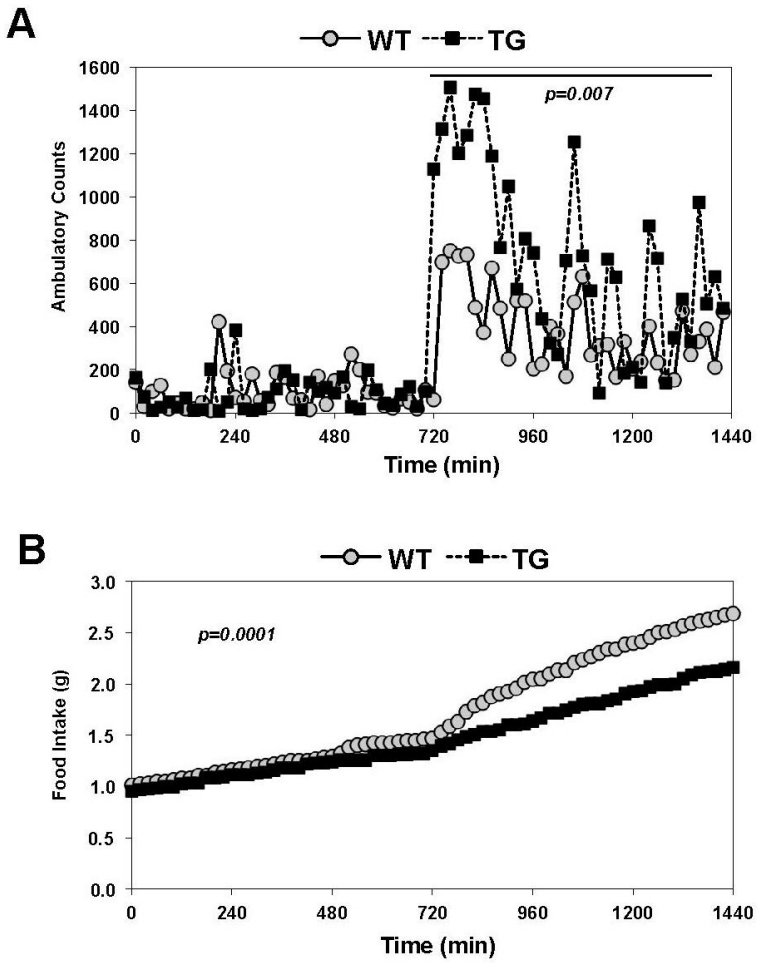


Villanueva Fig 7

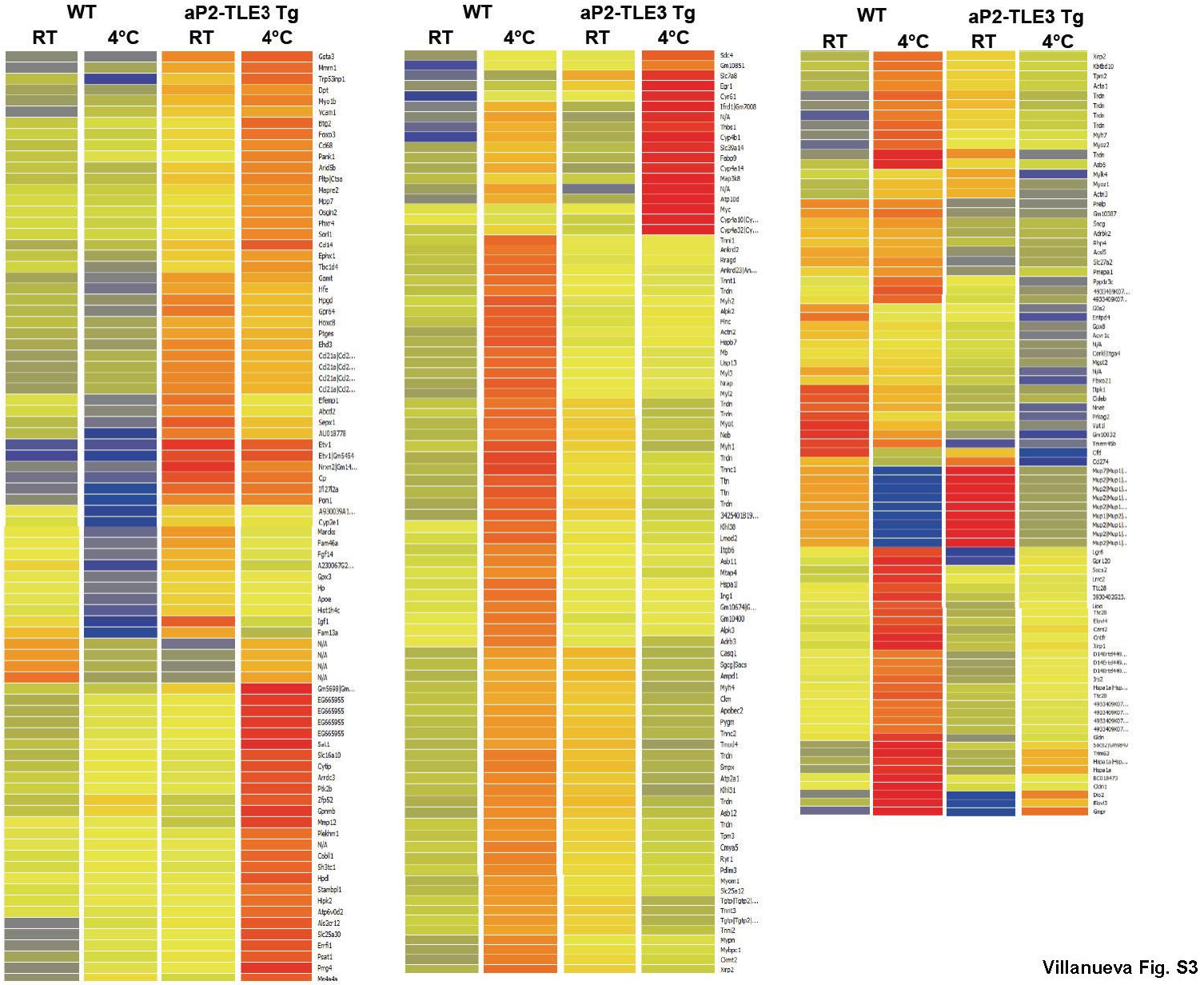




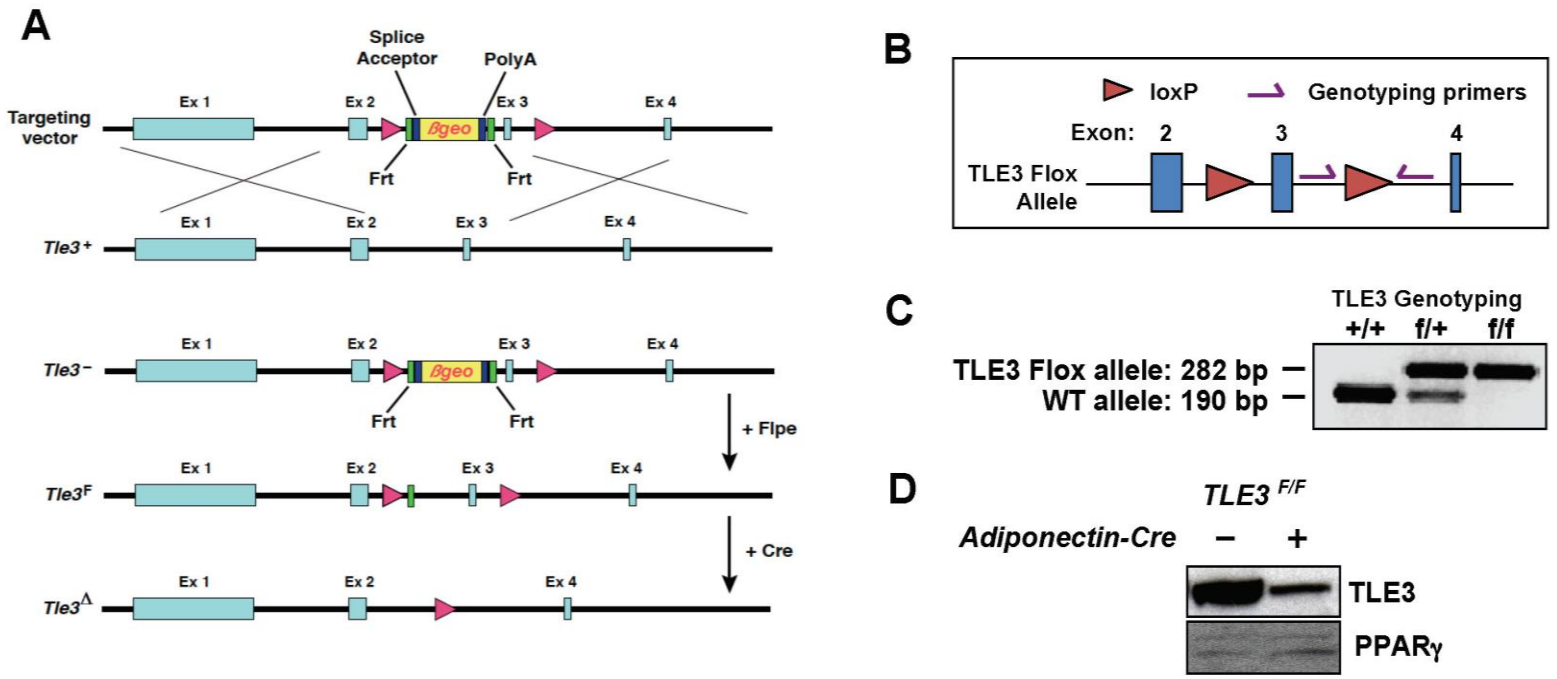
Villanueva Fig S1



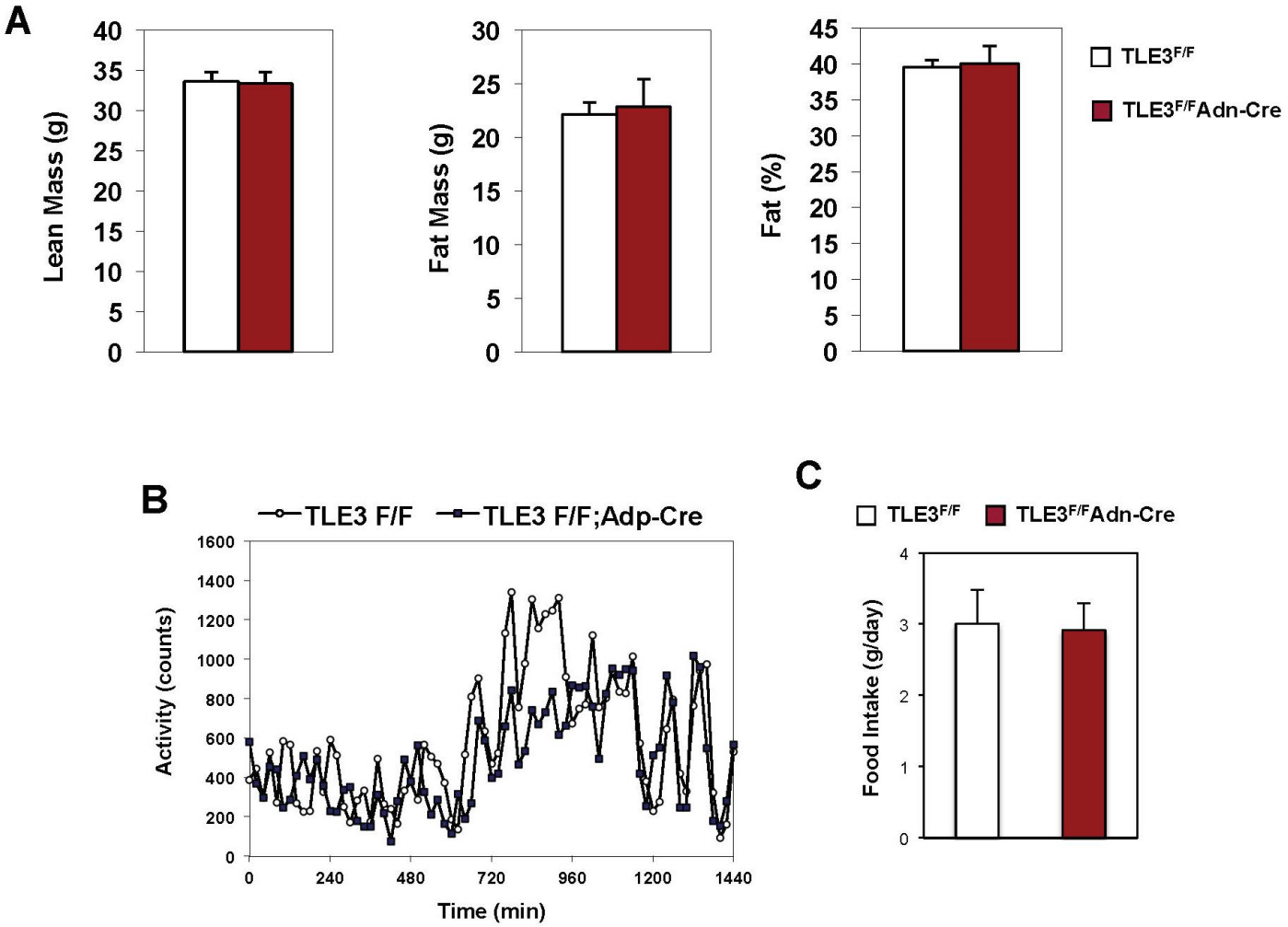
Villanueva Fig S2



Villanueva Fig. S3



Villanueva Fig S4



Villanueva Fig S5

Table S1. Murine qPCR Primers

aP2 F	caccgcagacgacaggaag	
aP2 R	gcacctgcaccagggc	
CD36 F	ttgaaaagtctcggacattgag	
CD36 R	tcagatccgaacacagcgta	
Plin F	ccatctctacccgccttcg	
Plin R	cttgtcagaggtgcttgcaatg	
Lyz2 F	gaatggaatggctggctact	
Lyz2 R	cgtgctgagctaaacacacc	
Serpina3k F	agccaacaaccctgaacatc	
Serpina3k R	tccccatagctacaatgaagg	
Ephx1 F	tccctcaattcctggctatg	
Ephx1 R	ggccaccgaatttaaacctt	
Pltp F	gtctaaaatgaatatggccttcg	
Ptlp R	ccagaagtgatgaacgtgga	
Otop1 F	actaggaccccgtcgaatct	
Otop1 R	accatgctctacgtgctgtg	
Cldn1 F	cttgacccccatcaatgc	
Cldn1 R	cacctcccagaaggcaga	
Dhrs9 F	atttggtggaggggggcta	
Dhrs9 R	tgcacaccaaaagctttcat	
Elovl3 F	tccgcgttctcatgtaggtct	
Elovl3 R	ggacctgatgcaaccctatga	
Eva1 F	gtcccaaccagaccatcaac	
Eva1 R	ctccatcttgctctggaagc	
Dio2 F	cagtgtggtgcacgtctccaatc	
Dio2 R	tgaaccaaagttgaccaccag	
Fgf21 F	agatggagctctctatggatcg	
Fgf21 R	gggcttcagactggtacacat	
UCP1 F	ggcctctacgactcagtcca	
UCP1 R	taagccggctgagatcttgt	
Prdm16 F	gccatgtgtcagatcaacga	
Prdm16 R	ccttctttcacatgcaccaa	
Fbxo21 F	cttgaacctctacatgcaccag	
Fbxo21 R	aagtggcttgggaagttgac	
Itpk1 F	cacatcagatcgtgagtccatc	
Itpk1 R	gaagactccggctttgacac	
Gmpr F	ctcaaggggcacatcatctc	
Gmpr R	aaaggctttggcgacatct	
Socs2 F	ccccttaggtagttttagctgaatg	
Socs2 R	tttaaaagggccatttgatctt	
36B4 F	agatgcagcagatccgcat	
36B4 R	gttcttgcccatcagcacc	

Murine ChIP Primers

Plin F	tcaccctcgcccttaggatc	PPRE
Plin R	tggctgcttctgtacggattc	
Adrp F	tgtaggtgaaagggcaaagaaag	PPRE
Adrp R	gtccaccgcttgttactccc	
Dhrs9 F	cctttggaaacctgtgacct	PPRE

Dhrs9 R	tgcaacaccaagtggtgacta	
aP2 F	gagagcaaatggagttcccaga	PPRE
aP2 R	ttgggctgtgacacttccac	
Chr. 15 F	tggtagcctcaggagcttgc	
Chr. 15 R	atccaagatgggaccaagctg	